공학박사학위논문

Study on the Synergistic Effect of Magnetic Nanoparticles and Magnetic Field on Cell Behavior

자성나노입자와 자기장이 세포에 미치는 상승효과에 대한 연구

2014 년 2 월

서울대학교 대학원

기계항공공학부

신 재 하

자성나노입자와 자기장이 세포에 미치는 상승효과에 대한 연구

Study on the Synergistic Effect of Magnetic Nanoparticle and Magnetic Field on Cell Behavior

지도교수 이 정 훈

이 논문을 공학박사 학위논문으로 제출함

2014 년 2 월

서울대학교 대학원

기계항공공학부

신 재 하

신재하의 공학박사 학위논문을 인준함

2014 년 2 월

위 원 장 : 전 누 리 (인)

부위원장 : 이 정 훈 (인)

위 원 : 현 택 환 (인)

위 원 : 이 윤 식 (인)

위 원 : 김 영 근 (인)

Abstract

Study on the Synergistic Effect of Magnetic Nanoparticles and Magnetic Field on Cell Behavior

Jaeha Shin

School of Mechanical and Aerospace Engineering

Seoul National University

Biomedical use of electric and magnetic fields have been studied extensively for decades. The electric field has been used in physical therapy, rehabilitation and cancer treatment, then commercial devices for electrical stimulation are being sold in the market. Static magnetic field (SMF) also has been investigated for treating medical problems such as chronic pain, wound healing, and arthritis, and is being used in MRI diagnosis.

Magnetic nanoparticles (MNPs) are widely used in biomedical applications such as imaging and targeting tool with advantage of their magnetic nature which allows for more efficient bioapplications by applying external magnetic fields. Electromagnetic fields assisted MNPs have been studied for many therapeutic applications with

varied frequency and amplitude and SMF has been employed for separation and targeting of cells. However the biological effects of magnetic fields combined with MNPs have not yet been much investigated. Therefore careful examination of the biological effect of magnetic particle and fields is required for safe use of them.

In this study, the synergistic effect of the communications between internalized bacterial magnetic nanoparticles (BMPs) and an external SMF on a standard human cell line was demonstrated. The BMPs are naturally synthesized magnetic nanoparticles by magnetotactic bacteria with enclosing inherent biocompatible lipid membrane, which are well taken up by cells. In addition, their ferrimagnetic property is suitable to study effect of MNPs on cells.

Diamagnetic anisotropy of lipid molecules comprising cell membrane was the primary factor leading to the alteration of cell structure under moderate strength of SMF. Additionally, ferrimagnetic characteristic of the BMPs gave rise to enhancement of magnetic flux density around them internalized in cell. This combination of the BMPs and SMF resulted in the improved cell growth and reduced apoptotic efficiency of human tumor cells induced by anticancer drugs.

The alteration of cell membrane initiated modulation of embedded transmembrane proteins in structure and function which influence gene regulation and finally cell growth, apoptosis and differentiation. Microarray analysis suggested that these

phenomena are caused by the alterations of GPCRs-mediated signal transduction originated in the interaction of internalized BMPs and the external SMF.

Specific targeting of cells to sites of tissue damage and delivery of high numbers of transplanted cells to lesion tissue in vivo are critical parameters for the success of cell-based therapies. The synergistic effects of the BMPs and SMF, enhancement of cell growth and differentiation could be employed for expeditious cell therapy with manipulation of the cells by virtue of magnetic controllability of the internalized BMPs. Rapid replacement of the damaged tissue would be achieved with the advantage of synergistic effects.

This work suggests a promising in vitro model system for studying the homing of transplanted cells, which may eventually be applicable for targeted regeneration of damaged neurons in spinal cord injury. In this model system, neurospheres derived from human neuroblastoma SH-SY5Y cells labeled with bacterial magnetic nanoparticles are guided by magnetic field and successfully accumulated near the focus site of the magnetic field. These results demonstrated the effectiveness of using an in vitro model for testing bacterial magnetic nanoparticles to develop successful stem cell targeting strategies during fluid flow, which may ultimately be translated to in vivo targeted delivery of cells through the circulation in various tissue-repair models.

This study may offer new approach towards targeted cell therapy with the advantage of controlling cell viability by synergistic effect of internalized BMPs and external exposure to SMF.

Keyword: Magnetic Nanoparticle, Magnetic field, Cell growth, Anti-apoptosis, Neuronal Differentiation, Neurosphere, Cell Therapy

Student Number: 2006-23090

Table of Contents

List of Figures

List of Tables

Chapter 1. Introduction

1.1 Bioapplications of Electric and Magnetic Fields

Electric and magnetic fields have been studied widely to use for medical treatment from the late 1900s. This area has been advanced along with a number of studies to investigate biological effects of the electric and magnetic fields such as cell metabolism, apoptosis and tumor growth. Therapeutic applications using electric and magnetic fields have been developed considerably and some of them were approved by the United States Food and Drug Administration (FDA).

The electric and magnetic field are usually analyzed more appropriately as separate below 100 kHz and they do not propagate. Above 100 kHz the fields are coupled and propagating at the speed of light, it is called electromagnetic fields. At very high frequencies such as light waves, the electromagnetic wave are considered as oscillating bundles or particles of energy called photons [1]. For biomedical applications the low frequency and intermediated frequency, 0 to 10 MHz, of electromagnetic fields have been investigated and practical uses have been reported for the physical therapy and tumor treatment.

Electrical stimulation is used for rehabilitative purposes in physical therapy such as relaxation of muscle spasms and prevention of disuse atrophy which can occur after musculoskeletal injuries. The capacity of electrical stimulation has been demonstrated for strengthening muscles, enhancing circulation and blood flow, reducing pain, healing

tissue, retarding muscle atrophy, and reducing spasticity [2]. In addition to the muscle stimulation, pulsed electromagnetic field therapy are used for bone healing in the field of orthopedics [3-4]. Transcranial magnetic stimulation is another noninvasive method to use electromagnetic field for treatment of neurological and psychiatric disorders including epilepsy, strokes, and depression [5-7]. For cancer therapy, tumor treating fields is a novel method using alternating electric fields in the frequency range of 100–300 kHz [8]. It is also reported that the nanosecond pulsed electric fields induce apoptosis which can be applied for cancer treatment [9].

Static magnetic field (SMF) generated by permanent magnets is a plain magnetic field uncombined with electric field. The applications of permanent magnets for treating medical problems such as chronic pain, wound healing, and arthritis have continuously investigated for decades [10-18]. In vitro study on the biological effects of the SMF has been conducted with various cell types under diverse exposure conditions, strength of the field, time, and orientation [19-31]. The advantage of using SMF is powerless, it is simply applied via many or a magnet attached to the specific site. The medical use of SMF is therefore an attractive field being investigated vigorously, though the efficacy of magnet therapy is a subject still under debate. Dosing parameters, e.g. optimal SMF strength, duration and the time point of exposure during the course of an illness or injury, are remained to be established for effective use of SMF.

A great interest in use of electric and magnetic field for medical applications have led to

development of the various therapies which could contribute to human health and wellbeing. These efforts to study biological effects and applications of the electric and magnetic field will be continued to advance technique of medical treatment.

1.2 Bioapplications of Magnetic Particle

1.2.1 In-vitro Applications

Magnetic particles are used to separate molecules from their surroundings, thereby the surroundings can be purified or the molecules can be concentrated for further study. The phase separation is a crucial step for in-vitro diagnosis and it is usually achieved by centrifugation, precipitation or filtration. The magnetic particles can offer rapid and easy separation upon applying an external magnetic field. Furthermore, large surface area of nano-sized magnetic particles is effective to functionalize large quantity of molecules. This separation is also applied to isolate specific cells from others for diagnosis or further use.

Gene delivery using magnetic particles has been called magnetofection. Efficient gene transfection and expression could be achieved by applying a magnetic field to the particles coated with gene. The magnetic field aids in holding the particles at the target cells, thereby increased duration of gene in contact with the cells induces improvement of transfection efficiency.

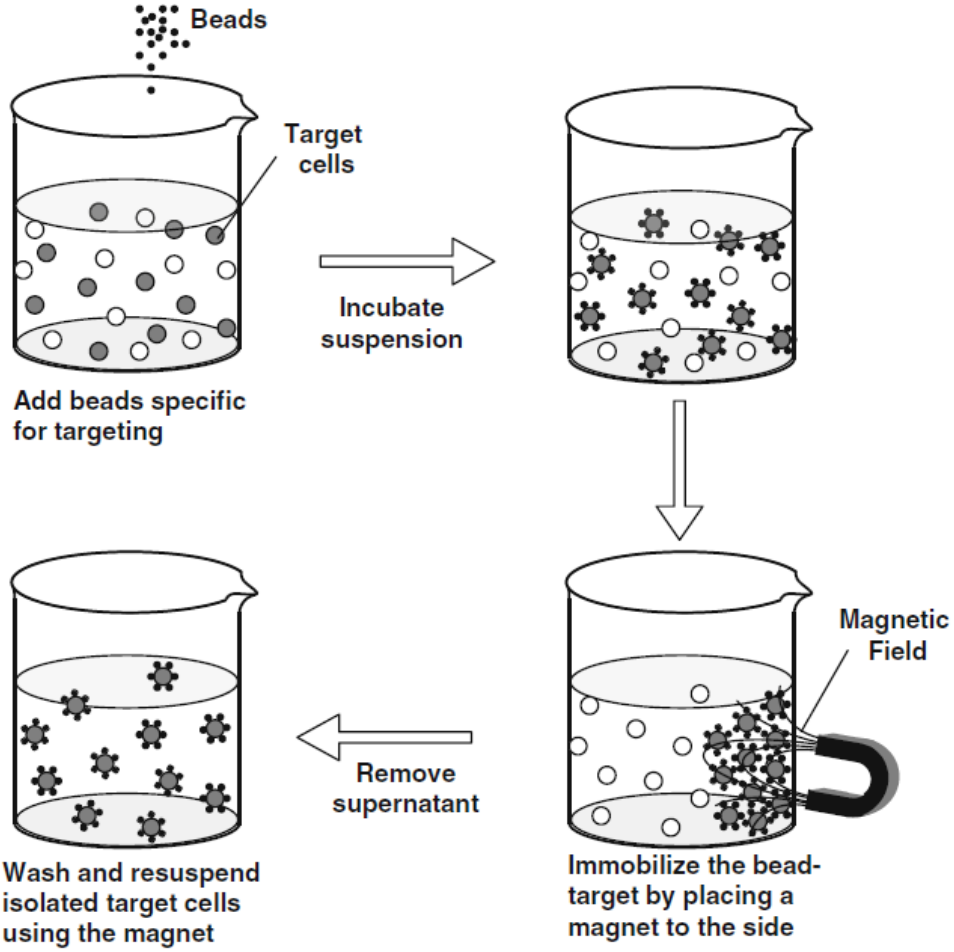

Figure 1-1. Magnetic separation [32]

For the in-vitro diagnosis, the magnetic particles can be more attractive by the benefit of the potential to detect more than one molecule at the same time. The magnetic particles have been employed as supports for the immobilization of biorecognition molecules in immunoassay. The magnetic controllability of the particles reduces time consuming

washing steps, so that the immunoassay can be carried out faster than typical methods. Another potential application of magnetic particles is the detection and monitoring of bacterial, viral and other pathogenic contamination combined with integrated sensor.

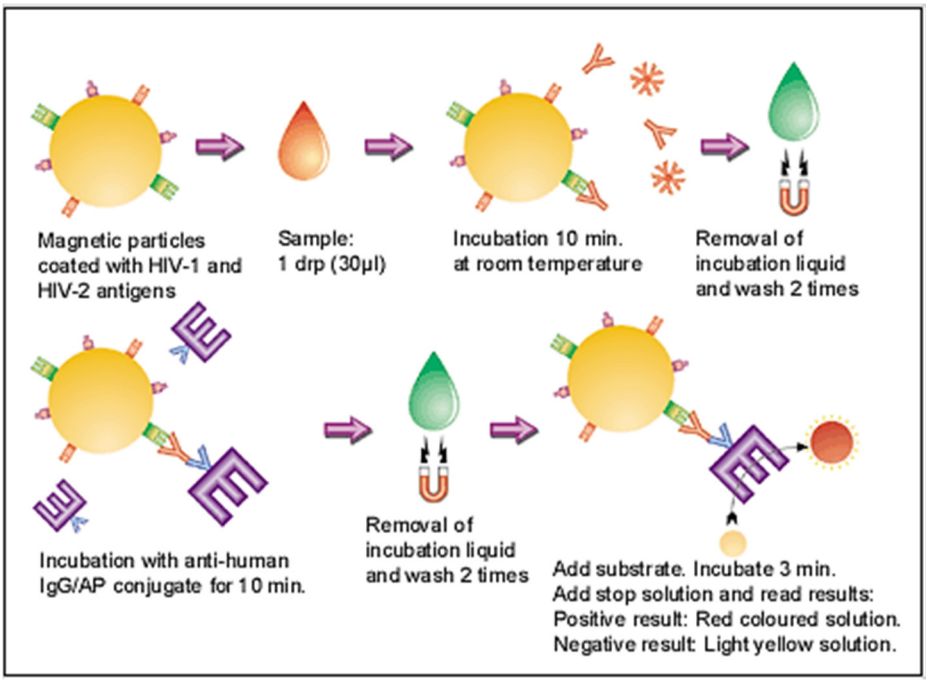

Figure 1-2. Immunoassay using magnetic particle [33-34]

1.2.2 In-vivo Applications

In-vivo biomedical applications of magnetic nanoparticles (MNPs) include drug delivery, hyperthermia and magnetic resonance imaging. Biocompatible and non-toxic MNPs, well dispersed in aqueous solutions, have a lot of potential for in-vivo applications. Superparamagnetic nanoparticles are of interest since any residual magnetism are not remained after removal of a magnetic field. Large surface-to-volume ratio of MNPs offers ample active sites for biomolecule conjugation, allowing delicate design and engineering of the MNPs for intended functions such as long-circulating in the blood stream, target specificity to lesion tissue, optical detectability, and therapeutic delivery.

Delivery of drug to specific site can prevent undesirable side effects caused by relatively non-specific common chemotherapy. The use of MNPs as a drug carrier can render drug to be effective on targeted site with benefit of guidance by applying magnetic fields [35-36]. Additionally, the release of the drug can be controlled to occur once the particle has reached or to be spread pulsatively on the target [37-39].

The idea that a localized rise in temperature, typically about 43°C, can be used to destroy malignant cells selectively is called hyperthermia. This method of treatment can be achieved using magnetic particles which are heated by an A.C. magnetic field [40]. The advantage of using magnetic particles is that the only the targeted region affected by heat generated from the particles under an external A.C. magnetic field. The targeted

hyperthermia is another promising therapeutic application along with drug delivery to treat cancer.

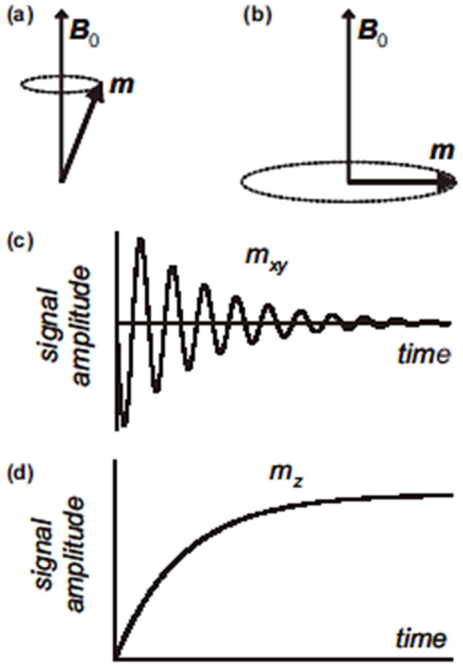

Figure 1-3. Magnetic resonance for protons with magnetic moment m in a field Bz. (a) the moment precesses around the field. (b) A second field excites the moment precession into the plane perpendicular to Bz. (c, d) the second field is removed and the in-plane (c) and longitudinal (d) moment amplitudes relax back to their initial values [41]

Magnetic resonance imaging (MRI) is one of most powerful for clinical diagnosis and in-vivo imaging. When a steady field of about 1 T apply to a material, a very small fraction of protons are to line up parallel to the field. Then, the net magnetic moment precesses

like a top around the direction of this field (Fig. 1-3). In order to measure the signal produced as a result of this alignment, a transverse radio frequency magnetic field is applied. After this second field is turned off, the amplitudes of the magnetic moments relax back to their initial values. This relaxation of the response is measured by pick-up coils and the relaxation time can be reduced by means of a magnetic particle [32]. The MNPs are used as MRI contrast agent [42-44].

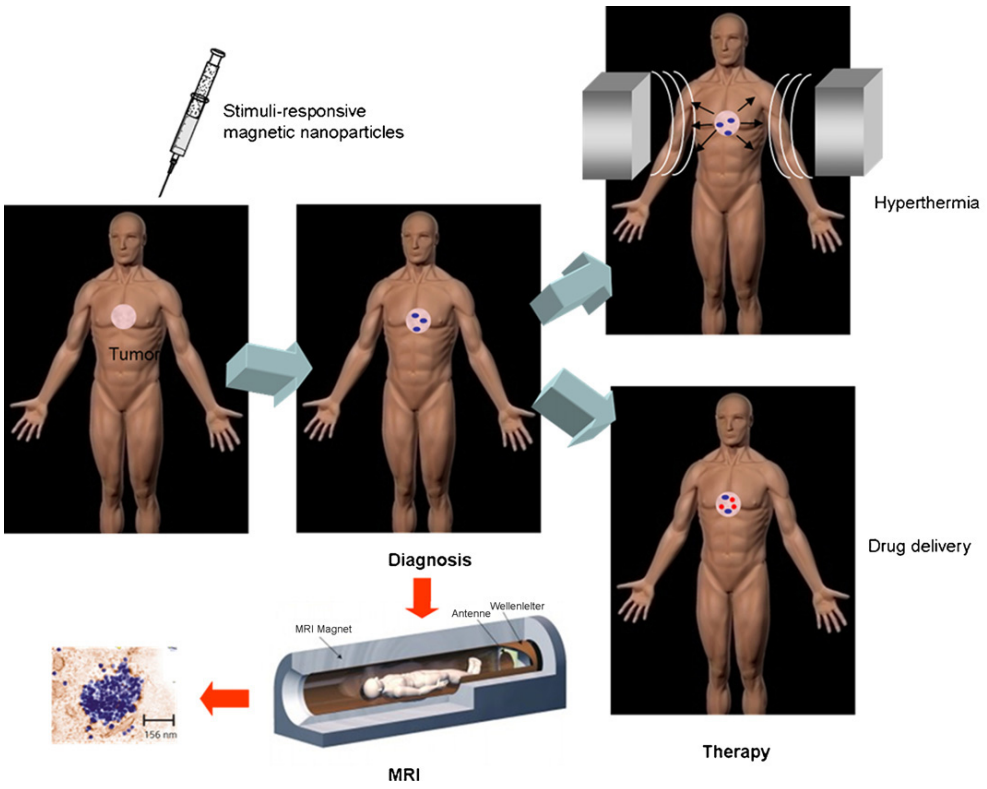

Figure 1-4. Schematic representation of the drug-loaded magnetic nanoparticles localization by MRI followed by the treatment of the tumour either by hyperthermia or by the drug release [45]

Recently, the MNPs has been designed and developed to contain complex function for theragnosis [46]. The theragnosis is a novel concept in clinic, which conduct diagnosis and therapy simultaneously (Fig. 1-4). Drug carried MNPs enable targeted drug delivery with observing MR images to check the location of the particles and efficacy of the drug treatment.

Likewise, the use of magnetic particles have been extensively researched for biomedical applications in-vitro and in-vivo.

1.3 Potential Use of Magnetic Particle and Magnetic Field

Destruction of tumor and regeneration of damaged tissue are completely opposite aim of the treatment in terms of cellular level. The magnetic particles and fields have potential to advance the medical techniques in both areas of the treatments. The combination of magnetic particles and field facilitate more effective treatment by targeting specific site.

Magnetic guide of the particles is a key factor to treat specific tissue like tumor. Hyperthermia and drug delivery are main therapeutic uses of magnetic particle and magnetic field for cancer treatment. The magnetic field guides movement of magnetic particles carried drugs to destroy only cancer cells rather than normal cells, it can reduce the side effect of general anti-cancer treatments. Hyperthermia with magnetic particle can induce heat locally by control of the position of particles, the heat affects only targeted cells.

Cell therapy is a therapeutic method in which stem or progenitor cells are injected into a patient, it is targeted to damaged and injured tissue for regeneration in body. Specific targeting of cells to sites of tissue damage and delivery of high numbers of transplanted cells to lesion tissue in vivo are important for the efficacy of cell therapy. Cells labeled with magnetic particles can be manipulated by magnetic field. This magnetic cell manipulation can facilitate more efficient cell delivery to target site of cell therapy [47-49].

Despite lots of studies are being investigated to use magnetic particle and field for biomedical applications, the biological effect of magnetic particles combined with magnetic field has not been extensively examined yet. The magnetic field should be applied to magnetic particle in any applications, irrespective of the aim. For the medical applications, careful examination of the biological effect of magnetic particle combined with fields is especially required for safe use of them.

Diamagnetic anisotropic properties of membrane phospholipids can result in the reorientation of cell membrane during exposure to SMF, although effect of diamagnetism is negligible in general. The sum of diamagnetic anisotropy can overcome thermal energy because the cell membrane is composed of lipid molecules arranged in parallel [50-53]. In addition, the magnetic particles can aid in enhancing the strength of field and extending the region affected by the SMF. This interaction between the magnetic particles and SMF would affect cell metabolism.

The biological effect of magnetic particles combined with SMF was investigated on three kind of cell system in-vitro, cancer, normal and neuronal cells. HeLa cell (human cervical cancer) was a case of cancer cell, C2C12 cell (rat myoblast) was a case of normal cells and SH-SY5Y cell (human neuroblastoma) was a case of neural stem cells. Furthermore the mechanism of the combined effect was studied with HeLa cells which are easy to handle and analyze. Based on the effect of magnetic particles combined with SMF, potential application of them was tested as an in-vitro model system of cell therapy.

1.4 References

(1) Carpenter, D. O.; Ayrapetyan, S., *Biological Effects of Electric and Magnetic Fields*. Academic Press, INC.: San Diego, California, 1994; Vol. 1.

(2) Doucet, B. M.; Lam, A.; Griffin, L., Neuromuscular Electrical Stimulation for Skeletal Muscle Function *Yale J. Biol. Med.* **2012,** *85*, 201.

(3) Haddad, J. B.; Obolensky, A. G.; Shinnick, P., The biologic effects and the therapeutic mechanism of action of electric and electromagnetic field stimulation on bone and cartilage: new findings and a review of earlier work *J. Altern. Complement. Med.* **2007,** *13*, 485.

(4) Markov, M. S., Expanding use of pulsed electromagnetic field therapies *Electromagnetic biology and medicine* **2007,** *26*, 257.

(5) MERTON, P. A.; MORTON, H. B., Stimulation of the cerebral cortex in the intact human subject *Nature* **1980,** *285*, 227.

(6) Theodore, W. H., Trnascranial Magnetic Stimulation in Epilepsy *Epilepsy Currents* **2003,** *3*, 191.

(7) Dimyan, M. A.; Cohen, L. G., Contribution of transcranial magnetic stimulation to the understanding of functional recovery mechanisms after stroke *Neurorehabil Neural Repair* **2010,** *24*, 125.

(8) Davies, A. M.; Weinberg, U.; Palti, Y., Tumor treating fields: a new frontier in cancer therapy *Ann. N. Y. Acad. Sci.* **2013,** *1291*, 86.

(9) Beebe, S.; Sain, N.; Ren, W., Induction of Cell Death Mechanisms and Apoptosis by Nanosecond Pulsed Electric Fields (nsPEFs) *Cells* **2013,** *2*, 136.

(10) Vallbona, C.; Hazlewood, C. F.; Jurida, G., Response of Pain to Static Magnetic

Fields in Postpolio Patients: A Double-Bllind Pilot Study *Arch. Phys. Med. Rehabil.* **1997,** *78*, 1200.

(11) Man, D.; Man, B.; Plosker, H., The Influence of Permanent Magnetic Field Therapy on Wound Healing in Suction Lipectomy Patients: A Double-Blind Study *Plast. Reconstr. Surg.* **1999,** *104*, 2261.

(12) Segal, N. A.; Toda, Y.; Huston, J.; Saeki, Y.; Shimizu, M.; Fuchs, H.; Shimaoka, Y.; Holcomb, R.; McLean, M. J., Two configurations of static magnetic fields for treating rheumatoid arthritis of the knee: a double-blind clinical trial *Arch. Phys. Med. Rehabil.* **2001,** *82*, 1453.

(13) Brown, C. S.; Ling, F. W.; Wan, J. Y.; Pilla, A. A., Efficacy of static magnetic field therapy in chronic pelvic pain: A double-blind pilot study *Am. J. Obstet. Gynecol.* **2002,** *187*, 1581.

(14) Carter, R.; Aspy, C. B.; Mold, J., The effectiveness of magnet therapy for treatment of wrist pain attributed to carpal tunnel syndrome *J. Fam. Pract.* **2002,** *51*, 38.

(15) Hinman, M. R.; Ford, J.; Heyl, H., Effects of static magnets on chronic knee pain and physical function: a double-blind study *Altern. Ther. Health Med.* **2002,** *8*, 50.

(16) Weintraub, M. I.; Wolfe, G. I.; Barohn, R. A.; Cole, S. P.; Parry, G. J.; Hayat, G.; Cohen, J. A.; Page, J. C.; Bromberg, M. B.; Schwartz, S. L., Static magnetic field therapy for symptomatic diabetic neuropathy: a randomized, double-blind, placebo-controlled trial *Arch. Phys. Med. Rehabil.* **2003,** *84*, 736.

(17) Harlow, T.; Greaves, C.; White, A.; Brown, L.; Hart, A.; Ernst, E., Randomised controlled trial of magnetic bracelets for relieving pain in osteoarthritis of the hip and knee *BMJ* **2004,** *329*, 1450.

(18) Wolsko, P. M.; Eisenberg, D. M.; Simon, L. S.; Davis, R. B.; Walleczek, J.; Mayo-Smith, M.; Kaptchuk, T. J.; Phillips, R. S., Double-blind placebo-controlled trial of static magnets for the treatment of osteoarthritis of the knee: results of a pilot study *Altern. Ther. Health Med.* **2004,** *10*, 36.

(19) Kale, P. G.; Baum, J. W., Genetic effects of strong magnetic fields in Drosophila melanogaster: I. Homogeneous fields ranging from 13,000 to 37,000 Gauss *Environ. Mutagen.* **1979,** *1*, 371.

(20) Fedrowitz, M.; Westermann, J. r.; Lo¨scher, W., Magnetic Field Exposure Increases Cell Proliferation but Does Not Affect Melatonin Levels in the Mammary Gland of Female Sprague Dawley Rats *Cancer Res.* **2002,** *62*, 1356.

(21) Jajte, J.; Grzegorczyk, J.; Zmys´lony, M.; Rajkowska, E. b., Effect of 7 mT static magnetic field and iron ions on rat lymphocytes: apoptosis, necrosis and free radical processes *Bioelectrochemistry* **2002,** *57*, 107.

(22) Teodori, L.; Göhde, W.; Valente, M. G.; Tagliaferri, F.; Coletti, D.; Perniconi, B.; Bergamaschi, A.; Cerella, C.; Ghibelli, L., Static magnetic fields affect calcium fluxes and inhibit stress-induced apoptosis in human glioblastoma cells *Cytometry* **2002,** *49*, 143.

(23) Aldinucci, C.; Garcia, J. B.; Palmi, M.; Sgaragli, G.; Benocci, A.; Meini, A.; Pessina, F.; Rossi, C.; Bonechi, C.; Pessina, G. P., The effect of strong static magnetic field on lymphocytes *Bioelectromagnetics* **2003,** *24*, 109.

(24) Dini, L.; Abbro, L., Bioeffects of moderate-intensity static magnetic fields on cell cultures *Micron* **2005,** *36*, 195.

(25) Kim, H. J.; Chang, I. T.; Heo, S. J.; Koak, J. Y.; Kim, S. K.; Jang, J. H., Effect of magnetic field on the fibronectin adsorption, cell attachment and proliferation on titanium

surface *Clin. Oral Implants Res.* **2005,** *16*, 557.

(26) Teodori, L.; Albertini, M. C.; Uguccioni, F.; Falcieri, E.; Rocchi, M. B.; Battistelli, M.; Coluzza, C.; Piantanida, G.; Bergamaschi, A.; Magrini, A.; Mucciato, R.; Accorsi, A., Static magnetic fields affect cell size, shape, orientation, and membrane surface of human glioblastoma cells, as demonstrated by electron, optic, and atomic force microscopy *Cytometry. Part A : the journal of the International Society for Analytical Cytology* **2005,** *69*, 75.

(27) Tenuzzo, B.; Chionna, A.; Panzarini, E.; Lanubile, R.; Tarantino, P.; Jeso, B. D.; Dwikat, M.; Dini, L., Biological effects of 6 mT static magnetic fields: A comparative study in different cell types *Bioelectromagnetics* **2006,** *27*, 560.

(28) Teodori, L.; Albertini, M. C.; Uguccioni, F.; Falcieri, E.; Rocchi, M. B. L.; Battistelli, M.; Coluzza, C.; Piantanida, G.; Bergamaschi, A.; Magrini, A.; Mucciato, R.; Accorsi, A., Static magnetic fields affect cell size, shape, orientation, and membrane surface of human glioblastoma cells, as demonstrated by electron, optic, and atomic force microscopy *Cytometry Part A* **2006,** *69A*, 75.

(29) Hashimoto, Y.; Kawasumi, M.; Saito, M., Effect of static magnetic field on cell migration *Electrical Engineering in Japan* **2007,** *160*, 46.

(30) Rosen, A. D.; Chastney, E. E., Effect of long term exposure to 0.5 T static magnetic fields on growth and size of GH3 cells *Bioelectromagnetics* **2009,** *30*, 114.

(31) Wang, Z.; Sarje, A.; Che, P. L.; Yarema, K. J., Moderate strength (0.23-0.28 T) static magnetic fields (SMF) modulate signaling and differentiation in human embryonic cells *BMC Genomics* **2009,** *10*, 356.

(32) Ramanujan, R., Magnetic Particles for Biomedical Applications. In *Biomedical*

Materials, Narayan, R., Ed. Springer US: 2009; pp 477-491.

(33) http://www.bionor.no/.

(34) Sommerfelt, M. A.; Ohlsson, I.; Flolid, I.; Thorstensson, R.; Sørensen, B., A simple semi-rapid HIV-1&2 confirmatory immunoassay using magnetic particles *J. Virol. Methods* **2004,** *115*, 191.

(35) Amirfazli, A., Magnetic nanoparicles hit the target *Nature nanotechnology* **2007,** *2*, 467.

(36) Arruebo, M.; Fernández-Pacheco, R.; Ibarra, M. R.; Santamaría, J., Magnetic nanoparticles for drug delivery *Nano Today* **2007,** *2*, 22.

(37) De Paoli, V. M.; De Paoli Lacerda, S. H.; Spinu, L.; Ingber, B.; Rosenzweig, Z.; Rosenzweig, N., Effect of an oscillating magnetic field on the release properties of magnetic collagen gels *Langmuir : the ACS journal of surfaces and colloids* **2006,** *22*, 5894.

(38) Liu, T. Y.; Hu, S. H.; Liu, K. H.; Liu, D. M.; Chen, S. Y., Study on controlled drug permeation of magnetic-sensitive ferrogels: effect of Fe3O4 and PVA *Journal of controlled release : official journal of the Controlled Release Society* **2008,** *126*, 228.

(39) Zhao, X.; Kim, J.; Cezar, C. A.; Huebsch, N.; Lee, K.; Bouhadir, K.; Mooney, D. J., Active scaffolds for on-demand drug and cell delivery *Proceedings of the National Academy of Sciences* **2011,** *108*, 67.

(40) Lee, J.-H.; Jang, J.-t.; Choi, J.-s.; Moon, S. H.; Noh, S.-h.; Kim, J.-w.; Kim, J.-G.; Kim, I.-S.; Park, K. I.; Cheon, J., Exchange-coupled magnetic nanoparticles for efficient heat induction *Nature nanotechnology* **2011,** *6*, 418.

(41) Pankhrust, Q. A.; Connolly, J.; Jones, S. K.; Dobson, J., Applications of magnetic

nanoparticles in biomedicine *Jounal of Physics D: Applied Physics* **2003,** *36*, R167.

(42) Leea, N.; Kim, H.; Choi, S. H.; Park, M.; Kim, D.; Kim, H.-C.; Choi, Y.; Lin, S.; Kim, B. H.; Jung, H. S.; Kim, H.; Park, K. S.; Moon, W. K.; Hyeon, T., Magnetosome-like ferrimagnetic iron oxide nanocubes for highly sensitive MRI of single cells and transplanted pancreatic islets *proceedings of the National Academy of Sciences* **2011,** *108*, 2662.

(43) Yim, H.; Seo, S.; Na, K., MRI Contrast Agent-Based Multifunctional Materials: Diagnosis and Therapy *Journal of nanomaterials* **2011,** *2011*, 1.

(44) Xu, W.; Kattel, K.; Park, J. Y.; Chang, Y.; Kim, T. J.; Lee, G. H., Paramagnetic nanoparticle T1 and T2 MRI contrast agents *PCCP* **2012,** *14*, 12687.

(45) Medeiros, S. F.; Santos, A. M.; Fessi, H.; Elaissari, A., Stimuli-responsive magnetic particles for biomedical applications *Int. J. Pharm.* **2011,** *403*, 139.

(46) Lim, E. K.; Sajomsang, W.; Choi, Y.; Jang, E.; Lee, H.; Kang, B.; Kim, E.; Haam, S.; Suh, J. S.; Chung, S. J.; Huh, Y. M., Chitosan-based intelligent theragnosis nanocomposites enable pH-sensitive drug release with MR-guided imaging for cancer therapy *Nanoscale research letters* **2013,** *8*, 467.

(47) Kyrtatos, P. G.; Lehtolainen, P.; Junemann-Ramirez, M.; Garcia-Prieto, A.; Price, A. N.; Martin, J. F.; Gadian, D. G.; Pankhurst, Q. A.; Lythgoe, M. F., Magnetic tagging increases delivery of circulating progenitors in vascular injury *JACC. Cardiovascular interventions* **2009,** *2*, 794.

(48) Loebinger, M. R.; Kyrtatos, P. G.; Turmaine, M.; Price, A. N.; Pankhurst, Q.; Lythgoe, M. F.; Janes, S. M., Magnetic resonance imaging of mesenchymal stem cells homing to pulmonary metastases using biocompatible magnetic nanoparticles *Cancer*

Res. **2009,** *69*, 8862.

(49) Singh, J. P., Enabling technologies for homing and engraftment of cells for therapeutic applications *JACC. Cardiovascular interventions* **2009,** *2*, 803.

(50) Maret, G.; Dransfeld, K., Macromolecules and membranes in high magnetic fields *Physica B+C* **1977,** *86–88, Part 3*, 1077.

(51) BOROSKE, E.; HELFRICH, W., Magnetic anisotropy of egg lecithin membranes *Biophys. J.* **1978,** *24*, 863.

(52) Speyer, J. B.; Sripada, P. K.; Das Gupta, S. K.; Shipley, G. G.; Griffin, R. G., Magnetic orientation of sphingomyelin-lecithin bilayers *Biophys. J.* **1987,** *51*, 687.

(53) Rosen, A. D., Studies on the effect of SMF on biological systems *PIERS online* **2010,** *6*, 133.

Chapter 2. Bacterial Magnetic Nanoparticles (BMPs) and Its Application

2.1 Introduction

2.1.1 Magnetic Nanoparticles

Magnetic nanoparticles (MNPs) have used for various biomedical applications such as magnetic resonance imaging (MRI), drug delivery, cell separation and magnetic hyperthermia [1-5]. This attention is derived from intriguing magnetic properties of nanoparticles. When size of the particles goes down to 20 nm, each nanoparticle becomes a single magnetic domain and shows superparamagnetic behavior at room temperature. The particles have a large constant magnetic moment and behave like a giant paramagnetic atom with a fast response to applied magnetic fields [6].

Preparation of fine magnetic particles by present techniques requires strict control of pH or/and temperature in the reaction process. Much effort has been devoted to the synthesis of nano-sized magnetic particles with well controlled size and shape. Also, surface coating of magnetic core is crucial to chemically stabilize the particles and functionalize with various molecules for bioapplications. The choice of materials used for the surface treatment of MNPs depends on applications and these could be either organic such as surfactants or polymers, or could be inorganic such as silicon or carbon.

Synthetic MNPs have been developed with tailored design for their purpose of use. Complex, multifunctional MNP systems with designed active sites, including

ligands, enzymes, chiral catalysts, drugs, and other species, seem to be promising for various applications. The surface modification of MNPs to introduce additional functionality will gain more and more attention [6]. Synthesis of stable and robust MNPs is critical for successful applications, therefore it will improve further.

2.1.2 Bacterial Magnetic Nanoparticles (BMPs)

Bacterial magnetic nanoparticles (BMPs) are naturally crystallized MNPs enveloped with biocompatible lipid layer by bacteria. Magnetotactic bacteria (MTB) were discovered from marine marsh muds in 1975 by Richard Blackmore (Fig. 2-1) [7], that orient along the geomagnetic field line. The MTB tend to swim downward of sediments away from oxygen in surface waters by virtue of the magnetic sensitivity, thus the name magnetotactic. Therefore, the MTB observed in the southern hemisphere showed to move towards the south, unlike the MTB in the northern hemisphere, which swim towards the north direction [8]. This geomagnetic sensitivity is originated from magnetic nanoparticles naturally synthesized by the MTB inside their body.

The MTB have magnetosomes which is lipid membrane template to produce the BMPs, and these particles are crystallized in a magnetosome by accumulating iron. BMPs are membrane-enclosed inorganic crystals consisting either of the magnetic minerals magnetite (Fe_3O_4) or greigite (Fe_3S_4) [9-12]. Iron oxides and iron sulfides are general types of minerals synthesized as the mineral phases of their magnetosomes; the iron oxides include only ferrimagnetic magnetite (Fe_3O_4) and the iron sulfides include ferrimagnetic greigite (Fe_3S_4) and non-magnetic pyrite (FeS_2) [12].

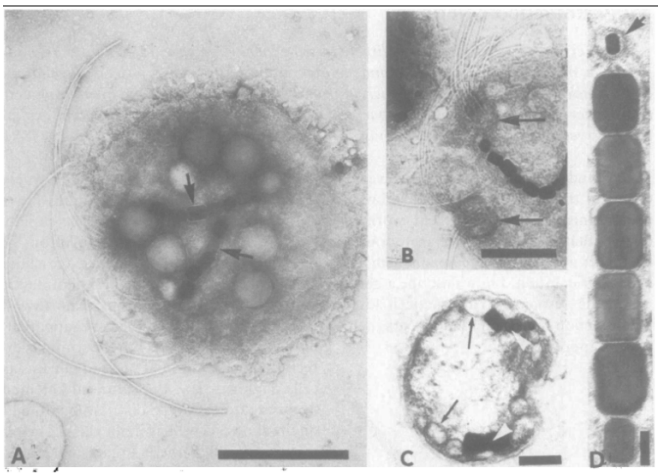

Figure 2-1. Transmission electron micrographs recorded on Kodak EM estar thick base film with a Hitachi HU-12 electron microscope operating at 75 kv. (A) Electron micrograph of a magnetotactic bacterium. Two bundles of flagella insert at one side of the cell. Two chains of iron-rich particles are present (arrows). Deposits believed to be polyphosphate are abundant. The outer cell layers appear disrupted. Cell stained with phosphotungstic acid (bar, 0.5 μm). (B) Electron micrograph of a portion of a magnetotactic bacterium showing the two disks (arrows) into which flagella insert. Osmotically lysed cell stained with phosphotungstic acid (bar, 0.25 μm). (C) Electron micrograph of a chemically fixed and thin-sectioned magnetotactic bacterium stained with lead and uranvl salts. The cell has a gram-negative type wall. The iron-rich particles (white arrowheads) have been unintentionally displaced during thin-sectioning revealing intracytoplasmic membranes arranged as vesicles (black arrows) adjacent to the cell plasma membrane. Much of the central portion of the cell appears to have been extracted during chemical preparation (bar, 0.25 μm). (D) Electron micrograph of a single chain of particles containing iron present in a cell prepared as described for (C). The particles are enclosed within vesicles consisting of triple-lasered membranes (arrow) (bar, 0.07 μm) [7].

Particle sizes are in narrow range, typically 35–120 nm, which is within the single magnetic domain size for magnetite and greigite [13-14]. The BMPs are arranged in line by their inherent magnetic dipole inside a bacterium and also the magnetosome are assembled by imbedded protein, which confer magnetic dipole moment to the bacterium [15-16]. In addition, a large variety of crystal morphologies such as cubo-octahedral, elongated hexagonal prismatic and bullet-shaped morphologies have been reported [17]. The size and shape of the BMPs are species- and/or strain-specific (Fig. 2-2) [12].

The BMPs were employed to investigate the synergistic effect of the MNPs and external magnetic field on cells in this study. The choice of BMPs among various MNPs is because of that the BMPs have innate lipid layer coating and stronger magnetic property, ferrimagnetic. The ferrimagnetic characteristic makes the BMPs suitable to study the effect of MNPs on cells rather than para- or superpara- magnetic particles.

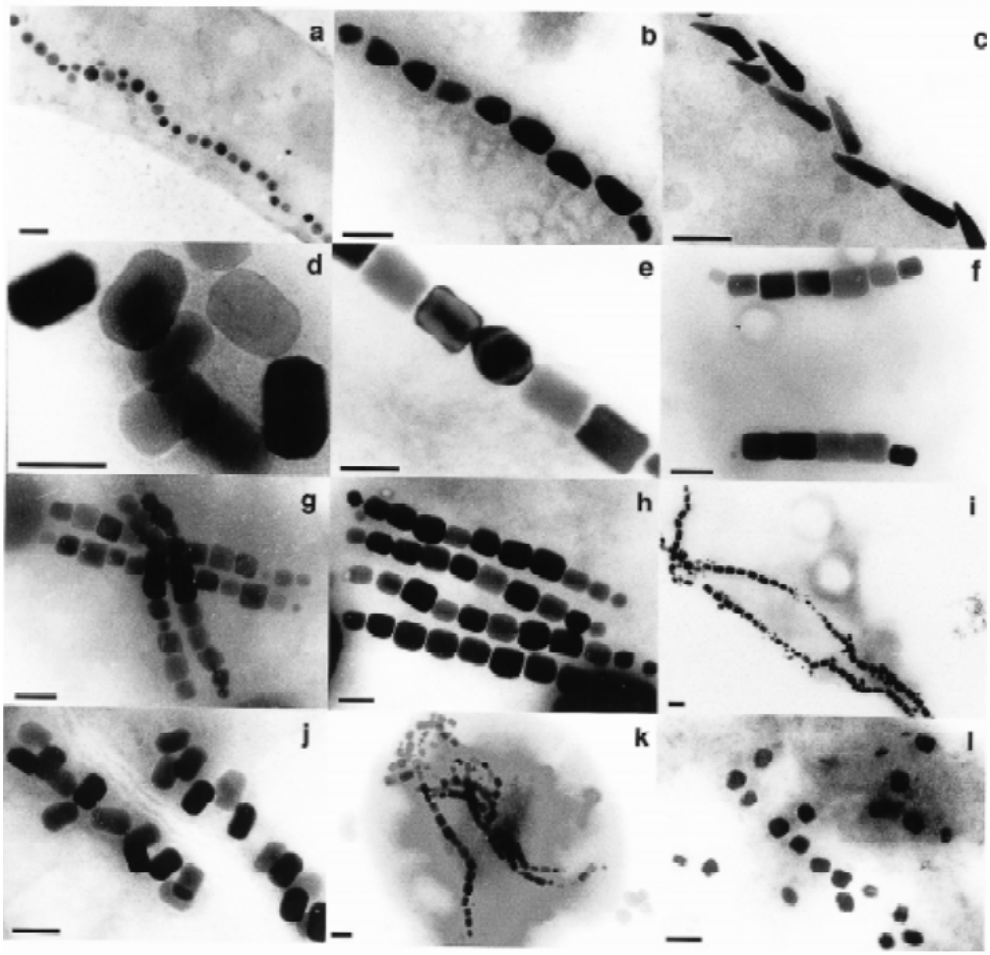

Figure 2-2. Electron Micrographs of Magnetosomes, Crystal morphologies and intracellular organization of magnetosomes found in various magnetotactic bacteria. Shapes of magnetic crystals include cubooctahedral (a), bullet-shaped (b, c) elongated prismatic (d, e, f, g, h, i, j, k) and rectangular morphologies (l). The magnetosome particles can be arranged in one (a, b, c, e), two (f, i) or multiple chains (g, h) or irregularly (j, k, l). The bar is equivalent to 0.1 μm [17].

2.1.3 Applicability of BMPs to Cell

BMPs have been predicted to be highly biocompatible because they are formed by bacteria rather than artificially synthesized. On the other hand, BMPs also pose potential risks as they are nano-size particles isolated from bacterial cells and their membrane contains various nonhuman proteins [18-19].

The biocompatibility of BMPs have studied in vivo and in vitro. The body tissue distribution and host tissue elimination following administration of BMPs into the vascular system were reported, BMPs were distributed in rat liver. It showed that BMPs may avoid incurring organ congestion or infarction in vivo since they can be transferred from the sublingual vein to the liver [20-21]. Further studies, with injection of 40 mg/kg BMPs, showed no significant difference between BMP-treated and non-treated control rats. The histological examination of major organs from the BMP-treated rats showed no obvious pathological changes, except increased number of vacuoles in livers and thicker interlobular septa in lungs [22]. In vitro cytotoxicity of BMPs has been investigated with mouse fibroblasts, endothelial progenitor cells and human cervical cancer cells; purified and sterilized BMPs were found to be nontoxic in vitro [1, 23-24].

As MNPs are widely used in biomedical applications [2-5], the BMPs also can be used for MRI, drug delivery, and magnetic hyperthermia. MTB embedded with

BMPs affect the T2-relaxation more greatly than T1-relaxation rate in MRI system [25] and then BMPs can be used as a negative contrast agent for MRI [26-27]. Heat production of BMPs was reported by applying oscillating magnetic field of frequency 108 kHz and field amplitudes of 23 and 88mT [28]. These studies indicate that the BMPs can be used in many biomedical applications alike synthetic MNPs.

2.1.4 Cellular Uptake of BMPs

With increasing interest to apply nanoparticles for biomedical applications, cellular uptake mechanism of nanoparticles has been studied by researchers to achieve successful delivery of the particles inside cells, cytoplasm or nucleus. Cells keep interacting with external environment for their developmental and functional programs. Endocytosis allows the communication across the cell membrane with continuous sampling of the external environment, which is essential for the uptake of nutrients and for the cellular and organismal response to infectious agents [29]. Polar molecules such as ions, macromolecules and nanomaterials are generally incapable of penetration through the lipid bilayer. Thus, the nanoparticles including BMPs mostly are internalized into cells via endocytosis (Fig. 2-3).

Endocytosis is divided into two different types according to the states of nanomaterials, phagocytosis is solid-uptake pathways of bacteria and yeast (cell eating) and pinocytosis is fluid-phase uptake pathway (cell drinking). Pinocytosis is subdivided into macropinocytosis, clathrin-mediated pinocytosis and caveolin-mediated pinocytosis, according to the different mechanism for uptake surrounding fluid. Macropinocytosis is trapping large amount of fluid in vesicles up to 5 μm in diameter, which is one of the non-specific uptake pathways of extracellular fluid. The clathrin-mediated and caveolin-mediated pinocytosis are ligand-specific pathways and generate smaller vesicles; about 80 nm by clathrin-mediated and

around 50-60 nm by caveolin-mediated pinocytosis. The nanoparticles internalized by endocytosis are translocated to endosome, lysosome, endoplasmic reticulum or Golgi apparatus [30]. The specific endocytic pathway for MNPs would be affected by their different properties such as size, shape and surface charge, also the pathway could be controlled using surface modification with specific ligands [31-36].

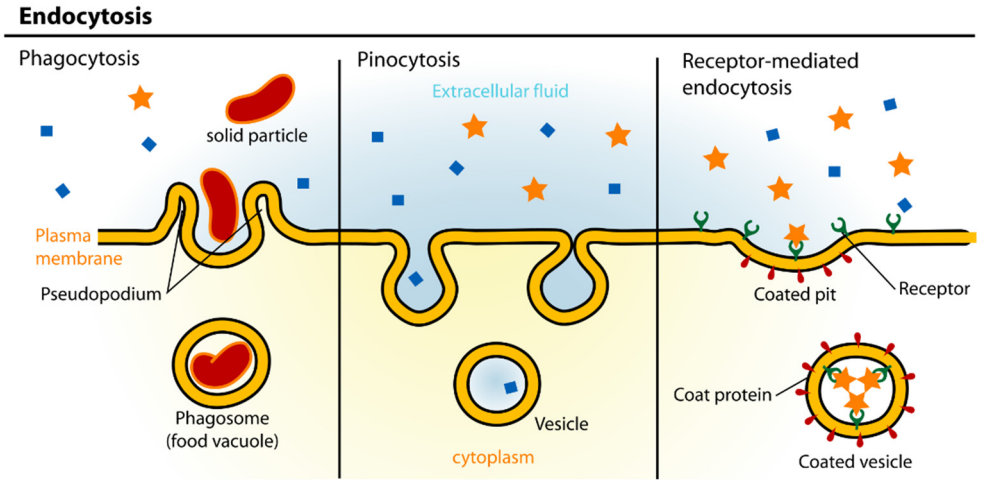

Figure 2-3. The different types of endocytosis [37]

The different pathways of endocytosis result in the translocation of endocytosed material to distinctive intracellular compartments and therewith correlated differential processing [35]. Intracellular localization and transport of the magnetic nanoparticles have been studied to use the particles for drug delivery vehicles or

contrast agents for magnetic resonance imaging [38-40].

The internalized MNPs by endocytosis pathways are translocated with enclosing vesicles through the pathways as shown in Figure 2-4. The particles internalized by macropinocytosis and clathrin-mediated endocytosis are transported to endosomes and finally to lysosomes or extracellular region (exocytosis) via late endosomes. In case of caveolae-mediated endocytosis, the transport vesicles could translocate to Golgi apparatus or endoplasmic reticulum. Thereby, the materials carried in vesicles are delivered to the organelles and give rise to further signaling process as their functions. Most of endocytosed MNPs are located in cytoplasm and then finally degraded in lysosomes or exocytosed.

Delivery of the MNPs inside nucleus is challenging to achieve with natural endocytosis because the constraint of nucleus membrane. It is needed to modify surface of MNPs with functional molecules for translocation into the nucleus.

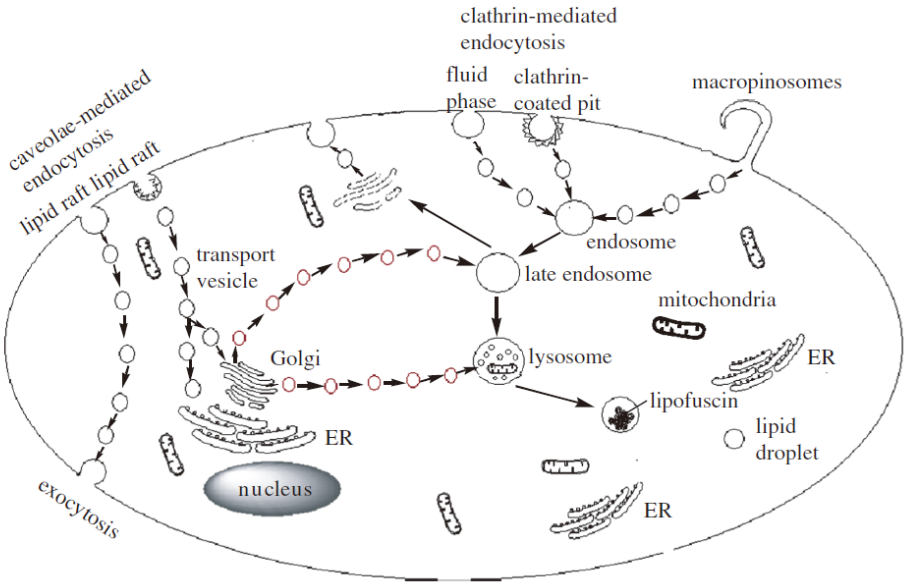

Figure 2-4. Three types of endocytic pathways for pinocytosis in the cell: macropinocytosis; clathrin-mediated pinocytosis; and caveolin-mediated pincytosis. Pinocytosis via clathrin-coated pits or macropinosomes transfer materials to the lysosomaldegradative compartment, while caveolae-mediated endocytosis can result in translocation to the endoplasmic reticulum (ER) and Golgi apparatus, or through the cell by transcytosis [30].

2.2 Materials and Methods

2.2.1 Extraction of BMPs

BMPs were extracted from magnetotactic bacteria (MTB), *Magnetospirillum* sp. AMB-1 (ATCC® 700264) which was cultured in magnetic spirillum growth medium (MSGM) for 5 days in shaking incubator at 30°C under anaerobic conditions [41]. After sufficient culture, the cells were centrifuged for 25 min at 5000 rpm and then lysed by homogenizer (VCX500, Sonics&Materials, USA) for 30 min. BMPs were collected using a neodymiumiron boron (NdFeB) magnet and washed 5 times with 1× PBS. Collected BMPs were dispersed in 1× PBS and sterilized by autoclave (121℃, 15 min) to deliver it to mammalian cells without cross contamination. Concentration of extracted BMPs was examined with inductive coupled plasma-atomic emission spectrometer (ICP-AES, ICPS-7500, Shimadzu, Japan). The 30 μl of extracted BMPs dissolved in 0.5 ml of HCl (37%) solution at 60°C overnight to prepare acceptable sample for ICP-AES measurement. The solution was diluted with distilled water and final volume of the solution was 10 ml. For the measurement the solution was filtered using syringe filter (0.20 μm pore, Advantec, Japan) to eliminate large impurities. The concentration of BMPs, Fe_3O_4, was calculated with measured ionic concentration of iron using atomic weight. Finally the BMPs were dispersed in 1× PBS with 0.5 mg/ml of concentration and used for further studies.

2.2.2 Cell Culture

Human cervical cancer HeLa cells were cultured in Dulbecco's modified Eagle's medium (DMEM/high glucose, Thermo Scientific, USA) containing 10% (v/v) fatal bovine serum (FBS, Thermo Scientific, USA) and 300 U/ml penicillin/streptomycin (Thermo Scientific, USA) at 37°C in a humidified atmosphere containing 5% CO_2. Subculture was performed before over-confluent culture of cells.

SH-SY5Y cells, a human neuroblastoma cell line, were cultured in Dulbecco's modified Eagle's medium (DMEM/low glucose, Thermo Scientific, USA) containing 10% (v/v) fatal bovine serum (FBS, Thermo Scientific, USA) and 100 U/ml penicillin/streptomycin (Thermo Scientific, USA) at 37°C in a humidified atmosphere containing 5% CO_2. The culture medium was changed every 3 days with fresh medium and subculture was performed when the cells were cultured to 80% confluency to maintain optimal condition for further studies.

2.2.3 Delivery of BMPs to Cells

The HeLa and C2C12 cells were seeded (5.0×10^4 cells/cm^2) in the BMP free culture medium and incubated for 2-24 h to stabilize adherent condition. After the pre-incubation, 10 μg/ml of the BMPs were added to the medium and then the cells were incubated overnight for internalization of BMPs. In case of SH-SY5Y cells, the BMPs were treated to cells of 80% confluency to keep differentiation potency of cells for further studies. The cells were treated with BMPs (10 μg/ml on more than 10^6 cells) dispersed in serum reduced medium (1% FBS) and incubated overnight for sufficient time to internalize BMPs on the same condition as cell culture. The medium containing remained BMPs were washed three times with 1× PBS after the overnight incubation, and fresh medium was added to cells for further studies.

2.2.4 Microscopy

2.2.4.1 Transmission Electron Microscopy

Transmission electron microscope (TEM) imaging of the cells was performed after overnight treatment with the BMPs to confirm internalization of the BMPs. The cells were treated with BMPs as aforementioned and the remnant medium containing non-translocated BMPs into cells were removed. After washing three times with 1×PBS, the cells were trypsinized and collected by centrifuge 5 min at 1000 rpm. The BMP-treated cells were fixed by immersing in modified Karnovsky's fixative solution (2% paraformaldehyde and 2% glutaraldehyde in 0.05 M sodium cacodylate buffer, pH 7.2) for 4 h at 4°C. After three washes for 10 min in 0.05 M sodium cacodylate buffer (pH 7.2), the cells were post-fixed with 1% osmium tetroxide in 0.05 M sodium cacodylate buffer (pH 7.2) for 2 h at 4°C. The cells were then briefly washed twice with distilled water, stained with 0.5% uranyl acetate for 30 min at 4°C, and dehydrated in a graded ethanol series (30%, 50%, 70%, 80%, 90%, and 100%) for 10 min each. The samples were treated with 100% propylene oxide twice for 10 min and embedded in Spurr's resin. Ultrathin sections of the cells were prepared using an ultramicrotome (MT-X, RMC, USA) and mounted on copper grids. The sections were examined using a TEM (JEM-1010, JEOL, Japan).

2.2.4.2 Confocal Microscopy

BMPs were labeled with the fluorescein isothiocyanate (FITC) which is used to track the location of internalized BMPs in the cells with a confocal laser scanning microscope. For the confocal microscopy measurement, the nucleus and actin filaments of cells were stained as following procedure. After delivery of FITC-labeled BMPs to cells overnight, the cells were fixed with 4% paraformaldehyde in 1× PBS for 15 min at room temperature. Following washing twice with wash buffer, 0.1% Triton X-100 in 1× PBS, the fixed cells were permeabilized and blocked with 1% BSA and 0.1 Triton X-100 in 1× PBS for 20 min. Then the actin filaments were stained by incubating cells with TRITC-conjugated phalloidin (1:200) for 50 min at room temperature. The cells were briefly washed three times with 1× PBS and nucleus staining was performed by incubating with a dilute DAPI in 1× PBS (1:1000) three times for 5 min each. Finally the cells were gently washed three times with 1× PBS and immersed in 1× PBS. The stained cells were examined using a confocal laser scanning microscope (LSM510 and LSM710, Carl Zeiss, Germany).

2.2.5 Uptake Efficiency

Uptake efficiency of BMPs to HeLa and SH-SY5Y cells were studied to determine magnetic force applied to the cells and proper amount of BMPs to deliver. HeLa cells were seeded on 24 well plate, 10^4 cells per well with 500 μl culture medium (DMEM/high glucose containing 10% FBS and 300 U/ml penicillin/streptomycin). After 24 h incubation for stabilization of cells, BMPs were added to the culture medium of each well with serial concentrations, 0, 4, 8, 16, 20 μg/ml. The remained BMPs in culture medium were collected after cellular uptake of them and the concentration was measured using ICP-AES (ICPS-7500, Shimadzu, Japan). The quantity of internalized BMPs to HeLa cells were estimated by subtracting measured amount from delivered amount of BMPs.

The uptake of BMPs by SH-SY5Y cells was assessed with similar procedure and the details were described as follows. The 10^6 cells were seeded on a well of 6 well plate with 2 ml culture medium (DMEM/low glucose containing 10% FBS and 100 U/ml penicillin/streptomycin) and incubated for 24 h to stabilize cell condition. Then the medium was changed to serum reduced medium (DMEM/low glucose containing 1% FBS and 100 U/ml penicillin/streptomycin) for expeditious uptake of BMPs. Serial concentrations, 0, 5, 10, 20, 40 μg/ml of BMPs were added to the serum reduced medium of each well and the cells were incubated for 24 h to take sufficient time for uptake of particles. After the incubation, the cells were collected by trypsinization

and lysed. The quantity of internalized BMPs to the cells were examined using ICP-AES (ICPS-7500, Shimadzu, Japan). The experiments were repeated three times and the data was summarized to analyse the uptake efficiency of BMPs to the cells.

2.2.6 Cytotoxicity

MTS assay (3-(4,5-dimethylthiazol-2-yl)-5-(3-carboxymethoxyphenyl)-2-(4-sulfophenyl)-2H-tetrazolium, Promega, USA) was used to evaluate the cytotoxicity of the BMPs to HeLa and SH-SY5Y Cells. The MTS is a novel tetrazolium compound and it requires fewer steps than procedures that use tetrazolium compounds such as MTT or INT [42]. The cells (5×10^3 cells/well) were seeded on 96-well plate with 100 μl of the culture medium firstly and then incubated for 24 h to stabilize adherent condition of cells. And then the BMPs were added to each well with various concentration, 0; 2; 4; 6; 8; 10; 15 μg per 10^4 HeLa cells, 0; 1.5; 3; 7.5; 15; 30 μg per 10^4 C2C12 cells, 0; 3; 6; 15; 30; 60 μg per 10^4 SH-SY5Y cells. After incubation of the cells in BMPs disperse medium for proper time (24 h; 48 h; 72 h for HeLa and C2C12 cells, 3 days; 6 days for SH-SY5Y cells) to assess, 20 μl of CellTiter 96® AQueous One Solution Reagent (Promega, USA) was added into each well. Then the plate was incubated at 37°C for 1–4 h in a humidified 5% CO_2 atmosphere and absorbance was recorded at 490 nm with a microplate reader (Sunrise, Tecan, Switzerland). Three wells in one experiment were employed to a concentration and the assessment was duplicated. The average absorbance value of control cells was normalized to 100% viability and the viability was calculated compared with control cells. The standard error of mean of the cell viability and p-value from unpaired t-test was calculated using Graphpad Prism 5 software.

2.3 Results and Discussion

2.3.1 Characteristic of BMPs

BMPs have considerable potential for various biomedical applications due to their narrow size and shape distribution, high magnetization and inherent biocompatibility [1, 43]. It has been known that the size and shape of BMP depend on the strain of magnetotatic bacteria [44]. Magnetosomes, which determine shape of BMPs, have various shapes in cubo-octahedral, elongated hexagonal prismatic, and bulletshaped morphologies [11, 21]. Typical size of BMPs are varied from 35 nm to 120 nm [21]. The BMPs used in this study consist of magnetite typically and were extracted from the *Magnetospirillum* sp. AMB-1, magnetotatic bacteria. *Magnetospirillum* sp. AMB-1 is widely used because it grows well under laboratory conditions. BMPs from AMB-1 contain a well-crystallized magnetite (Fe_3O_4) core and an enveloping magnetosome membrane that has a lipid bilayer and embedded proteins [45-47]. These BMPs are highly crystallized, with few defects, a uniform size, and ferromagnetic properties that are difficult to achieve in synthesized magnetic nanoparticles at room temperature [45-47]. Isolated and purified BMPs were observed with TEM (Fig. 2-5 (a)). Average diameter of the BMPs was 50 nm and particles were relatively homogeneous as shown in Figure 2-5 (a). As single domain particles, these ferrimagnetic particles (Fe_3O_4) have a strong and relatively stable magnetic moment even in the absence of an external magnetic field [48-49].

Magnetospirillum sp. AMB-1 has a saturation magnetization of 6.8×10^{-17} Am^2 per cell and the remnant magnetization is just below half of the saturation value [50]. The room-temperature-bulk coercivity is ~13 mT in isolated particles and ~25 mT in aligned short chains [51-52]. Each particle has own magnetization like magnet below Curie temperature (585°C for magnetite). Thereby the particles attract mutually and align with the opposite magnetic poles facing (Fig. 2-5 (b)). Furthermore, the innate lipid bilayer allows BMPs to be well dispersed in aqueous solutions and easily translocated into cells without any surface modifications. The proteins embedded in the lipid layer permit the immobilization of biomolecules such as DNA, proteins, and peptides on the surface of the BMPs [53].

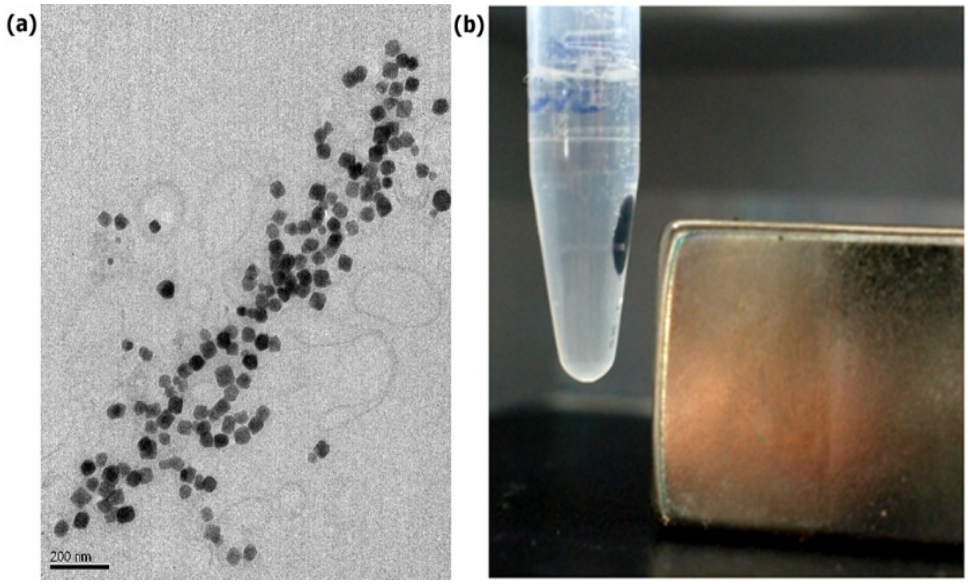

Figure 2-5. (a) TEM image of BMPs, scale bar: 200 nm (b) Magnetic attraction of BMPs

2.3.2 Cellular Uptake of BMPs

2.3.2.1 Internalization of BMPs

Confocal microscopy has been used mostly to study cellular uptake of nanoparticles with fluorescence labelled nanoparticles. The limited resolution of the confocal microscopy causes uncertainity about whether the nanoparticles are taken up or just attached on the surface of cell membrane. Sectional views of the confocal microscopy facilitate to validate the cellular uptake of the nanoparticles. Additionally, transmission electron microscopy (TEM) is also exploited to confirm cellular uptake of nanoparticles with ultrathin sectioned cells. The nanoparticles and vesicles, such as endosome and lysosome, inside cells could be observed with TEM which have higher resolution than confocal microscopy. TEM images may give lots of information regarding the cellular uptake mechanism and intracellular localization of nanoparticles [54].

The uptake of BMPs by HeLa and SH-SY5Y cells was directly confirmed and cross-checked using the confocal microscopy and TEM. The BMPs were labeled with FITC to track the location of internalized BMPs by using a confocal laser scanning microscope. BMPs were successfully internalized into HeLa cells and the internalized BMPs were mostly localized to endosomal or lysosomal vesicles (Fig. 2-6 (a)). In addition the FITC tagged BMPs were observed in all sectional views of

the confocal microscopy (Fig. 2-6(b)). As shown in Figure 2-7 (a), the BMPs were also internalized well internalized into the SH-SY5Y cells, and most of the internalized BMPs were found in the cytosol. The TEM images clearly showed that the internalized BMPs were mostly located in the endosome or lysosome in the cytosol (Fig. 2-7 (b), right upper box). Interestingly, a few BMPs escaped from endosome were found in the cytosol of SH-SY5Y cells after overnight uptake (Fig. 2-7 (b), lower box).

Endocytosis is a well-known mechanism for cellular uptake of nanoparticles and it can usually be classified according to the different state of nanomaterials, phagocytosis and pinocytosis. Phagocytosis is usually related to cellular internalization of solid particles and pinocytosis is known as fluid-phase uptake pathway [29]. Most of the internalized nanoparticles by endocytosis were finally transferred to the endosome or lysosome [29, 54-55]. In addition, some of the positively charged nanoparticles, in case of SH-SY5Y cells were observed to escape from endosome and then penetrate into the cytoplasm or nucleus [56-61]. The intracellular localization of BMPs in the presented TEM images is clearly explained by the mechanism for internalization of nanoparticles. The BMPs are suitable for using magnetic stimulation of cells in the context of that is well taken up by cells.

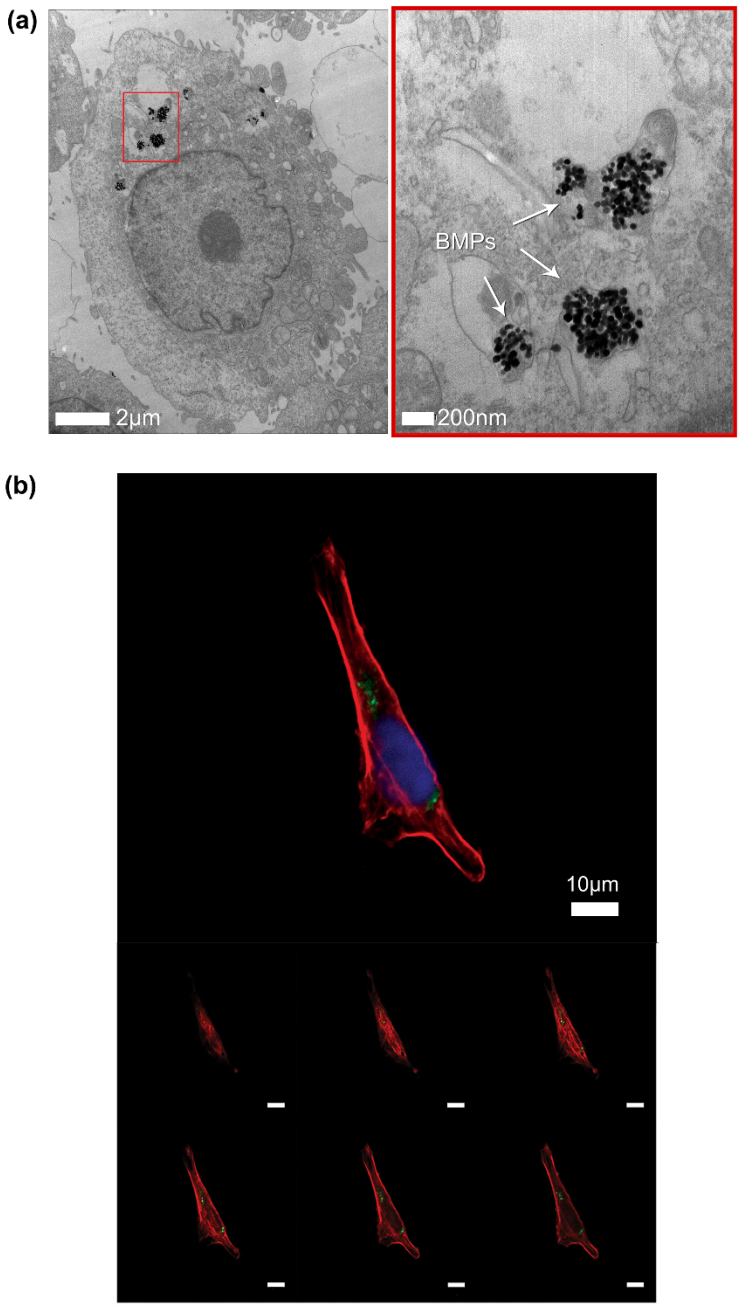

Figure 2-6. Observation of BMPs internalized HeLa cells using (a) TEM (b) confocal microscope with sectional view of the cell, scale bars: 10 μm, red: actin filaments, blue: nucleus, green: BMPs

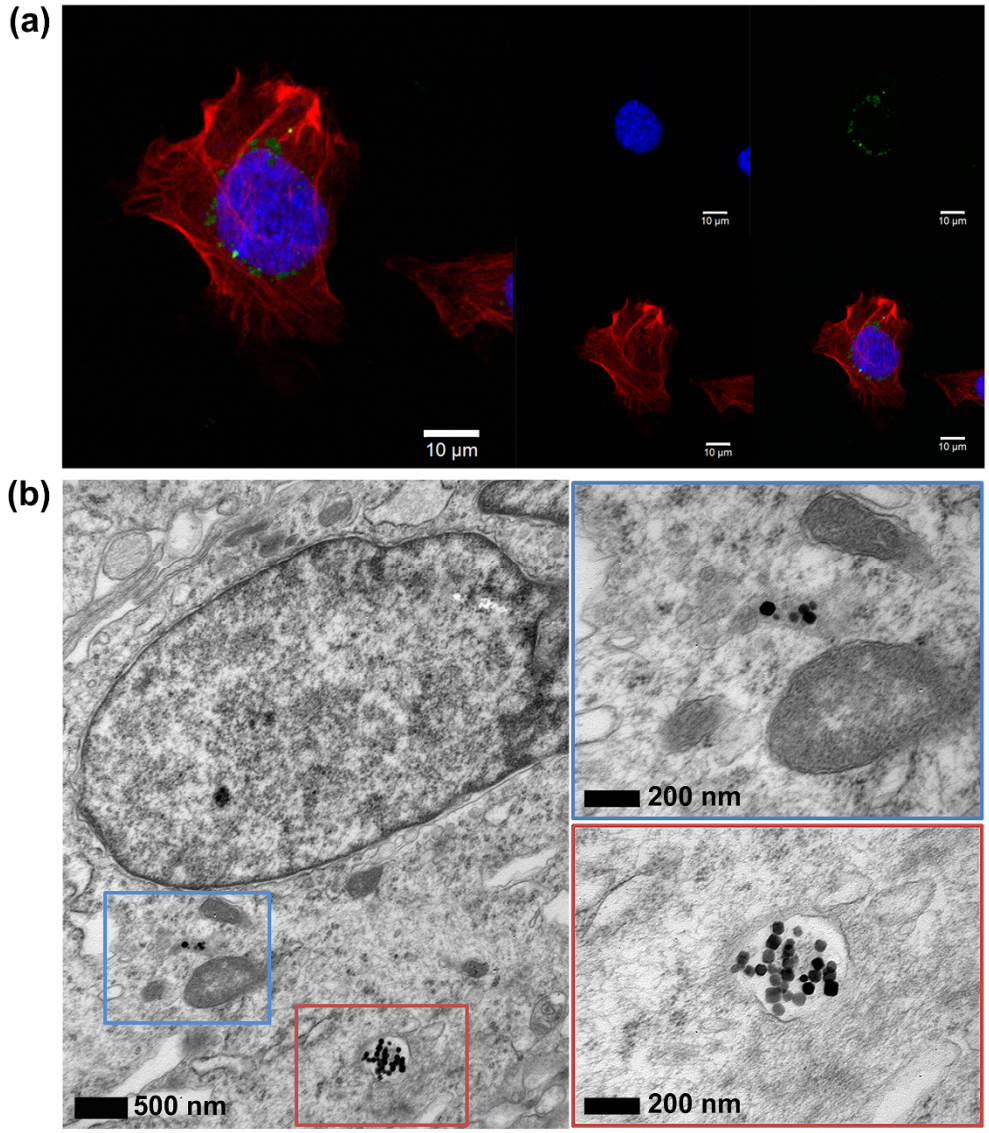

Figure 2-7. Observation of BMPs internalized SH-SY5Ycells using (a) confocal microscopy, scale bars: 10 μm, red: actin filaments, blue: nucleus, green: BMPs (b) TEM

2.3.2.2 Uptake Efficiency

In increasing attention to nanoparticles as a drug carrier, many researchers have studied about factors related to effective intracellular delivery of nanoparticles. Properties of nanoparticles such as shape, size, charge and surface modification are known to affect cellular uptake efficiency of nanoparticles as well as external factors (e.g., temperature, pH, concentration of nanoparticles, incubation time, cell type) [30].

The intracellular uptake quantity of spherical nanoparticles was five times compared to that of rod-like nanoparticles through endocytosis [62] and 50 nm-sized nanoparticles were more effectively delivered into cells than smaller or larger nanoparticles (≤100 nm) [62-64]. The positively charged nanoparticles are much easier to be taken up by cells than negatively charged ones, because cell membranes generally have many negatively charged groups on the surface. It implies that the positively charged nanoparticles have more chance to be adsorbed on the cell membrane surface, which will be followed by intracellular translocation of the nanoparticles via endocytosis [34].

The BMPs used in this research have good properties in terms of the efficient intracellular uptake, such as 50 nm size in diameter, almost spherical shape and envelopment with lipid membrane including amine functional groups.

The cellular uptake ratio of BMPs was evaluated with HeLa and SH-SY5Y cells which were dealt with mainly in this research. For the cellular uptake of BMPs, the cells were cultured in BMPs added culture medium overnight. After washing extra suspended BMPs in the medium, the quantity of BMPs in the cells was assessed by ICP-AES. In fact, concentration of iron ions was measured and the mass of BMPs was calculated with the molecular weight of iron oxide (Fe_3O_4).

The 162 pg/cell of BMPs was internalized when 8 μg/ml was added to 10^4 of HeLa cells (Fig. 2-8). In case of SH-SY5Y cells, the BMPs were added to 10^6 cells with serial concentration from 5 to 40 μg/ml. The 8.69 pg/cell of BMPs were taken up at a concentration of 20 μg/ml were delivered to 10^6 cells (Fig. 2-9). These results showed that larger amount of BMPs were internalized into the cells as increasing quantity of the adding particles, other than the 20 μg/ml of BMPs delivered to HeLa cells. The uptake by HeLa cells was likely to be saturated at which the concentration of added BMPs was 16 μg/ml, thus the uptake was not increased at the 20 μg/ml. In the concentration range, maximum amount of intracellular BMPs was 391.71 pg/cell for 10^4 of HeLa cells and 16.24 pg/cell for 10^6 of SH-SY5Y cells.

The uptake of BMPs by endothelial progenitor cells (EPCs) was reported using BMPs from same magnetotactic bacteria AMB-1 in 2008 [1]. The 40% of BMPs were internalized into the EPCs at a low dose of added BMPs, from 2 to 4 μg per 10^4 cells and this internalization efficiency gradually decreased at higher dose. At a high

level of dose, over 15 μg per 10^4 cells, about 25% of the BMPs were taken up by EPCs. The cellular uptake of BMPs was not saturated within the tested range in this study [1]. The HeLa and EPCs showed higher capacity to internalize the BMPs than SH-SY5Y cells with endocytosis. This difference is considered that the cellular uptake of BMPs might depend on the cell type.

Careful consideration of the size and property of the magnetic particle is needed because of the efficiency of delivery and available magnetic force. Larger magnetic particles, such as micro beads, can be used to produce more force by an external field, but require a different mechanism for delivery, such as injection, which has an adverse effect on the cell. On the other hand, smaller particles, such as paramagnetic nanoparticles, can be delivered relatively easily by endocytosis, but the amount of force that can be exerted by an external field is very small. Some researchers suggested magnetofection, applying magnetic field with delivery of magnetic nanoparticles, to enhance the cellular uptake efficiency [65-66]. However, the magnetofection was not used for internalization of BMPs into cells in this study. Instead, the BMP-loaded cells were isolated from BMP-free cells using a magnet and separately investigated biological effect of magnetic nanoparticles with external magnetic field.

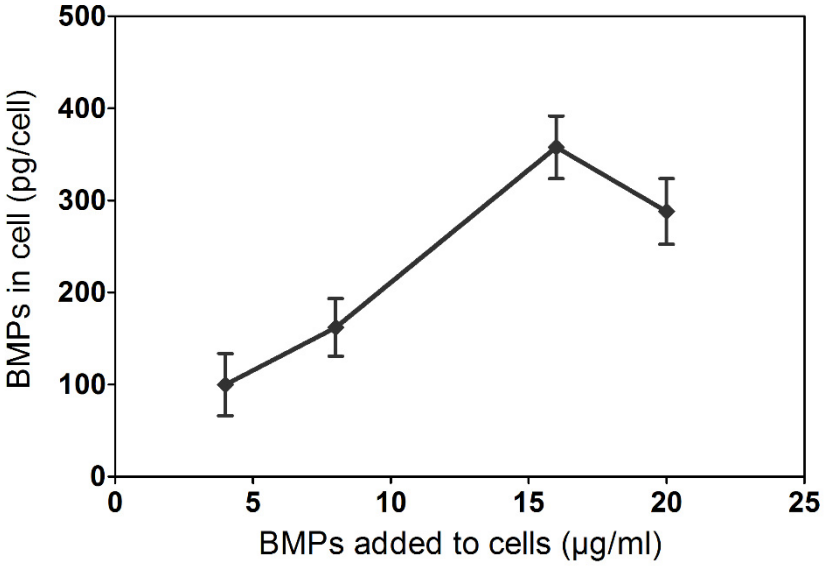

Figure 2-8. Uptake ratio of BMPs by HeLa cells

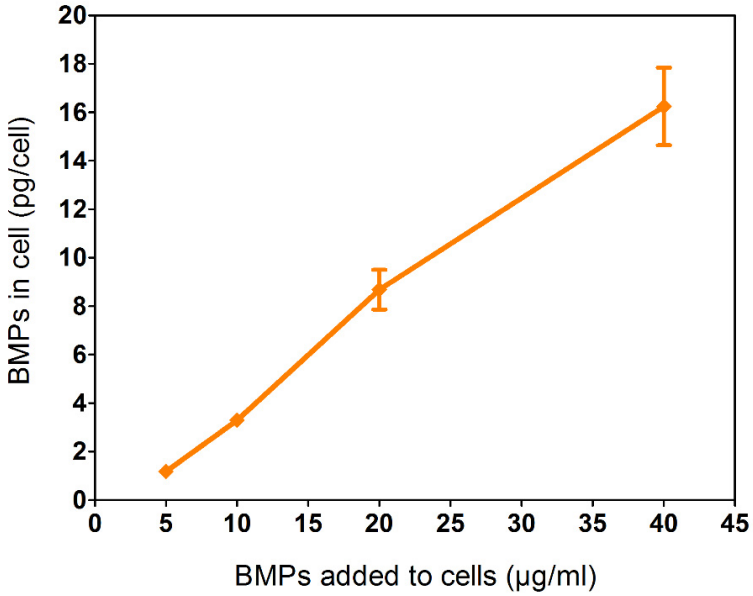

Figure 2-9. Uptake ratio of BMPs by SH-SY5Y cells

2.3.2.3 Cytotoxicity

Cytotoxicity test is essential to use nanomaterials for biomedical applications. The cytotoxicity of BMPs, a kind of nanomaterials, should be investigated for future applications and the information of toxicity could be a guidance on the use of BMPs.

The cytotoxicity of BMPs was examined with HeLa, C2C12 and SH-SY5Y cells that were handled in this study. Control cells without treatment of BMPs were normalized to 100% viability in the results of MTS assay. The BMPs did not affect significantly the viability of the HeLa cells up to the concentration of 15 μg per 10^4 cells during 72 h (Fig. 2-10). The viability of C2C12 cells was decreased about 10% after 24 h culture, but the viability was recovered during another 24 h culture up to the concentration of 15 μg per 10^4 cells. With 30 μg of BMPs per 10^4 cells, the BMPs showed a slight cytotoxicity as reduced viability of C2C12 cells about 15% during 72 h. In case of the SH-SY5Y cells, the BMPs showed no cytotoxicity up to the concentration of 60 μg for 10^4 cells during culture for 3 days. The viability of the cells, however, decreased at BMP concentrations over 15 μg after 6 days of incubation (Fig. 2-12). Thus, the C2C12 and SH-SY5Y cells were treated with lower amount of BMPs than 15 μg per 10^4 cells in subsequent studies.

The doubling time for HeLa and C2C12 cells is about 24 h and for SH-SY5Y cells is over 48 h. This difference in doubling time was considered to determine incubation

time after treatment of BMPs. The test was performed until that cell division was occurred twice at least, HeLa and C2C12 cells for 72 h and SH-SY5Y cells for 6 days. All subsequent experiments were carried out within this time.

BMPs are easily separated and purified from disrupted magnetic bacteria by magnetic separation using magnet. Moreover, these BMPs can be distinguished from artificially synthesized magnetite by the presence of an organic membrane approximately 2-4 nm in thickness enveloping the particles as well as the regular size and morphology. Major component of organic membrane in strain AMB-1 used by in this study is phospholipids, which mainly consist of phosphatidylethanolamin. Phospholipids provide good dispersion of BMPs in aqueous solutions [67-68]. These properties of BMPs allow intrinsic biocompatibility.

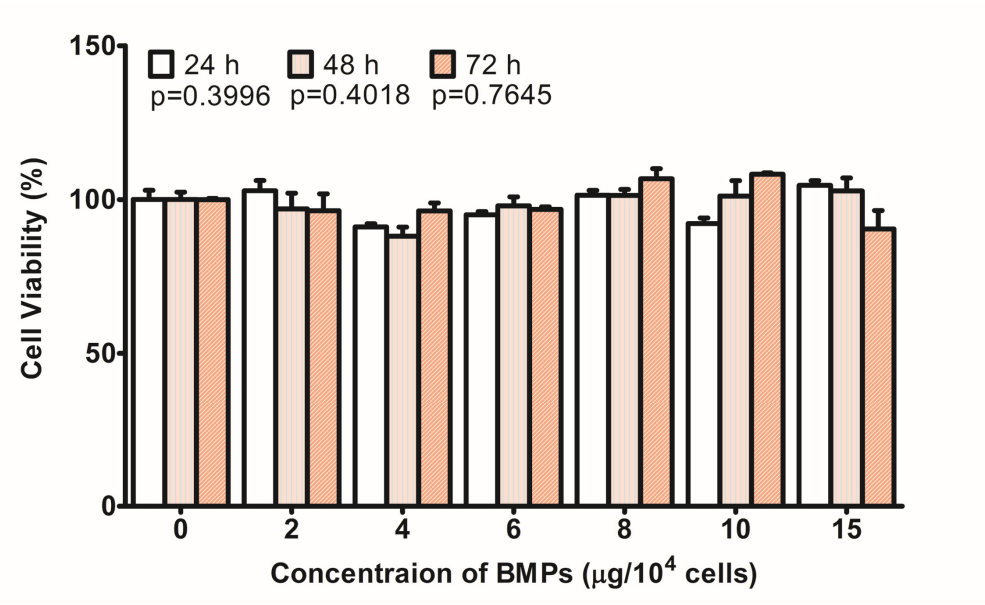

Figure 2-10. Cytotoxicity test of BMPs to HeLa cells with serial concentration with standard error of the mean (SEM) and p-value from unpaired t-test

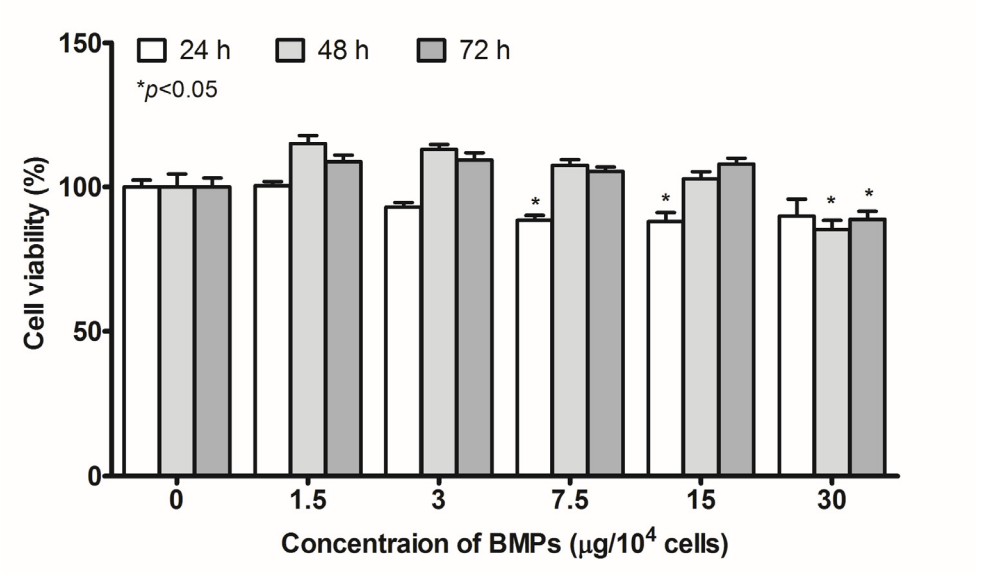

Figure 2-11. Cytotoxicity test of BMPs to C2C12 cells with serial concentration with SEM and p-value from unpaired t-test

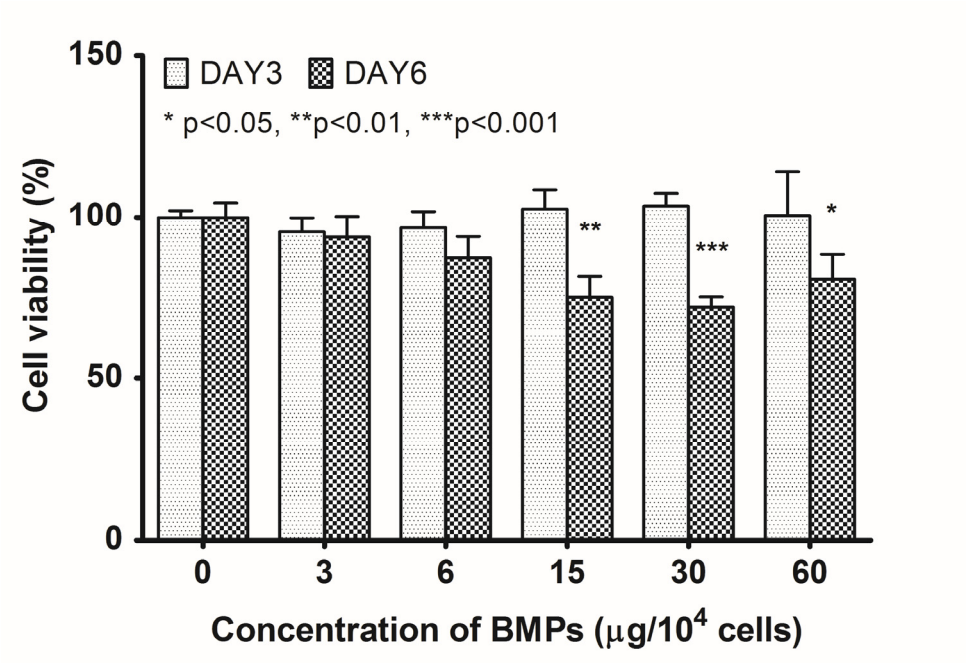

Figure 2-12. Cytotoxicity test of BMPs to SH-SY5Y cells with serial concentration with SEM and p-value from unpaired t-test

2.4 References

(1) Kim, J. A.; Lee, H. J.; Kang, H.-J.; Park, T. H., The targeting of endothelial progenitor cells to a specific location within a microfluidic channel using magnetic nanoparticles *Biomed. Microdevices* **2008,** *11*, 287.

(2) Bhattarai, S. R.; Kc, R. B.; Kim, S. Y.; Sharma, M.; Khil, M. S.; Hwang, P. H.; Chung, G. H.; Kim, H. Y., N-hexanoyl chitosan stabilized magnetic nanoparticles: Implication for cellular labeling and magnetic resonance imaging *J. Nanobiotechnol* **2008,** *6*, 1.

(3) Gupta, A. K.; Wells, S., Surface-modified superparamagnetic nanoparticles for drug delivery: preparation, characterization, and cytotoxicity studies *IEEE Trans. NanoBiosci.* **2004,** *3*, 66.

(4) McBain, S. C.; Yiu, H. H.; Dobson, J., Magnetic nanoparticles for gene and drug delivery *Int. J. Nanomedicine* **2008,** *3*, 169.

(5) Villanueva, A.; Presa, P. d. l.; Alonso, J. M.; Rueda, T.; Martínez, A.; Crespo, P.; Morales, M. P.; Gonzalez-Fernandez, M. A.; Valdés, J.; Rivero, G., Hyperthermia HeLa cell treatment with silica-coated manganese oxide nanoparticles *J. Phys. Chem. C* **2010,** *114*, 1976.

(6) Lu, A. H.; Salabas, E. L.; Schuth, F., Magnetic nanoparticles: synthesis, protection, functionalization, and application *Angew. Chem. Int. Ed. Engl.* **2007,** *46*, 1222.

(7) Blakemore, R., Magnetotactic Bacteria *Science* **1975,** *190*, 377.

(8) Blakemore, R. P.; Frankel, R. B.; Kalmijn, A. J., South-seeking magnetotatic bacteria in the Southern Hemisphere *Nature* **1980,** *286*, 384.

(9) Bazylinski, D. A.; Frankel, R. B., Magnetosome formation in prokaryotes *Nature reviews. Microbiology* **2004,** *2*, 217.

(10) Flies, C. B.; Peplies, J.; Schuler, D., Combined approach for characterization of uncultivated magnetotactic bacteria from various aquatic environments *Appl. Environ. Microbiol.* **2005,** *71*, 2723.

(11) Schüler, D.; Frankel, R. B., Bacterial magnetosomes: microbiology, biomineralization and biotechnological applications *Appl. Microbiol. Biotechnol.* **1999,** *52*, 464.

(12) Bazylinski, D. A., Controlled biomineralization of magnetic minerals by magnetotactic bacteria *Chem. Geol.* **1996,** *132*, 191.

(13) Moskowitz, B. M., Biomineralization of magnetic minerals *Rev. Geophys.* **1995,** *33*, 123.

(14) Dunin-Borkowski, R. E.; McCartney, M. R.; Pósfai, M.; Frankel, R. B.; Bazylinski, D. A.; Buseck, P. R., Off-axis electron holography of magnetotactic bacteria: magnetic microstructure of strains MV-1 and MS-1 *Eur. J. Mineral.* **2001,** *13*, 671.

(15) D. L. Balkwill; D. Maratea; Blakemore, R. P., Ultrastructure of a magnetotactic spirillum *J. Bacteriol.* **1980,** *141*, 1399.

(16) Sonkaria, S.; Fuentes, G.; Verma, C.; Narang, R.; Khare, V.; Fischer, A.; Faivre, D., Insight into the assembly properties and functional organisation of the magnetotactic bacterial actin-like homolog, MamK *PloS one* **2012,** *7*, e34189.

(17) Schüler, D., Formation of magnetosomes in magnetotactic bacteria *J. Mol. Microbiol. Biotechnol.* **1999,** *1*, 79.

(18) Nakamura, N.; Hashimoto, K.; Matsunaga, T., Immunoassay method for the determination of immunoglobulin G using bacterial magnetic particles *Anal. Chem.* **1991,** *63*, 268.

(19) Tanaka, M.; Okamura, Y.; Arakaki, A.; Tanaka, T.; Takeyama, H.; Matsunaga, T., Origin of magnetosome membrane: proteomic analysis of magnetosome membrane and comparison with cytoplasmic membrane *Proteomics* **2006,** *6*, 5234.

(20) Sun, J. B.; Wang, Z. L.; Duan, J. H.; Ren, J.; Yang, X. D.; Dai, S. L.; Li, Y., Targeted distribution of bacterial magnetosomes isolated from Magnetospirillum gryphiswaldense MSR-1 in healthy Sprague-Dawley rats *J Nanosci Nanotechnol* **2009,** *9*, 1881.

(21) Sun, J.; Li, Y.; Liang, X. J.; Wang, P. C., Bacterial Magnetosome: A Novel Biogenetic Magnetic Targeted Drug Carrier with Potential Multifunctions *Journal of nanomaterials* **2011,** *2011*, 469031.

(22) Sun, J.; Tang, T.; Duan, J.; Xu, P. X.; Wang, Z.; Zhang, Y.; Wu, L.; Li, Y., Biocompatibility of bacterial magnetosomes: acute toxicity, immunotoxicity and cytotoxicity *Nanotoxicology* **2010,** *4*, 271.

(23) Xiang, L.; Wei, J.; Jianbo, S.; Guili, W.; Feng, G.; Ying, L., Purified and sterilized magnetosomes from Magnetospirillum gryphiswaldense MSR-1 were not toxic to mouse fibroblasts in vitro *Lett. Appl. Microbiol.* **2007,** *45*, 75.

(24) Choi, J.; Shin, J.; Lee, J.; Cha, M., Magnetic response of mitochondria-targeted cancer cells with bacterial magnetic nanoparticles *Chem Commun (Camb)* **2012,** *48*, 7474.

(25) Felfoul, O.; Mohammadi, M.; Martel, S., Magnetic resonance imaging of Fe3O4

nanoparticles embedded in living magnetotactic bacteria for potential use as carriers for in vivo applications *Conference proceedings : ... Annual International Conference of the IEEE Engineering in Medicine and Biology Society. IEEE Engineering in Medicine and Biology Society. Conference* **2007,** *2007*, 1463.

(26) Herborn, C. U.; Papanikolaou, N.; Reszka, R.; Grunberg, K.; Schuler, D.; Debatin, J. F., Magnetosomes as biological model for iron binding: relaxivity determination with MRI *RoFo : Fortschritte auf dem Gebiete der Rontgenstrahlen und der Nuklearmedizin* **2003,** *175*, 830.

(27) Hu, L. L.; Zhang, F.; Wang, Z.; You, X. F.; Nie, L.; Wang, H. X.; Song, T.; Yang, W. H., Comparison of the H NMR Relaxation Enhancement Produced by Bacterial Magnetosomes and Synthetic Iron Oxide Nanoparticles for Potential Use as MR Molecular Probes *IEEE TRANSACTIONS ON APPLIED SUPERCONDUCTIVITY* **2010,** *20*, 822.

(28) Alphandéry, E.; Faure, S.; Raison, L.; Duguet, E.; Howse, P. A.; Bazylinski, D. A., Heat Production by Bacterial Magnetosomes Exposed to an Oscillating Magnetic Field *The Journal of Physical Chemistry C* **2010,** *115*, 18.

(29) Riezman, H.; Woodman, P. G.; van Meer, G.; Marsh, M., Molecular Mechanisms of Endocytosis *Cell* **1997,** *91*, 731.

(30) Ma, N.; Ma, C.; Li, C.; Wang, T.; Tang, Y.; Wang, H.; Mou, X.; Chen, Z.; He, N., Influence of Nanoparticle Shape, Size, and Surface Functionalization on Cellular Uptake *Journal of Nanoscience and Nanotechnology* **2013,** *13*, 6485.

(31) CAÑETE, M.; SORIANO, J.; VILLANUEVA, A.; ALEJANDRO G. ROCA; VEINTEMILLAS, S.; SERNA, C. J.; MIRANDA, R.; MORALES, M. D. P., The

endocytic penetration mechanism of iron oxide magnetic nanoparticles with positively charged cover: A morphological approach *Int. J. Mol. Med.* **2010,** *26*.

(32) Wittrup, A.; Zhang, S.-H.; Svensson, K. J.; Kucharzewska, P.; Johansson, M. C.; Mörgelin, M.; Belting, M., Magnetic nanoparticle-based isolation of endocytic vesicles reveals a role of the heat shock protein GRP75 in macromolecular delivery *Proc. Natl. Acad. Sci. U. S. A.* **2010,** *107*, 13342.

(33) Schlorf, T.; Meincke, M.; Kossel, E.; Gluer, C. C.; Jansen, O.; Mentlein, R., Biological properties of iron oxide nanoparticles for cellular and molecular magnetic resonance imaging *International journal of molecular sciences* **2010,** *12*, 12.

(34) Harush-Frenkel, O.; Debotton, N.; Benita, S.; Altschuler, Y., Targeting of nanoparticles to the clathrin-mediated endocytic pathway *Biochem. Biophys. Res. Commun.* **2007,** *353*, 26.

(35) Georgieva, J. V.; Kalicharan, D.; Couraud, P. O.; Romero, I. A.; Weksler, B.; Hoekstra, D.; Zuhorn, I. S., Surface characteristics of nanoparticles determine their intracellular fate in and processing by human blood-brain barrier endothelial cells in vitro *Molecular therapy : the journal of the American Society of Gene Therapy* **2011,** *19*, 318.

(36) Tran, N.; Webster, T. J., Understanding magnetic nanoparticle osteoblast receptor-mediated endocytosis using experiments and modeling *Nanotechnology* **2013,** *24*, 185102.

(37) LadyofHats, M. R. V., Endocytosis types. Wikimedia Commons: 2007.

(38) Thorek, D. L.; Tsourkas, A., Size, charge and concentration dependent uptake of iron oxide particles by non-phagocytic cells *Biomaterials* **2008,** *29*, 3583.

(39) Sauer, A. M.; de Bruin, K. G.; Ruthardt, N.; Mykhaylyk, O.; Plank, C.; Brauchle, C., Dynamics of magnetic lipoplexes studied by single particle tracking in living cells *Journal of controlled release : official journal of the Controlled Release Society* **2009,** *137*, 136.

(40) Miyoshi, S.; Flexman, J. A.; Cross, D. J.; Maravilla, K. R.; Kim, Y.; Anzai, Y.; Oshima, J.; Minoshima, S., Transfection of neuroprogenitor cells with iron nanoparticles for magnetic resonance imaging tracking: cell viability, differentiation, and intracellular localization *Molecular imaging and biology : MIB : the official publication of the Academy of Molecular Imaging* **2005,** *7*, 286.

(41) Blakemore, R. P.; Maratea, D.; Wolfe, R. S., Isolation and pure culture of a freshwater magnetic spirillum in chemically defined medium *J. Bacteriol.* **1979,** *140*, 720.

(42) Mosmann, T., Rapid colorimetric assay for cellular growth and survival: Application to proliferation and cytotoxicity assays *J. Immunol. Methods* **1983,** *65*, 55.

(43) Matsunaga, T.; Okamura, Y.; Tanaka, T., Biotechnological application of nano-scale engineered bacterial magnetic particles *J. Mater. Chem.* **2004,** *14*, 2099.

(44) Frankel, R. B.; Bazylinski, D. A., *Nanobiotechnology*. WILEY-VCH: 2004.

(45) Matsunaga, T.; Okamura, Y., Genes and proteins involved in bacterial magnetic particle formation *Trends Microbiol.* **2003,** *11*, 536.

(46) Nishio, H.; Takahashi, T.; Taguchi, H.; Kamiya, S.; Matsunaga, T., Magnetic Characterization of Bacterial Magnetic Particles *Le Journal de Physique IV* **1997,** *07*, C1.

(47) Matsunaga, T.; Sato, R.; Kamiya, S.; Tanaka, T.; Takeyama, H., Chemiluminescence enzyme immunoassay using ProteinA-bacterial magnetite complex *J. Magn. Magn. Mater.* **1999,** *194*, 126.

(48) Hergt, R.; Hiergeist, R.; Zeisberger, M.; Schuler, D.; Heyen, U.; Hilger, I.; Kaiser, W., Magnetic properties of bacterial magnetosomes as potential diagnostic and therapeutic tools *J. Magn. Magn. Mater.* **2005,** *293*, 80.

(49) Mann, S.; Frankel, R. B.; Blakemore, R. P., Structure morphology and crystal growth of bacterial magnetite *Nature* **1984,** *310*, 405.

(50) Krichevsky, A.; Smith, M. J.; Whitman, L. J.; Johnson, M. B.; Clinton, T. W.; Perry, L. L.; Applegate, B. M.; O'Connor, K.; Csonka, L. N., Trapping motile magnetotactic bacteria with a magnetic recording head *J. Appl. Phys.* **2007,** *101*, 014701.

(51) Kopp, R. E.; Kirschvink, J. L., The identification and biogeochemical interpretation of fossil magnetotactic bacteria *Earth-Sci. Rev.* **2008,** *86*, 42.

(52) Weiss, B. P.; Sam Kim, S.; Kirschvink, J. L.; Kopp, R. E.; Sankaran, M.; Kobayashi, A.; Komeili, A., Ferromagnetic resonance and low-temperature magnetic tests for biogenic magnetite *Earth. Planet. Sci. Lett.* **2004,** *224*, 73.

(53) Xie, J.; Chen, K.; Chen, X., Production, Modification and Bio-Applications of Magnetic Nanoparticles Gestated by Magnetotactic Bacteria *Nano research* **2009,** *2*, 261.

(54) Iversen, T.-G.; Skotland, T.; Sandvig, K., Endocytosis and intracellular transport of nanoparticles: Present knowledge and need for future studies *Nano Today* **2011,** *6*, 176.

(55) Kim, J.-S.; Yoon, T.-J.; Y, K.-N.; Noh, M. S.; Woo, M.; Kim, B.-G.; Lee, K.-H.; Sohn, B.-H.; Park, S.-B.; Lee, J.-K.; Cho, M.-H., Cellular uptake of magnetic nanoparicle is mediated through energy dependent endocytosis in A549 cells *Journal of Veterinary Science* **2006,** *7*, 321.

(56) Fuller, J. E.; Zugates, G. T.; Ferreira, L. S.; Ow, H. S.; Nguyen, N. N.; Wiesner, U. B.; Langer, R. S., Intracellular delivery of core–shell fluorescent silica nanoparticles *Biomaterials* **2008,** *29*, 1526.

(57) Choudhari, K.; Xavier, P. L.; Pradeep, T., Size Evolution of Luminescent Lactoferrin Protected Gold Clusters *Journal of Biomedical Nanotechnology* **2011,** *7*, 70.

(58) Goyal, R.; Tripathi, S. K.; Tyagi, S.; Sharma, A.; Kumar, P.; Ravi Ram, K.; Chowdhuri, D. K.; Shukla, Y.; Gupta, K. C., In Vitro and In Vivo Evaluation of Linear Polyethylenimine Nanoparticles *Journal of Biomedical Nanotechnology* **2011,** *7*, 52.

(59) Roy, R.; Tripathi, A.; Das, M.; Dwivedi, P. D., Cytotoxicity and Uptake of Zinc Oxide Nanoparticles Leading to Enhanced Inflammatory Cytokines Levels in Murine Macrophages: Comparison with Bulk Zinc Oxide *Journal of Biomedical Nanotechnology* **2011,** *7*, 110.

(60) Sharma, V.; Anderson, D.; Dhawan, A., Zinc Oxide Nanoparticles Induce Oxidative Stress and Genotoxicity in Human Liver Cells (HepG2) *Journal of Biomedical Nanotechnology* **2011,** *7*, 98.

(61) Zhang, X.; He, X.; Wang, K.; Yang, X., Different Active Biomolecules Involved in Biosynthesis of Gold Nanoparticles by Three Fungus Species *Journal of*

Biomedical Nanotechnology **2011,** *7*, 245.

(62) Chithrani, B. D.; Ghazani, A. A.; Chan, W. C. W., Determining the Size and Shape Dependence of Gold Nanoparticle Uptake into Mammalian Cells *Nano Lett.* **2006,** *6*, 662.

(63) Osaki, F.; Kanamori, T.; Sando, S.; Sera, T.; Aoyama, Y., A Quantum Dot Conjugated Sugar Ball and Its Cellular Uptake. On the Size Effects of Endocytosis in the Subviral Region *J. Am. Chem. Soc.* **2004,** *126*, 6520.

(64) Sabuncu, A. C.; Grubbs, J.; Qian, S.; Abdel-Fattah, T. M.; Stacey, M. W.; Beskok, A., Probing nanoparticle interactions in cell culture media *Colloids and surfaces. B, Biointerfaces* **2012,** *95*, 96.

(65) Liu, Q.; Zhang, J.; Xia, W.; Gu, H., Magnetic field enhanced cell uptake efficiency of magnetic silica mesoporous nanoparticles *Nanoscale* **2012,** *4*, 3415.

(66) Scherer, F.; Anton, M.; Schillinger, U.; Henke, J.; Bergemann, C.; Kru¨ger, A.; Ga¨nsbacher, B.; Plank, C., Magnetofection: enhancing and targeting gene delivery by magnetic force in vitro and in vivo *Gene Ther.* **2002,** *9*, 102.

(67) Sakaguchi, T.; Burgess, J. G.; Matsunaga, T., Magnetite formation by a sulphate-reducing bacterium *Nature* **1993,** *365*, 47.

(68) Nakamura, N.; Matsunaga, T., Highly sensitive detection of allergen using bacterial magnetic particles *Anal. Chim. Acta* **1993,** *281*, 585.

Chapter 3. Synergistic Effect of BMPs and Static Magnetic Field on Cells

3.1 Introduction

3.1.1 Biological Effect of External Magnetic Fields Exposure on Cells

Humans are continuously exposed to electromagnetic fields (EMFs) due to expanding use of electronic devices in their life. Static magnetic field (SMF) is also required to consider for protecting human health because it could be employed in magnetically levitated trains and therapeutic use, e.g. MRI, coupling of magnetic fields (MFs) exposure with chemotherapy. For the increasing concern, biological effects of the MFs exposure on cells have been reported in various conditions [1-6]. The effects were studied in different exposure systems and conditions, therefore it is considered in terms of MF intensity (from 10^{-7} to 10 T), type of field (static or alternating), and subjects exposed to MFs (from in vitro cultured cells to humans). In this study, the MFs exposure on cells is confined to SMF to investigate synergistic effects of BMPs and SMF exposure.

The influence of SMFs on biological systems has been a topic of considerable interest for many years [2, 7]. In terms of the intensity, SMFs could be classified as weak (<1 mT), moderate (1 mT to 1 T), strong (1-5 T) and ultrastrong (>5 T).

Experimental data on the biological effects of weak SMPs are limited and several different mechanisms have been considered to explain the effect. Endogenous radicals was the primary targets and another theory is based on a possible modulation

of high frequency oscillations in the cell nuclei [8-9]. Various response of weak SMFs on cells were reported such as modifications of neuronal and behavioral functions [10-12] including influence on brain function and enhancement of efflux of Ca^{2+} ions [13-14], and interaction with microfilaments in microvilli [15].

The interest in the bioeffects of strong and ultrastrong SMFs is related to the risk associated with exposure to the strong magnetic fields required to perform MRI. Some changes were observed in many cells, alteration of cleavage planes of Xenopus eggs (16.7 T) [16]; reorientation of the mitotic apparatus in frog eggs [17]; changes to proliferation and intracellular concentration of Ca^{2+} ions in Jurkat cells (4.75 T) [18]. Conversely, it was reported that the strong or ultrastrong SMFs failed to affect increasing mutations of *Drosophila melanogaster* eggs, larvae and adults (3.7 T) [19]; physiological behavior of normal lymphomonocytes (4.75 T) [18]; inducing aggregation of melanophores in cod fish (8, 14 T) [20].

The moderate-intensity SMFs also have been studied and their bioeffects on cultured cells are well summarized in a review [2]. A number of biological properties are influenced by moderate-intensity SMFs. The major effects on cells are considered to be plasma membrane changes, modulation of intracellular concentration and flux of Ca^{2+} ion, cell shape alteration, cytoskeleton reorganization, increase or decrease of apoptosis; proliferation and differentiation (Table 3-1) [1, 5, 21-27]. These studies showed that the bioeffects on cells could be contradictory on the basis of the

differences between the cell types. In spite of the differences in exposure time and cell types, the morphological modifications of cells and cell surfaces might be considered a common response of cells to exposure to SMFs [2-3, 28].

Table 3-1. Summaries of the major effects, most of which are exposure time- and cell type-dependent, of moderate-intensity SMFs on cultured cells [2]

Cellular structures and functions	Effects
Plasma membrane	–reorientation of diamagnetic molecular domains –proteic pattern changes –rotation of the membrane's phospholipids –rearrangement of lectin binding sites
$[Ca^{2+}]i$	–fluxes intracellular and extracellular –transport across cell membrane –Ca^{2+} signalling
Cell shape	–elongation for in suspension growing cells –detachment for in adhesion growing cells –lamellar or buble-like microvilli
Cytoskeleton	–reorganization and breakdown of F-actin filaments and microtubules
Apoptosis	–perturbation of the apoptotic rate (increase as well decrease)

Table 3-1.–Continued	
Necrosis	–not induced
Apoptotic related genes	–modulation (increase as well as decrease)
Apoptotic cell surface	–partially reverted the expression of ‘eat me’ epitopes
Phagocytosis of apoptotic cells	–decreased
Differentiation of macrophages	–delayed

3.2 Materials and Methods

3.2.1 Magnetic Field Exposure

Static Magnetic Fields (SMFs) were generated with a neodymium iron boron (NdFeB) magnet (50 × 25 × 25 mm) with an average flux density of 480 ± 10 mT, as measured by a Gauss meter (TM-701, Kanetec, Japan). Magnets were placed under the plastic culture dishes when changes in cell growth were evaluated. Because the SMF intensity decreases according to the square of the distance from the magnet, the magnetic force on the cells was calculated taking the thickness of the bottom of the culture dish (1.0 mm) into account. The SMF was applied continuously at the bottom of the culture dish for up to 72 h with HeLa cells, and 6 days with SH-SY5Y cells. For neurite outgrowth was measured, two NdFeB magnets (50 × 25 × 15 mm) were placed laterally on both sides of the culture dish and the cells were treated with retinoic acid (RA, all trans-retinoic acid; Sigma, USA) for 1 week.

3.2.2 Cell Culture

HeLa (human cervical cancer) cells and C2C12 (mouse myoblast cells) were cultured in DMEM/high glucose (Thermo Scientific, USA) containing 10% (v/v) FBS (Thermo Scientific, USA) and 300 U/ml penicillin/streptomycin (Thermo Scientific, USA) at 37°C in a humidified atmosphere containing 5% CO_2. For culture of SH-SY5Y cells, a human neuroblastoma cell line, culture medium consisted of DMEM/low glucose (Thermo Scientific, USA) containing 10% (v/v) FBS (Thermo Scientific, USA) and 100 U/ml penicillin/streptomycin (Thermo Scientific, USA) at 37°C in a humidified atmosphere containing 5% CO_2. The culture medium was changed every 3 days with fresh medium and subculture was performed when the cells were cultured to 80% confluency to maintain optimal condition for further studies. Moreover, the cells of passage number from 4 to 15 were used to maintain identical condition of the cell lines for reliability of experiments. The hemocytometer was used to count number of the cells and certain number of cells were seeded on proper culture plates or dishes.

3.2.3 Delivery of BMPs and Isolation of BMP-loaded Cells

The HeLa and C2C12 cells were seeded with density of 5.0×10^4 cells/cm^2 in the culture medium and incubated for 2-24 h for stabilization of cell condition. After the pre-incubation, 10 μg/ml of the BMPs were added to the medium and then the cells were incubated overnight to allow internalization of BMPs. In case of SH-SY5Y cells, the BMPs were applied when the cells have 80% confluency to keep differentiation potency for subsequent study. The BMPs (10 μg/ml on more than 10^6 cells) were dispersed in serum reduced medium (1% FBS) and then the culture medium was changed to BMPs containing medium. The SH-SY5Y cells showed lower uptake rate of BMPs than HeLa cells, thereby the serum reduced medium was employed for SH-SY5Y cells. After the delivery of BMPs, the cells were incubated overnight for sufficient time to internalize BMPs.

The BMP-loaded cells (BMP-HeLa, BMP-SH) were collected separately from BMP-free cells using a magnet as following description. The cells incubated with BMPs were washed three times with 1× PBS gently and then trypsinized for 3 min. After neutralization of trypsin with FBS containing medium, the cells were harvested by centrifuge for 5 min at 1000 rpm. The cells dispersed in the culture medium were transferred to centrifuge tube and an NdFeB magnet was placed at the side of the tube for 5 min to separate BMP-loaded cells. Remnant medium including BMP-free cells were removed after enough separation of the BMP-loaded cells. Then the

separated BMP-loaded cells were dispersed in fresh culture medium and seeded moderate number of cells on culture dish or plate for subsequent investigations.

3.2.4 Cell Staining

To check morphological and structural changes of the HeLa cells induced by internalized BMPs and external SMF, indirect immunofluorescence analysis to actin cytoskeleton staining was accomplished. DNA was counterstained with DAPI. HeLa cells were cultured under 4 different conditions, control HeLa; BMP-HeLa; control HeLa under the SMF; BMP-HeLa under the SMF, for 24 h. Then, the cells were fixed with 4% paraformaldehyde in 1× PBS for 15 min at room temperature. After washing twice with wash buffer, 0.1% Triton X-100 in 1× PBS, the fixed cells were permeabilized and blocked by immersing in 1% BSA and 0.1 Triton X-100 in 1× PBS for 20 min. The actin filaments were stained by incubating cells with TRITC-conjugated phalloidin (1:200) for 50 min at room temperature. The cells were gently washed three times with 1× PBS and nucleus staining was performed by incubating with a dilute DAPI in 1× PBS (1:1000) three times for 5 min each. The cells were gently washed three times with 1× PBS and finally immersed in 1× PBS. The stained cells were examined using an inverted microscope (Nikon, Japan).

Area of each cell was measured to get quantitative data using Image J. The numerical values obtained from 85-150 cells in each condition were fitted to normal distribution.

3.2.5 Proliferation

3.2.5.1 MTS assay

The MTS assay was performed to investigate viability of HeLa and SH-SY5Y cells in various conditions, with or without BMP loading and with or without SMF exposure. The cells (1×10^3 cells/well for HeLa and 5×10^3 cells/well for SH-SY5Y cells) were seeded on 96-well plate with 100 μl of the aforementioned culture medium. After incubation in various conditions for proper time to assess, 20 μl of CellTiter 96® AQueous One Solution Reagent (Promega, USA) was introduced into each well. Then the plate was incubated at 37°C for 1–4 h in a humidified 5% CO_2 atmosphere and absorbance was recorded at 490 nm with a microplate reader (Sunrise, Tecan, Switzerland). Six wells in one assay were employed to a culture condition and the assay was triplicated. The average absorbance value of control cells was normalized to 100% viability and the viability of cells were calculated compared to control cells. The standard error of mean of the cell viability and p-value from unpaired t-test was calculated using Graphpad Prism 5 software.

3.2.5.2 ATP assay

The HeLa cells (2×10^3 cells/well) were seeded on opaque-walled 96-wells plate with 100 µl of the culture medium and cultured for 48 h in the aforementioned various condition to evaluate ATP content of the cells. ATP content was measured in accordance with the protocol of CellTiter-Glo luminescent cell viability assay kit (Promega, USA). This procedure followed the protocol provided by manufacturer. In brief, 100 µl of reagent was added to each well and mixed for 2 min at room temperature. After then the intracellular ATP content was measured using luminometer (Thermo Fisher Scientific Inc., USA). Four wells were employed to a condition of cell culture in an assay. The assays were performed in three separate sets of experiments, and the luminescence value of control cells was defined as 100% of ATP content in every assay. The standard error of mean of the ATP content and p-value from unpaired t-test was calculated using Graphpad Prism 5 software.

3.2.6 Induced Apoptosis

3.2.6.1 Cisplatin Treatment

Cisplatin, a DNA-damaging anticancer drug, was treated to the HeLa cells and BMP-HeLa cells to investigate synergistic effect of BMP internalization and SMF exposure on apoptosis. Cisplatin was prepared with concentration of 10 mg/ml by dissolving in dimethyl sulfoxide (DMSO), which is to minimize toxicity effect of DMSO to cells. To determine concentration of cisplatin to induce LD50 of HeLa cells, the cells (5×10^3 cells/well) were seeded on 96-well plate and incubated to stabilize cell condition for 24 h. The sensitivity of HeLa cells to cisplatin was determined by treatment with serial concentration of cisplatin (5, 10, 20 μg/ml) for 24 h in normal culture condition. After that cell viability was evaluated by MTS assay as following the aforementioned procedure. The HeLa cells and BMP-HeLa cells were treated with cisplatin at 10 μg/ml concentration (LD50) to investigate the effect of SMF and BMP internalization on apoptosis, DNA fragmentation and progress of apoptosis.

3.2.6.2 DNA Extraction and Gel Electrophoresis

To confirm the DNA fragmention induced by cisplatin, genomic DNA of the cells was extracted from cisplatin treated cells and examined by agarose gel electrophoresis. The genomic DNA was extracted using Blood & Tissue genomic DNA extraction miniprep system (Viogene, Taiwan). The procedure was followed protocol provided by the manufacturer with some modifications as described below.

Tree samples of 10^7 cells, control cells, cisplatin treated BMP-HeLa cells with and without SMF exposure, were prepared in 200 µl of 1×PBS. The cells were mixed with 20 µl of Proteinase K (10 mg/ml) and 200 µl of EX buffer (included in the product) by vortexing for 20 s and incubated at 60°C water bath for 20 min to lyse. During incubation the samples were mixed by vortexing or inverting every 3-5 minutes. After 20 min incubation, the sample were moved to another water bath set 70°C and incubated for 10 min more. Meanwhile, TE buffer (pH 8.0, 500 µl/sample) was prepared and preheated at 70°C for DNA elution step. Then 210 µl of absolute ethanol was mixed with the samples by vortexing and all the mixture from a sample was put into a B/T genomic DNA mini column (included in the product) placed onto a collection tube. After centrifuge at 8,000 rpm for 2 min, the column was moved to a new collection tube. The column was washed twice with 500 µl of WS buffer (included in the product) by centrifuging at 8,000 rpm for 2 min each, and then the solution collected in the collection tube was discarded. To remove residual ethanol,

the column was centrifuged at 13,000 rpm for another 2 min. DNA was eluted by adding 20 μl of the preheated elution solution into the column which was placed onto a new 1.5 ml ep-tube. After standing the column for 5 min, DNA was collected by centrifuging 8,000 rpm for 2 min. The eluted DNA was stored at 4°C.

The extracted DNA was run on a 2% agarose gel and observed under UV light.

3.2.6.3 Reverse Transcriptase-Polymerase Chain Reaction (RT-PCT)

P53 gene expression was analysed by reverse transcriptase-polymerase chain reaction (RT-PCR). Total RNA was isolated from subconfluent cultures by using easy spinTM [DNA free] total RNA extraction kit (iNtRON Biotechnology, Inc., Korea). RNA yields were determined by duplicate absorbance measurements. RT–PCR was performed using One-Step RT–PCR PreMix kit (iNtRON Biotechnology, Inc., Korea). The primer sequences and sizes of the amplified products were designed as follows for

p53:

5’-CTGAGGTTGGCTCTGACTGTACCACCATCC-3’

5’-CTCATTCAGCTCTCGGAACATCTCGAAGCG-3’

β-actin:

5’-CAAGAGATGGCCACGGCTGCT-3’

5’-TCCTTCTGCATCCTGTCGGCA -3’

β-actin was usually amplified for 30 cycles, p53 for 28 cycles respectively. PCR products of the size of 371 bp (p53), 275 bp (β-actin) were run on a 1.5% agarose gels and then observed under UV light.

3.2.7 Neurite Outgrowth

Differentiation of SH-SY5Y and BMP-loaded SH-SY5Y cells (BMP-SHs) was induced by treating them with 10 μM retinoic acid (RA) in serum-reduced medium; the medium was changed every 3 days. Neurite outgrowth of the cells was assessed after 7 days of differentiation induction with or without exposure to SMF. Neurite length was measured from captured image using an inverted microscope and classified into three levels according to the length, i.e., 0–50 μm, 50–100 μm, or over 100 μm. In total, 200 cells in each condition were analyzed in three separate sets of the experiments, with the standard error of the mean being recorded.

3.3 Results and Discussion

3.3.1 Applied Magnetic Field and Force

To evaluate the synergistic effects of the BMPs within the cell and an external SMF, BMP-loaded cells were separated from non-loaded cells using a magnet, and cultured under an SMF. The SMF was applied continuously at the bottom of the culture dish using a permanent magnet with the magnetic field strength of 480 mT (Fig. 3-1).

The magnetic force on a BMP was estimated using a magnetofection model to understand physical effect of the internalization of BMPs with SMF exposure on a cell. When the BMP is internalized into a cell and exposed to an SMF externally at the bottom of the cell, the environment is similar with magnetofection. Cytoplasm could be substituted for the transport fluid in the magnetofection model [29]. The magnetic force on a BMP is modeled using the effective dipole moment method in which a magnetic particle is replaced by an equivalent point dipole with a moment $m_{p,\text{eff}}$ [29-30]. The force on the dipole (and hence on the particle) is given by

$$\mathbf{F}_m = \mu_f \mathbf{m}_{p,eff} \cdot \nabla \mathbf{H}_a$$

where μ_f is the permeability of transport fluid, $m_{p,\text{eff}}$ is the effective dipole moment of the particle, and H_a is the externally applied magnetic field intensity at the center of a particle, where the equivalent point dipole is located. The $m_{p,\text{eff}}$ is depends on H_a

as following equation.

$$\mathbf{m}_{p,\text{eff}} = V_p f(H_a)\mathbf{H}_a$$

where,

$$f(H_a) = \begin{cases} \dfrac{3(\chi_p - \chi_f)}{(\chi_p - \chi_f) + 3} & \text{if } H_a < \left(\dfrac{(\chi_p - \chi_f) + 3}{3\chi_p}\right) M_{sp} \\ \dfrac{M_{sp}}{H_a} & \text{if } H_a \geq \left(\dfrac{(\chi_p - \chi_f) + 3}{3\chi_p}\right) M_{sp} \end{cases}$$

χ_p is magnetic susceptibility of the particle and χ_f is magnetic susceptibility of the fluid. It was assumed that the cytoplasm is nonmagnetic ($\chi_f = 0$) with a viscosity and density equal to that of water. The BMP consists of Fe_3O_4 and have a density ρ_p = 5170 kg/m^3 and saturation magnetization of the particle M_{sp} = 4.52 x 10^5 A/m. When, $\chi_p >> 1$

$$f(H_a) = \begin{cases} 3 & \text{if } H_a < M_{sp}/3 \\ \dfrac{M_{sp}}{H_a} & \text{if } H_a \geq M_{sp}/3 \end{cases}$$

In the SMF exposure condition, employing a rectangular NdFeB magnet (50 x 25 x 25 mm), 1-D distribution of H_a is described as following equation which is provided from the international magnetic solutions (IMS) [31].

$$H_a = \frac{M_s}{\pi}\left[\left[\tan^{-1}\frac{WL}{2x(4x^2 + W^2 + L^2)^{1/2}}\right] - \tan^{-1}\left[\frac{WL}{2(x+T)[4(x+T)^2 + W^2 + L^2]^{1/2}}\right]\right]$$

W is width and L is length of the magnet. The Flux density H_a is calculated along the center axis at a distance x from the magnet and saturation magnetization of the magnet M_s is 9.09 x 10^5 A/m (Fig. 3-2). When the distance from center of the magnet $x < 0.10$ m, $H_a \geq M_{sp}/3$.

Finally, the magnetic force on a BMP could be described as following.

$$\mathbf{F}_m(x) = \mu_f V_p \left(\frac{M_{sp}}{H_a}\right) \mathbf{H}_a \cdot \nabla \mathbf{H}_a = \mu_f V_p \left(\frac{M_{sp}}{H_a}\right) H_a \frac{dH_a}{dx} = \mu_f V_p M_{sp} \frac{dH_a}{dx}$$

where V_p is volume of a magnetic nanoparticle (6.54 x 10^{-23} m^3, radius of a magnetic nanoparticle is 25 nm). The distance x was 1 mm which is the thickness of the culture dish. The BMPs internalized cells attached right on the dish and ignored the height of a cell. Based on the experiment condition, the magnetic force on a BMP was 0.81 *f*N toward the magnet. BMP-HeLa cells had an average of 162 pg of BMPs in cytosol based on the cellular uptake study, which means the cells experienced 388.09 pN under 480 mT of SMF. Otherwise, BMP-SH cells have taken up 8.69 pg of BMPs in average and the cells experienced 20.82 pN under 480 mT of SMF.

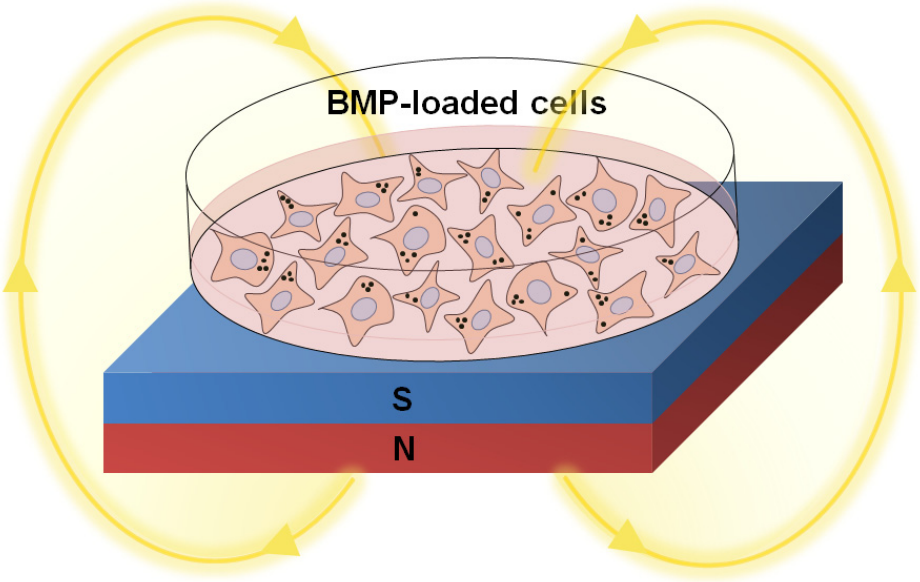

Figure 3-1. Schematic of SMF exposure to study effects of BMPs and SMF on cell

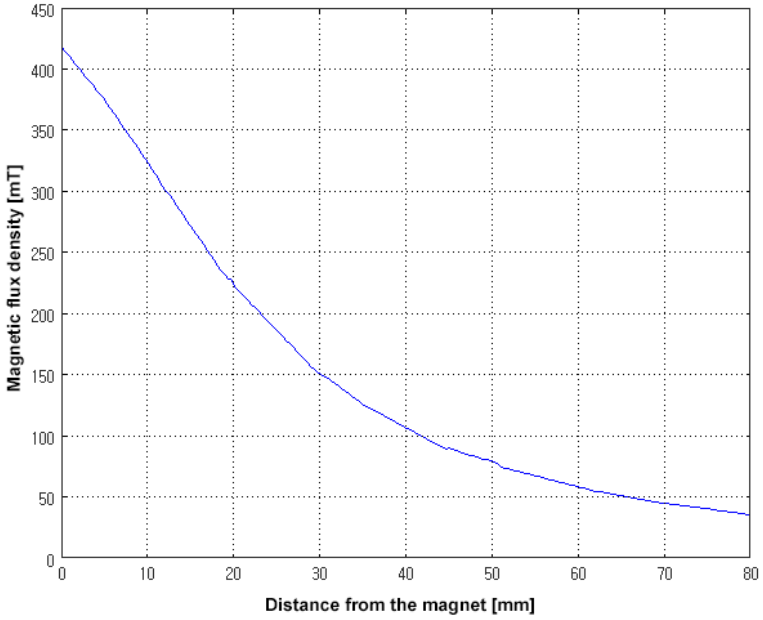

Figure 3-2. Calculated Magnetic flux density from the magnet

The SMF was applied constantly to SH-SY5Y cells with lateral direction as shown in Figure 3-3 during induction of the neuronal differentiation by RA treatment. The lateral direction of magnetic field gradient was expected to simulate neurite outgrowth, which is parallel to each other. The cells were placed in the magnetic field strength range of 100 to 220 mT (Fig. 3-4) when the neuronal differentiation was induced by RA treatment.

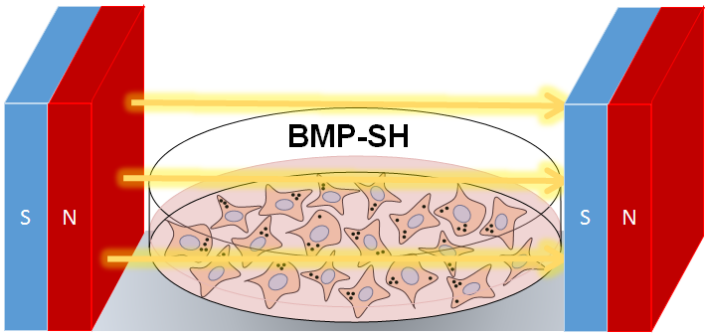

Figure 3-3. Schematic of SMF exposure to SH-SY5Y cells during induction of differentiation

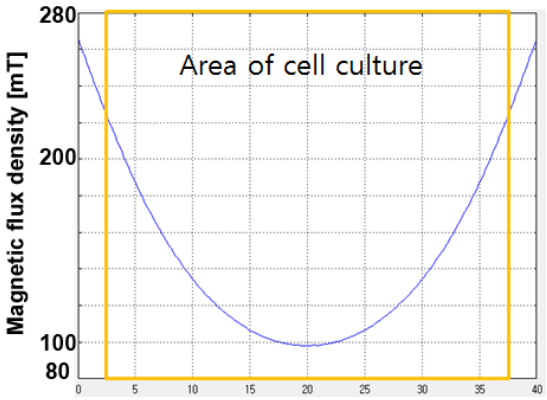

Figure 3-4. Magnetic flux density in cell culture area during induction of differentiation

3.3.2 Morphology Changes

Morphological and structural changes of HeLa cells induced by internalized BMPs and an external SMF were observed with indirect immunofluorescence analysis to actin cytoskeleton staining (DNA counterstained with DAPI). As shown in Figure 3-5, the interplay of BMPs within the cell and external SMF cause the deformed cytoskeletal networks of cells. The deformation of cell shape was checked by measuring area of each cell cultured in different conditions using image J, then it was fitted to normal distribution (Fig. 3-6). Interestingly, BMPs itself did not much affect to the cytoskeletal deformation without SMF exposure; however the morphology of the cells significantly changed after exposure to the SMF and also these deformations were induced by the SMF independently.

The cytoskeleton plays a major role in many important fields such as cell shape, motility, division, adhesion and the connections the cell can realize with its environment [32]. Strong and replicable alterations of cell shape and plasma membrane have been reported to produce with the SMF exposure in different cell types [3]. It is considered that the SMF influences dominantly for alteration of cellular structure.

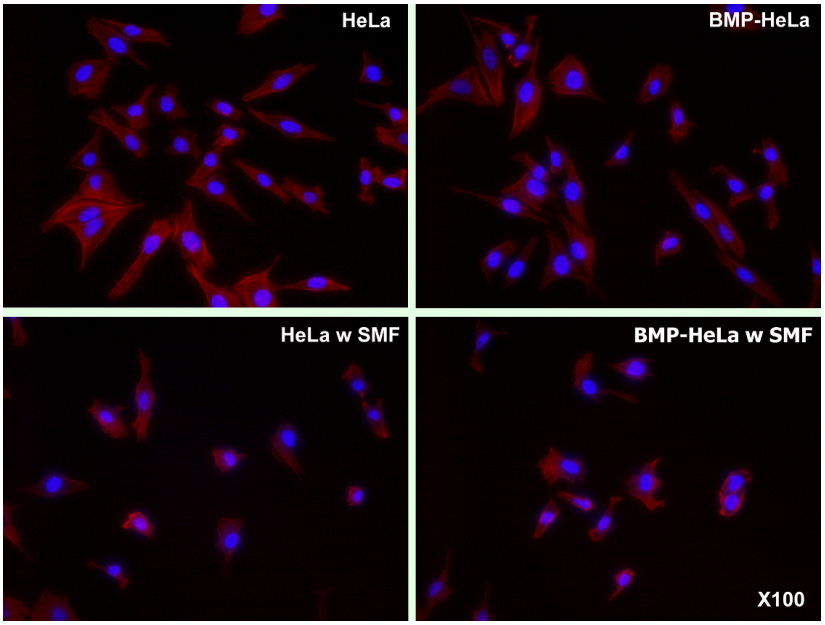

Figure 3-5. Fluorescence images of cytoskeletal stained cells magnified to 100 times, (a) Control (Hela cell), (b) BMP loaded Hela cells, (c) HeLa cells under the SMF exposure (d) BMP loaded HeLa cells under the SMF exposure, blue: nucleus, red: actin filaments

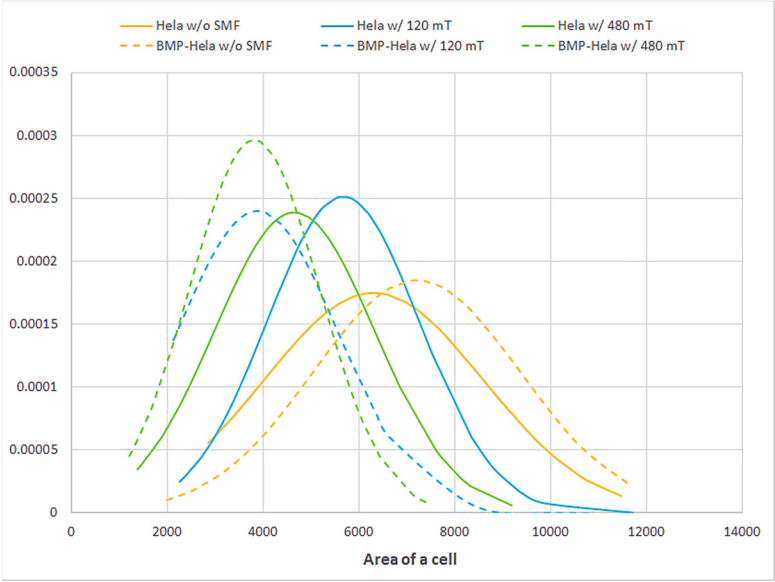

Figure 3-6. Measured area of one cell indicating shape change

3.3.3 Growth Enhancement

An SMF with moderate strength (1 mT–1 T) is supposed to influence the viability of cells, because of the diamagnetic properties of cell membrane molecular structure [2]. However, HeLa cells have been reported to be essentially unaffected by the exposure to the SMF with strength from 0.3 to 1.1 T [21]. Interestingly, the growth of the BMPs loaded HeLa (BMP-HeLa) cells notably improved, up to 23 %, under the exposure to the SMF over 48 h (Fig. 3-7).

The increased growth can be ascribed to the ATP content of the BMP-HeLa cells exposed to the SMF that increased about 11% higher compared with those under other conditions (Fig. 3-8). The intracellular ATP level strictly reflects the number of viable cells. When cells die, the tricarboxylic acid cycle stops the production of ATP, and intracellular ATP level immediately decreases. Therefore, the intracellular ATP level is proportional to the number of healthy and functional cells.

The enhancement was further confirmed that the growth of another cell system, mouse myoblast C2C12 cells transfected with the BMPs, was more dramatically enhanced (up to 44%) under the SMF condition over 48 h (Fig. 3-9). However, a synergetic effect of the BMPs and SMF was not observed in SH-SY5Y cell. Internalization of BMPs induced a substantial increase in SH-SY5Y cell growth (up to 30% in 6 days), whereas the effect of SMF exposure was negligible regardless of

BMP internalization (Fig. 3-10).

Interestingly, the higher improvement of cell growth was induced as increasing applied magnetic field strength in the range below 480 mT (Fig. 3-11). In addition, the growth was enhanced only by the combined condition, internalized BMPs and external SMF, under the 120 mT of SMF. These results suggest that the interaction between the internalized BMPs and the external SMF is a key factor leading to the enhanced cell growth. Moreover the sensitivity to the combined stimulation could depend on the cell type. The interplay with external SMF and BMPs within the cell induce the alteration of the diamagnetic anisotropy of membrane phospholipids, which was described in section 3.3.2. Thereby, cell growth could be enhanced as the cell signaling related to the membrane protein may be modulated. The detailed mechanism will be discussed in chapter 4.

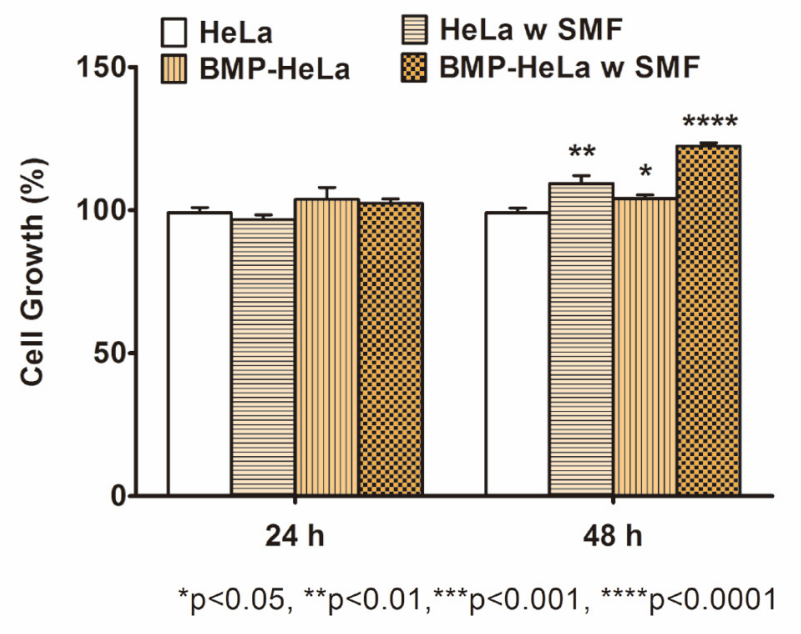

Figure 3-7. Cell growth of HeLa cells with SEM and *p*-value from unpaired *t*-test

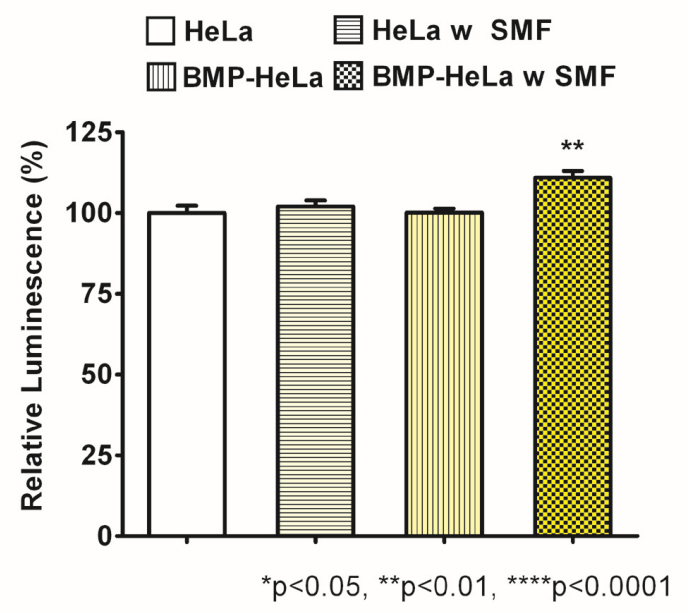

Figure 3-8. ATP level of HeLa cells with SEM and *p*-value from unpaired *t*-test

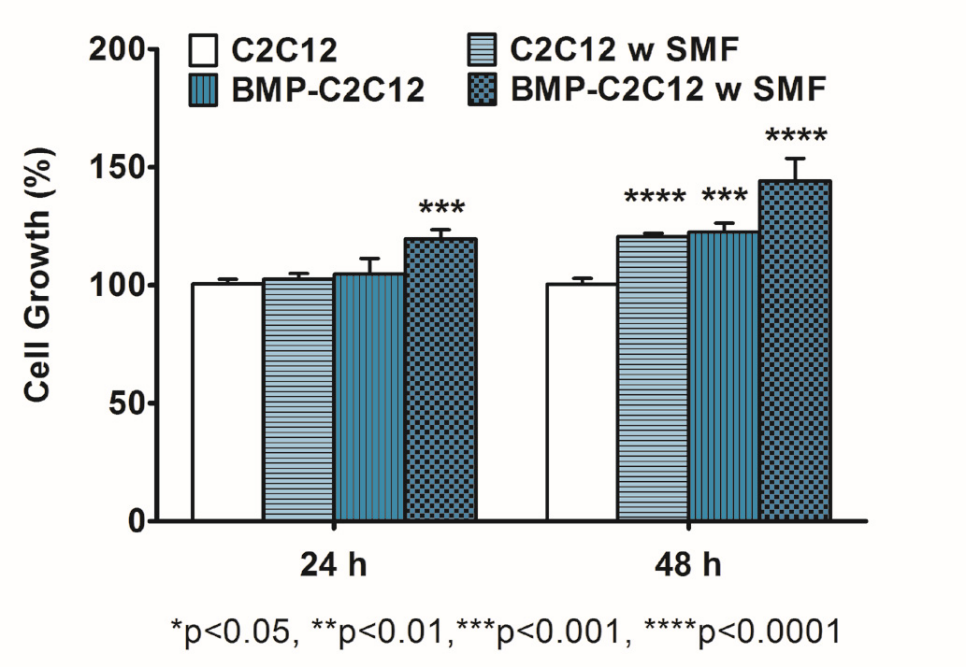

Figure 3-9. Cell growth of C2C12 cells with SEM and *p*-value from unpaired *t*-test

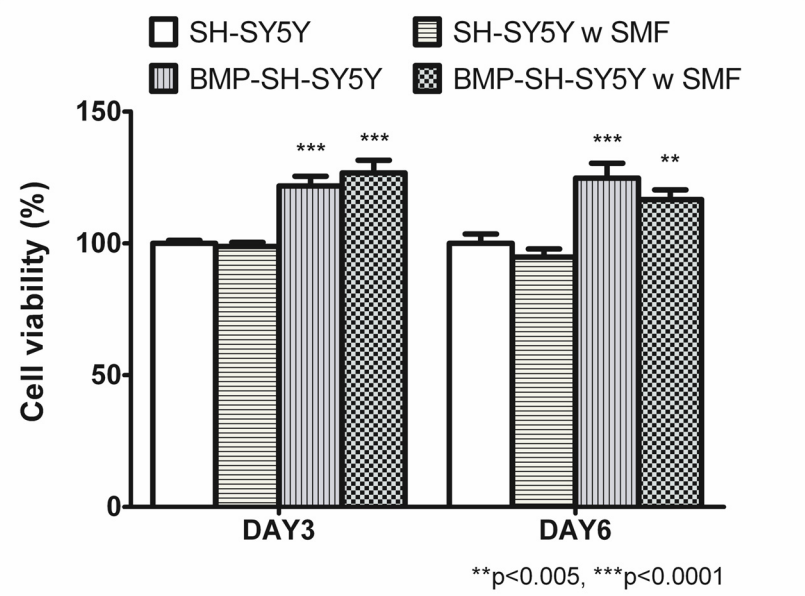

Figure 3-10. Cell growth of SH-SY5Y cells with SEM and *p*-value from unpaired *t*-test

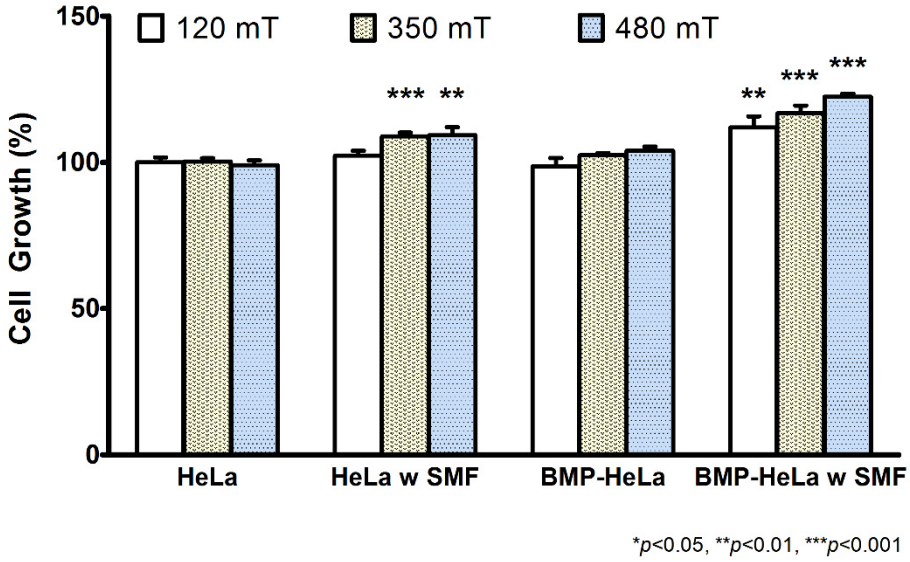

Figure 3-11. Enhancement of cell growth as increasing flux density of SMF after 48 h incubation (*p<0.05, **p<0.01, ***p<0.001 from unpaired t-test)

3.3.4 Apoptosis Inhibition

The apoptotic effect on human tumor cells induced by DNA-damaging agents was reduced as a result of the synergetic interaction between the internalized BMPs and the external SMF. While continuously exposed to the SMF, the BMP-HeLa cells were treated for 24 h with cisplatin (10 μg/ml), which is primarily thought to be a DNA-damaging anticancer drug [33]. As shown in Figure 3-12 and 3-13, the apoptotic progression of these BMP-HeLa cells was meaningfully inhibited under the SMF in various concentrations of cisplatin. Decrease in apoptosis was always paralleled by a corresponding increase in the fraction of viable cells, excluding the possibility that the reduction in apoptosis merely reflects a change in the mode of cell death from apoptosis to necrosis.

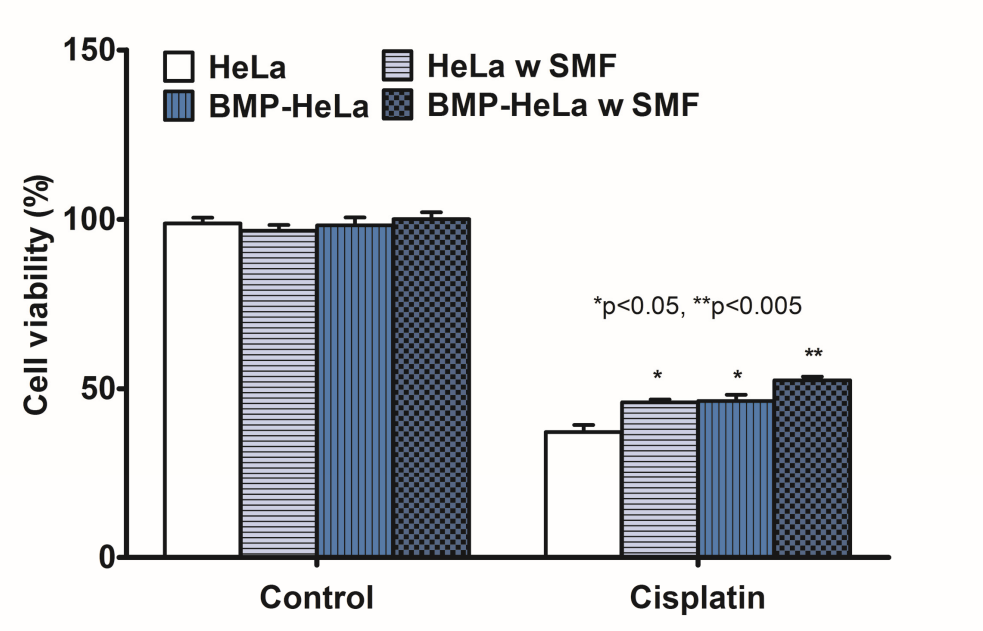

Figure 3-12. Cell viability of HeLa cells treated with 10 μg/ml of cisplatin for 24 h

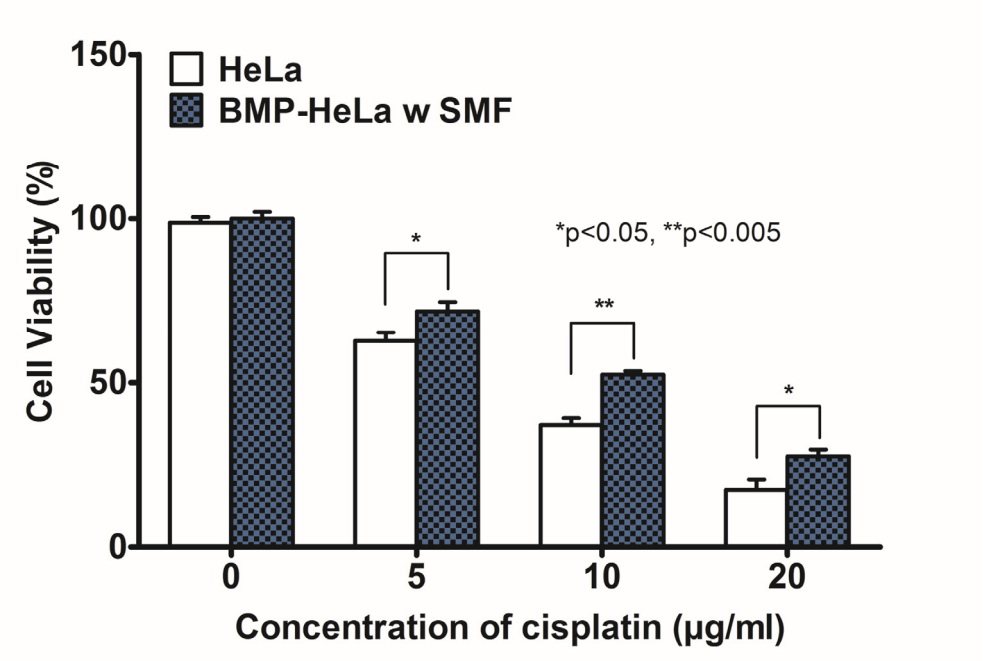

Figure 3-13. Cell viability of HeLa cells treated with various concentration of cisplatin

DNA fragmentation was also investigated using gel electrophoresis to ascertain reduced progress of apoptosis in BMP-HeLa cells under the SMF. The top band presents original DNA and the thickness indicates amount of them in Figure 3-14. The top band of the middle lane was thinner than others, in other words more DNA was fragmented. Lager amount of DNA which is extracted from apoptosis induced HeLa cells were fragmented into short pieces (middle lane in figure 3-14). On the other hand the DNA of BMP-HeLa cells, which treated with cisplatin for 24 h under the magnetic field, slightly fragmented into longer pieces as shown the right lane in Figure 3-14. In this aspect, the BMPs suppressed the progress of apoptosis along with magnetic field.

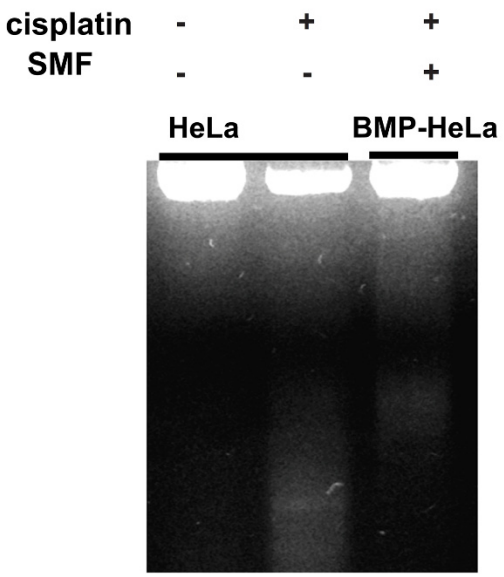

Figure 3-14. DNA gel electrophoresis to confirm DNA fragmentation

This inhibition process was further examined the expression level of *p53* gene in the cisplatin-treated BMP-HeLa cells under the external SMF condition. *p53* gene is regarded as a key regulator of the cellular response to anticancer agents [34-36]. After cisplatin treatment, the p53 mRNA level was modulated in the BMP-HeLa cells exposed to the SMF (Fig. 3-15). HeLa cells show little functional *p53* activity [37] due to the constitutive expression of human papilloma virus E6 protein [38]; thus, these cells appear to be intrinsically resistant to genotoxic stress-induced apoptosis mediated by a *p53* gene product. In the results of experiments, this resistance was pronounced via the magnetic effect.

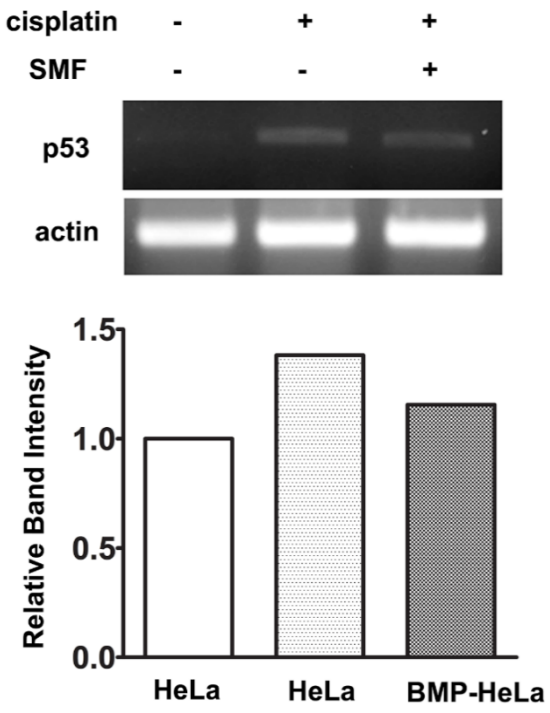

Figure 3-15. p53 gene expression from RT-PCR

3.3.5 Promoted Neuronal Differentiation

Neuronal differentiation of the BMP-SH cells was induced by constant treatment with RA (10 μM/ml) for 7 days under SMF condition. The SMF (100–220 mT) was applied to cells laterally as neuronal differentiation was induced by RA treatment. The neurite length was measured and classified according to three levels of length, i.e., 0–50 μm, 50–100 μm, or over 100 μm, after 7 days of induction of differentiation. The length of the neurites was significantly higher in BMP-SH cells (regardless of their exposure to SMF) than in BMP-free cells, particularly with regard to the ratio of neurites longer than 50 μm (Fig. 3-16, 17).

Neurite outgrowth is a major morphological alteration in neuronal differentiation induced by RA [39]. Improvement of neurite outgrowth with magnetic nanoparticles has been previously reported in another neural cell line, PC12 cells [40]. It has been proposed that magnetic nanoparticles could be exploited to enhance or accelerate nerve regeneration and to provide guidance for regenerating axons [40]. Nanoparticles may also be used to create mechanical tension to stimulate the growth and elongation of axons. These results imply that targeted magnetic cell delivery to injury sites without side effects may be possible using SMF and that BMP-SH cells delivered to lesion sites magnetically may afford efficient regeneration and healing.

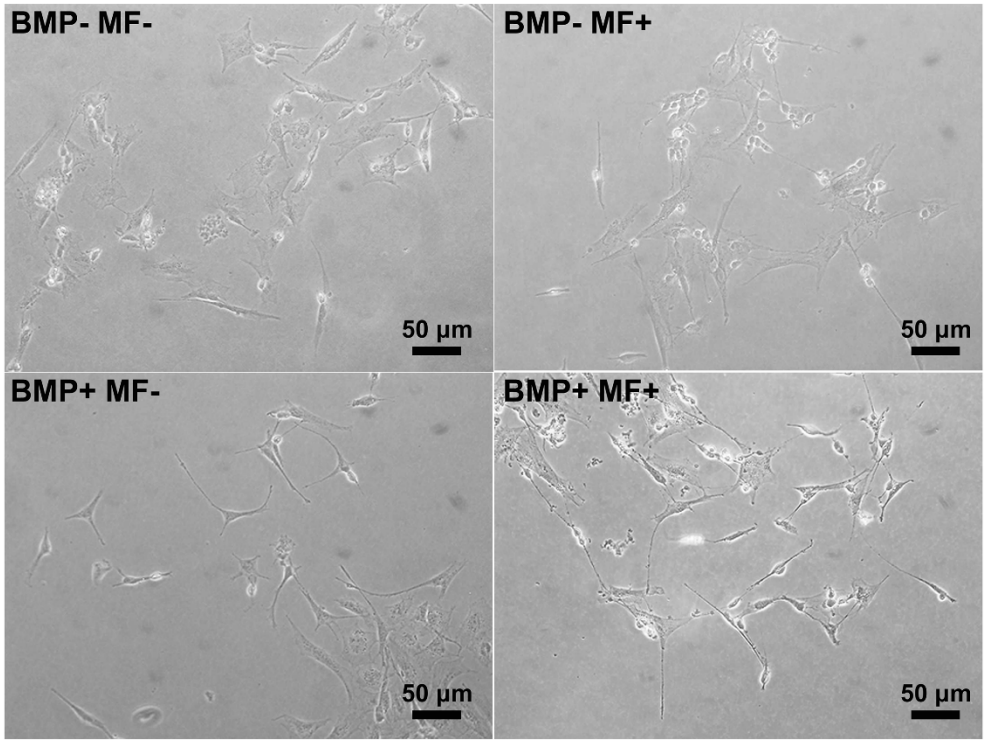

Figure 3-16. Microscope images of SH-SY5Y cells with treatment of RA (10 μM)

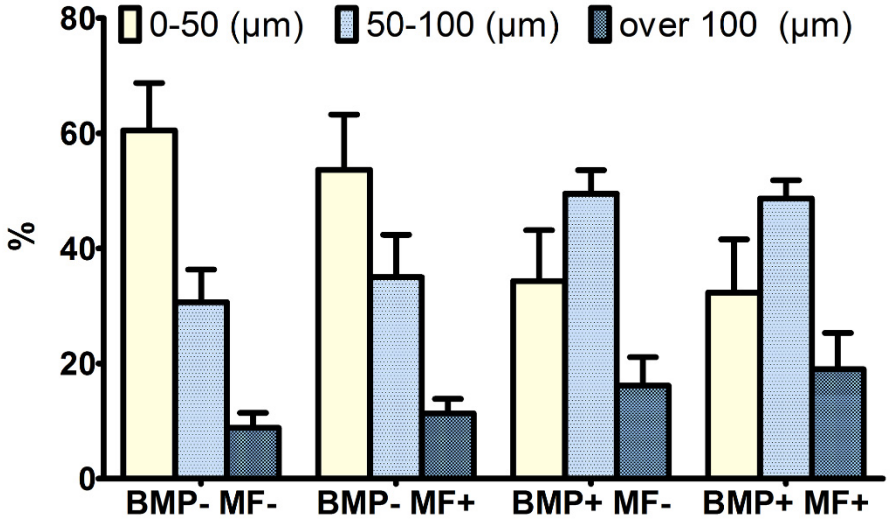

Figure 3-17. Neurite outgrowth length distribution of SH-SY5Y cells

3.4 References

(1) Rosen, A. D.; Chastney, E. E., Effect of long term exposure to 0.5 T static magnetic fields on growth and size of GH3 cells *Bioelectromagnetics* **2009,** *30*, 114.

(2) Dini, L.; Abbro, L., Bioeffects of moderate-intensity static magnetic fields on cell cultures *Micron* **2005,** *36*, 195.

(3) Chionna, A.; Dwikat, M.; Panzarini, E.; Tenuzzo, B.; Carlà, E. C.; Verri, T.; Pagliara, P.; Abbro, L.; Dini, L., Cell shape and plasma membrane alterations after static magnetic fields exposure *Eur. J. Histochem.* **2003,** *47*, 299.

(4) Gartzke, J.; Lange, K., Cellular target of weak magnetic fields: ionic conduction along actin filaments of microvilli *American journal of physiology. Cell physiology* **2002,** *283*, C1333.

(5) Tenuzzo, B.; Chionna, A.; Panzarini, E.; Lanubile, R.; Tarantino, P.; Jeso, B. D.; Dwikat, M.; Dini, L., Biological effects of 6 mT static magnetic fields: A comparative study in different cell types *Bioelectromagnetics* **2006,** *27*, 560.

(6) Kim, J.; Ha, C. S.; Lee, H. J.; Song, K., Repetitive exposure to a 60-Hz time-varying magnetic field induces DNA double-strand breaks and apoptosis in human cells *Biochem. Biophys. Res. Commun.* **2010,** *400*, 739.

(7) Ghodbane, S.; Lahbib, A.; Sakly, M.; Abdelmelek, H., Bioeffects of static magnetic fields: oxidative stress, genotoxic effects, and cancer studies *BioMed research international* **2013,** *2013*, 602987.

(8) Brocklehurst, B.; McLauchlan, K. A., Free radical mechanism for the effects of environmental electromagnetic fields on biological systems *Int. J. Radiat. Biol.* **1996,** *69*, 3.

(9) Belyaev, I. Y.; Alipov, Y. D.; Harms-Ringdahl, M., Effects of zero magnetic field on the conformation of chromatin in human cells *Biochimica et Biophysica Acta (BBA) - General Subjects* **1997,** *1336*, 465.

(10) Thomas, J. R.; Schrot, J.; Liboff, A. R., Low-intensity magnetic fields alter operant behavior in rats *Bioelectromagnetics* **1986,** *7*, 349.

(11) Reiter, R., A review of neuroendocrine and neurochemical changes associated with static and extremely low frequency electromagnetic field exposure *Integr. Physiol. Behav. Sci.* **1993,** *28*, 57.

(12) Kavaliers, M.; Ossenkopp, K. P., *Effects of magnetic and electric fields in invertebrates and lower vertebrates*. Academic-Press: New York, 1994; Vol. 1.

(13) Blackman, C. F.; Benane, S. G.; Rabinowitz, J. R.; House, D. E.; Joines, W. T., A role for the magnetic field in the radiation-induced efflux of calcium ions from brain tissue in vitro *Bioelectromagnetics* **1985,** *6*, 327.

(14) Vorobyov, V. V.; Sosunov, E. A.; Kukushkin, N. I.; Lednev, V. V., Weak combined magnetic field affects basic and morphine-induced rat's EEG *Brain Res.* **1998,** *781*, 182.

(15) Gartzke, J.; Lange, K., Cellular target of weak magnetic fields: ionic conduction along actin filaments of microvilli *American journal of physiology. Cell physiology* **2002,** *283*, C1333.

(16) Denegre, J. M.; Valles, J. M., Jr.; Lin, K.; Jordan, W. B.; Mowry, K. L., Cleavage planes in frog eggs are altered by strong magnetic fields *Proc. Natl. Acad. Sci. U. S. A.* **1998,** *95*, 14729.

(17) Valles, J. M., Jr., Model of magnetic field-induced mitotic apparatus

reorientation in frog eggs *Biophys. J.* **2002,** *82*, 1260.

(18) Aldinucci, C.; Garcia, J. B.; Palmi, M.; Sgaragli, G.; Benocci, A.; Meini, A.; Pessina, F.; Rossi, C.; Bonechi, C.; Pessina, G. P., The effect of strong static magnetic field on lymphocytes *Bioelectromagnetics* **2003,** *24*, 109.

(19) Kale, P. G.; Baum, J. W., Genetic effects of strong magnetic fields in Drosophila melanogaster: I. Homogeneous fields ranging from 13,000 to 37,000 Gauss *Environ. Mutagen.* **1979,** *1*, 371.

(20) Testorf, M. F.; Ake Oberg, P.; Iwasaka, M.; Ueno, S., Melanophore aggregation in strong static magnetic fields *Bioelectromagnetics* **2002,** *23*, 444.

(21) Sato, K.; Yamaguchi, H.; Miyamoto, H.; Kinouchi, Y., Growth of human cultured cells exposed to a non-homogeneous static mangetic field generated by Sm-Co magnets *Biochim. Biophys. Acta* **1992,** *1136*, 231.

(22) Teodori, L.; Göhde, W.; Valente, M. G.; Tagliaferri, F.; Coletti, D.; Perniconi, B.; Bergamaschi, A.; Cerella, C.; Ghibelli, L., Static magnetic fields affect calcium fluxes and inhibit stress-induced apoptosis in human glioblastoma cells *Cytometry* **2002,** *49*, 143.

(23) Jajte, J.; Grzegorczyk, J.; Zmys´lony, M.; Rajkowska, E. b., Effect of 7 mT static magnetic field and iron ions on rat lymphocytes: apoptosis, necrosis and free radical processes *Bioelectrochemistry* **2002,** *57*, 107.

(24) Teodori, L.; Albertini, M. C.; Uguccioni, F.; Falcieri, E.; Rocchi, M. B.; Battistelli, M.; Coluzza, C.; Piantanida, G.; Bergamaschi, A.; Magrini, A.; Mucciato, R.; Accorsi, A., Static magnetic fields affect cell size, shape, orientation, and membrane surface of human glioblastoma cells, as demonstrated by electron, optic,

and atomic force microscopy *Cytometry. Part A : the journal of the International Society for Analytical Cytology* **2005,** *69*, 75.

(25) Wang, Z.; Sarje, A.; Che, P. L.; Yarema, K. J., Moderate strength (0.23-0.28 T) static magnetic fields (SMF) modulate signaling and differentiation in human embryonic cells *BMC Genomics* **2009,** *10*, 356.

(26) YUGE, L.; KATAOKA, K., DIFFERENTIATION OF MYOBLASTS IS ACCELERATED IN CULTURE IN A MAGNETIC FIELD *In Vitro Cell. Dev. Biol. Animal* **2000,** *36*, 383.

(27) Kim, H. J.; Chang, I. T.; Heo, S. J.; Koak, J. Y.; Kim, S. K.; Jang, J. H., Effect of magnetic field on the fibronectin adsorption, cell attachment and proliferation on titanium surface *Clin. Oral Implants Res.* **2005,** *16*, 557.

(28) Smith, C. A.; de la Fuente, J.; Pelaz, B.; Furlani, E. P.; Mullin, M.; Berry, C. C., The effect of static magnetic fields and tat peptides on cellular and nuclear uptake of magnetic nanoparticles *Biomaterials* **2010,** *31*, 4392.

(29) Furlani, E. P.; Ng, K. C., Nanoscale magnetic biotransport with application to magnetofection *Physical Review E* **2008,** *77*, 061914.

(30) Furlani, E.; Ng, K., Analytical model of magnetic nanoparticle transport and capture in the microvasculature *Physical Review E* **2006,** *73*, 061919.

(31) http://www.imstrading.com/magnet-formula.html#drs.

(32) Yang, Y.; Bauer, C.; Strasser, G.; Wollman, R.; Julien, J.-P.; Fuchs, E., Integrators of the cytoskeleton that stabilize microtubules *Cell* **1999,** *98*.

(33) Muggia, F. M., Recent updates in the clinical use of platinum compounds for the treatment of gyneclogic cancers *Semin. Oncol.* **2004,** *31*, 17.

(34) Lane, D. P., p53, guardian of the genome *Nature* **1992,** *358*, 15.

(35) Kastan, M. B.; Onyekwere, O.; Sidransky, D.; Vogelstein, B.; Craig, R. W., Participation of p53 protein in the celluar response to DNA damage *Cancer Res.* **1991,** *51*, 6304.

(36) Kuerbitz, S. J.; Plunkett, B. S.; Walsh, W. V.; Kastan, M. B., Wild-type p53 is a cell cycle checkpoint determinant following irradiation *Proc. Natl. Acad. Sci. USA* **1992,** *89*, 7491.

(37) Matlashewski, G.; Banks, L.; PIM, D.; Crawford, L., Analysis of human p53 proteins and mRNA levels in normal and transformed cells *Eur. J. Biochem.* **1986,** *154*, 665.

(38) Scheffner, M.; Werness, B. A.; Huibregtse, J. M.; Levine, A. J.; Howley, P. M., The E6 oncoprotein encoded by human papillomavirus types 16 and 18 promotes the degradation of p53 *Cell* **1990,** *63*, 1129.

(39) Påhlman, S.; Ruusala, A.-I.; Abrahamsson, L.; Mattsson, M. E. K.; Esscher, T., Retinoic acid-induced differentiation of cultured human neuroblastoma cells: a comparison with phorbolester-induced differentiation *Cell Differ.* **1984,** *14*, 135.

(40) Kim, J. A.; Lee, N.; Kim, B. H.; Rhee, W. J.; Yoon, S.; Hyeon, T.; Park, T. H., Enhancement of neurite outgrowth in PC12 cells by iron oxide nanoparticles *Biomaterials* **2011,** *32*, 2871.

Chapter 4. Mechanism of the Synergistic Effect

4.1 Introduction

4.1.1 Diamagnetic Anisotropy of Biomolecules

Diamagnetism is a property of an object or materials that causes it to create a magnetic field in opposition to an externally applied magnetic field. Diamagnetic materials are repelled by magnetic fields and the magnetic permeability (μ) of the materials is smaller than the permeability of free space (μ_0). Molecules have tendency to orient in a magnetic field as a result of anisotropy in their diamagnetic susceptibility.

The diamagnetic anisotropy of molecules is defined by the difference between parallel; axial ($\chi_{\parallel}$ or χ_a) and perpendicular; radial ($\chi_{\perp}$ or χ_r) diamagnetic susceptibility as below equation.

$$\Delta\chi = \chi_a - \chi_r$$

Figure 4-1 shows diamagnetic anisotropy of a rod-like molecule with cylindrical coordinate. The diamagnetic anisotropy of biological molecules has been reported and it is summarized in Table 4-1. The negative value of the diamagnetic anisotropy ($\chi_a < \chi_r < 0$) implies that lipids will orient with their long axis perpendicular to the field, and the positive value ($\chi_r < \chi_a < 0$) would cause a molecule to align parallel to the field.

The orientation of various molecular components in magnetic fields of several

kilogauss have been reported, which occurred due to their magnetic anisotropic properties, retinal rod [1-2]; chloroplasts [3], photosynthetic algae and bacteria [4]; purple membranes [5]; and nucleic acids [6]. Earlier studies related to magnetic anisotropy was also reported in cellulosic materials [7], in silks, keratins, and collagens, and in muscle fibers [8]. The diamagnetic anisotorpy in protein was studied that is attributed to the diamagnetic anisotropy of the planar peptide bonds [9]. The anisotopy values of chemical groups and proteins are summarized in Table 4-2.

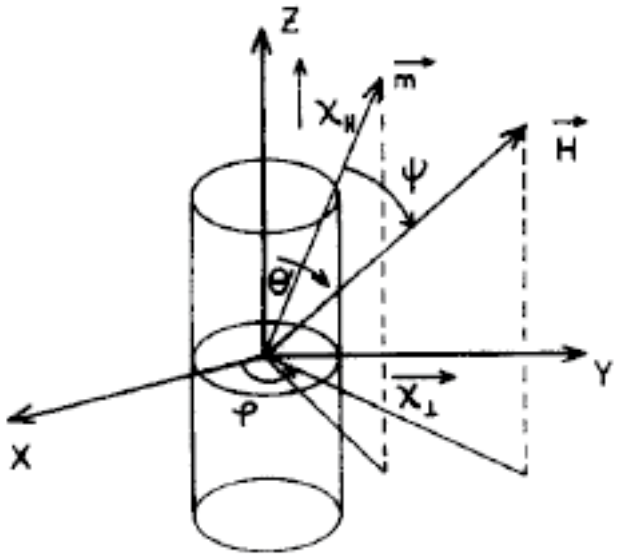

Figure 4-1. Rod-like diamagnetically anisotropic molecule with indication of the applied magnetic field, H, the induced magnetic moment, m, and the magnetic susceptibilities, parallel (χ_{II}) and perpendicular ($\chi_{\perp}$) to the longer molecular axis [10]

Table 4-1. Diamagnetic anisotropy of biological molecules

Molecules	**Diamagnetic anisotropy (SI units)**
Egg lecithin vesicles	-3.5×10^{-6} [11]
	-5.98×10^{-6} [12]
Lipids ($DC_{23}PC$)	-0.09×10^{-6} [13]
DMPC lecithin	-12.3×10^{-6} [12]
Red blood cell dry membranes	$-(2.8 \pm 0.1) \times 10^{-6}$ [14]

$DC_{23}PC$: 1,2-bis(10,12-tricosadiynoyl)-sn-glycero-3-phosphocholine

DMPC: 1,2-dimyristoyl-sn-glycero-3-phosphocholine

Table 4-2. Diamagnetic anisotropy of chemical groups and proteins [9]

Chemical groups and proteins	**Diamagnetic anisotropy (SI units)**
Ester, Peptide	8.8×10^{-6}
Carboxyl	4.5×10^{-6}
Benzene	54×10^{-6}
α-helix	4.4×10^{-6}
β-Sheet	1.1×10^{-6}
Collagens	-2.2×10^{-6}

The degree of orentation, β, is directly proportional to the diamagnetic anisotropy, $\Delta\chi$, and is described as below equation.

$$\beta = \frac{\Delta\chi H^2}{k_B T},$$

where k_B is Boltzmann's constant and T is the absolute temparture, it is the ratio of magnetic to thermal energy. The degree of orentation is usually quite small even for molecules with large values of $\Delta\chi$. However, the anisotorpy and the degree of orentation are proportional to the number of moclecules (N) in a system which is composed of parallely arranged diamagnetically anisotropic molecules [15].

$$\beta = \frac{N\Delta\chi H^2}{k_B T}$$

When β>1, the orientation of a molecular system would occur. This magnetic alignment of biological membranes has been reported in magnetic fields and Figure 4-2 clearly showed the experimental observation [11, 16]. The diamagnetic anisotropic properties of membrane phospholipids would result in the reorientation of the cell membrane during exposure to SMF [17-18].

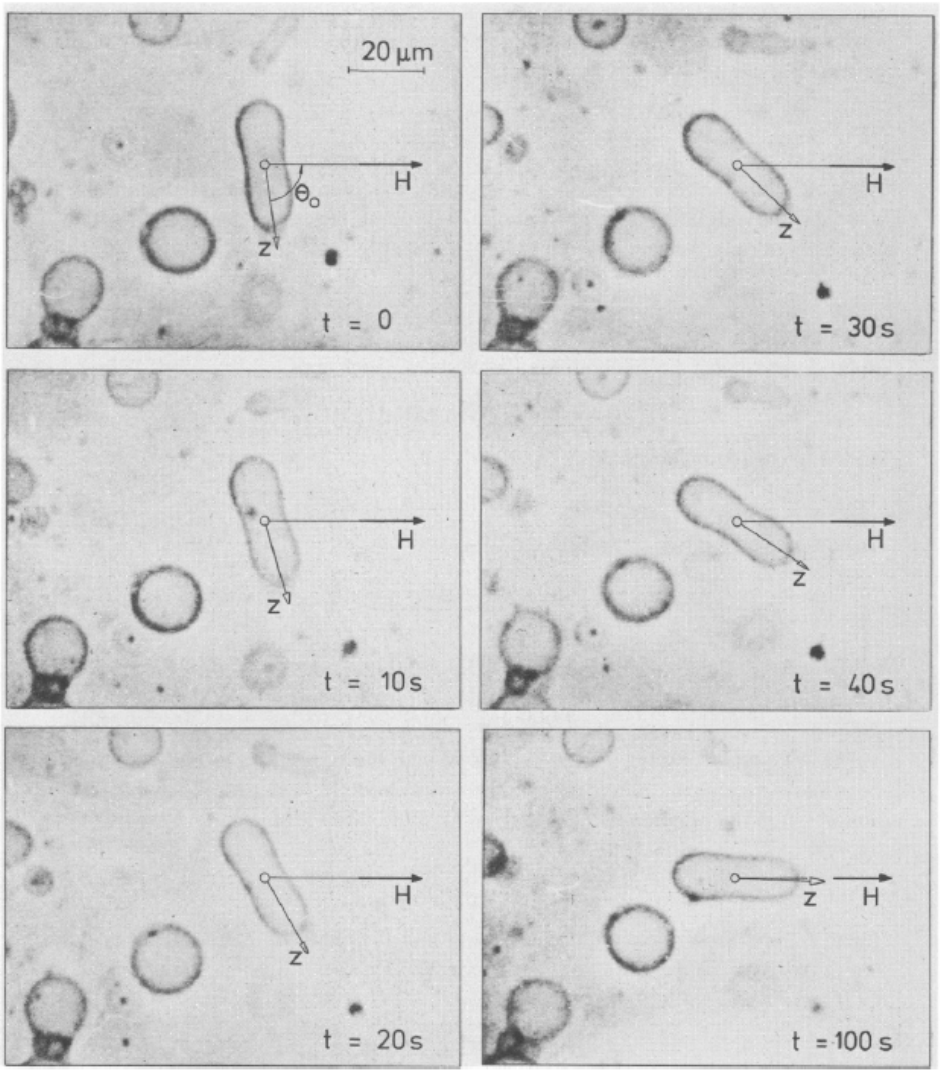

Figure 4-2. Time sequence of alignments of a cylindrical vesicle in a magnetic field, *H* [11]

4.1.2 Cell Membrane Composition

Cell membrane, plasma membrane, consists of a variety of biological molecules, notably lipids and proteins (Fig. 4-3). The fundamental structure of the membrane is the phospholipid bilayer, which forms a stable barrier between two aqueous compartments; inside (cytoplasm) and outside of the cell. Proteins embedded within the phospholipid bilayer fulfill the specific functions of the plasma membrane, including selective transport of molecules and cell-cell communication [19]. The cell membranes are complex and dynamic environments, the lipid components of the bilayer specifically and nonspecifically interact with membrane proteins affecting both structure and function [20].

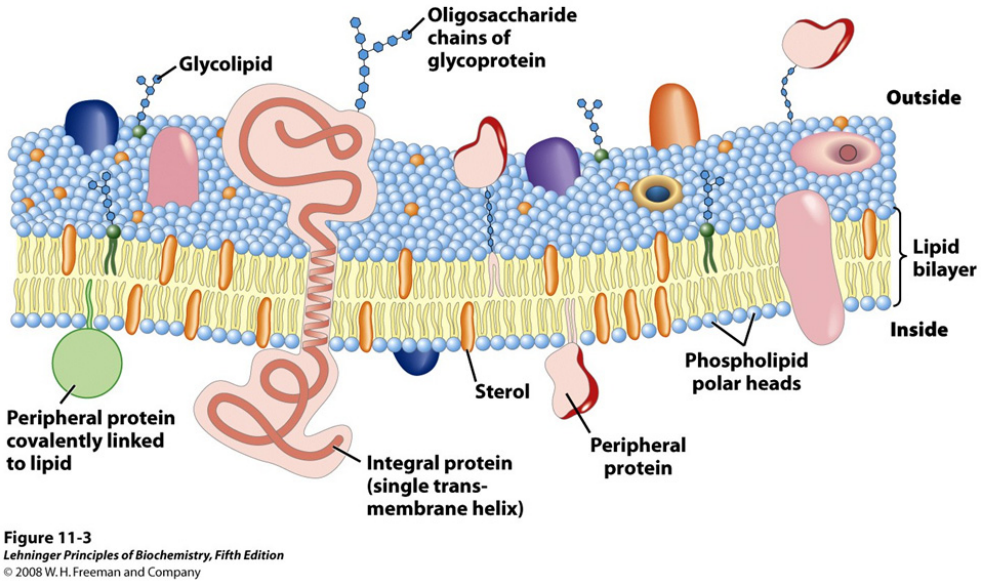

Figure 4-3. Structure of the cell membrane [21]

4.1.3 G-protein Coupled Receptor (GPCR)

An efficient system of cellular communication allows cells to respond to environmental stimuli as well as to each other by integrating the numerous extracellular and intercellular cues that they are constantly receiving into a coordinated response [22]. G-protein coupled receptors (GPCR) constitute a large protein family of receptors that perceive many extracellular signals as major mediators of intercellular communication. More than 800 distinct GPCRs are estimated to exist in the human genome, about half are predicted to be olfactory receptors. Activated GPCRs regulate a wide spectrum of intracellular biochemical changes resulting in the modulation of many aspects of physiology, growth, development and disease control [23]. Despite diversity in function, GPCRs are structurally similar, which is characterized by an extracellular N-terminus, followed by seven transmembrane (7-TM) α-helices connected by three intracellular and three extracellular loops, and finally an intracellular C-terminus (Fig. 4-4).

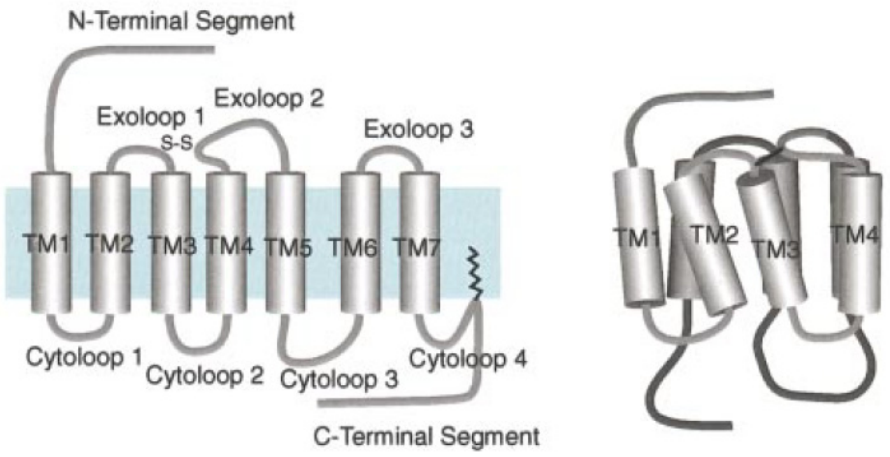

Figure 4-4. Schematic presentation of the general structure and terminology of GPCRs [24]

Upon stimulation, GPCRs activate specific members of a smaller family of G proteins that act as signal transducers that, in turn, activate a variety of second messenger systems [25]. A general mechanism of signal transduction through GPCR and G-proteins is shown in Figure 4-5. In the inactive state, Gα is bound to Gβγ dimer and GDP. The G-protein mediated signaling is triggered by binding of a ligand molecule that gives rise to activation of GPCR. The activated GPCR catalyzes exchange of guanosine triphosphate (GTP) for guanosine diphosphate (GDP) on the Gα subunit and then conformational changes occur in the GPCR, which leads to dissociation of Gβγ dimer from Gα. The dissociated Gα and Gβγ proteins bind to various effectors and then the effectors pass the signal to different kinds of second messengers. Inactivation of GPCR is caused by re-associating the Gα with Gβγ.

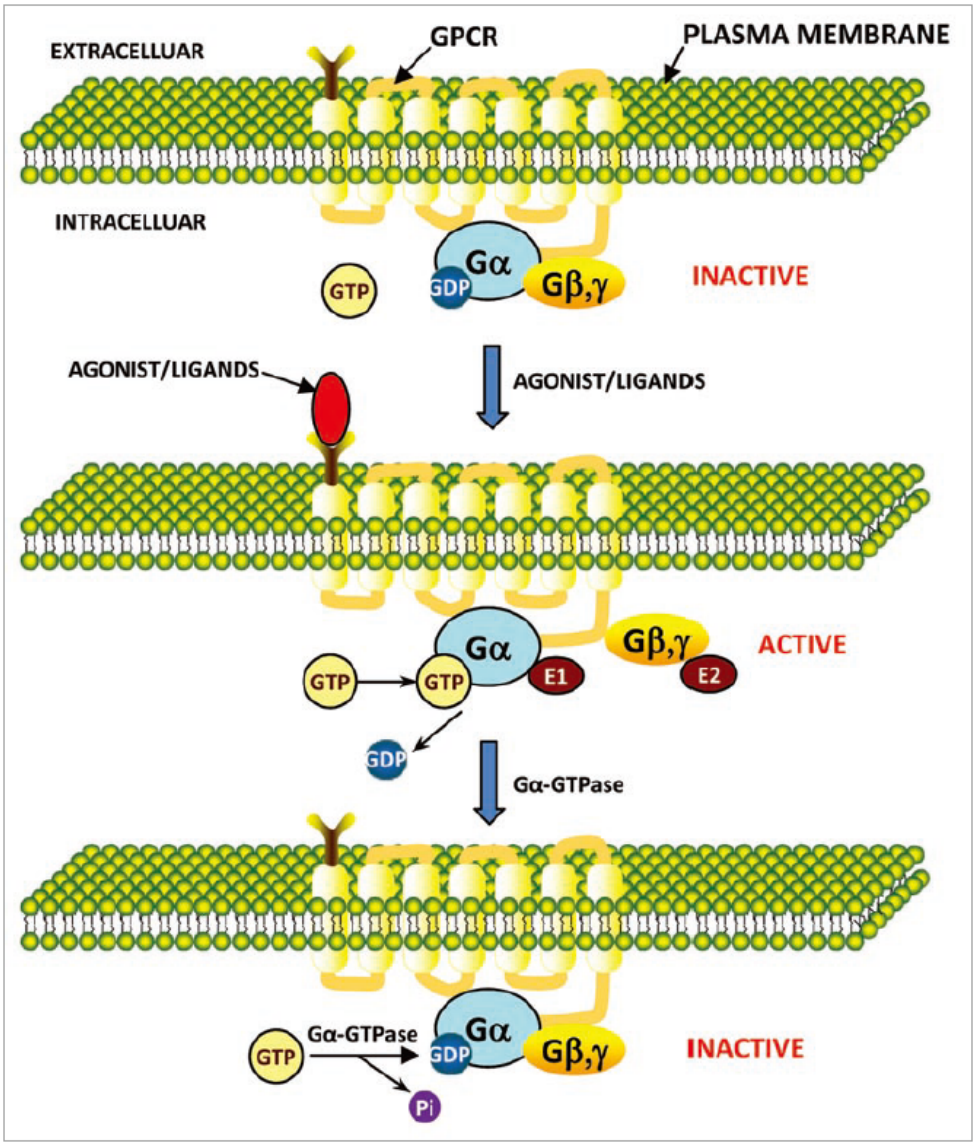

Figure 4-5. Model for signal transduction by activation/inactivation of heterotrimeric G proteins through GPCR [26]

As GPCRs are involved in regulation of many aspects of cellular physiology, the diversity of biological effects is function of both the size of the GPCR family and cell types. In case, the same receptor may induce different responses in different cell types. These diverse regulation of GPCRs offer a wide range of opportunities as therapeutic drug targets in areas including cancer, cardiac dysfunction, diabetes, central nervous system disorders, obesity, inflammation, and pain [27]. Thus, many drug discovery firms and researchers focus exclusively on these receptors.

4.2 Materials and Methods

4.2.1 Microarray

Total RNA was extracted as described above and then RNA yields were measured using UV absorbance (NanoDrop Technologies, Wilmington, DE). The quality of total RNA was assessed using the Agilent 2100 Bioanalyzer (Agilent Technologies, USA). 1 μg of total RNA were added to mixture in a final volume of 12 μl, containing T7 oligo dT primer. The mixture was incubated for 10 min at 70°C and then chilled into ice for 5 min. 2 μl of 10X first-strand buffer, 4 μl of 5 mM dNTP mix, 1 μl of RNase inhibitor (20 U/μl) and 1 μl of SuperscriptTM II RNase H– reverse transcriptase (200 U/μl) were added into mixture to make a final volume of 20 μl. The reaction mixture was incubated for 2 h at 42°C. To synthesize second-strand cDNA, 10 μl of 10X second-strand buffer, 63 μl of nuclease free water, 4 μl of 5 mM dNTP mix, 2 μl of DNA polymerase mix (20 U/μl) and 1 μl of RNase H (2 U/μl) were added into the mixture of 20 μl. The reaction mixture was incubated for 2 h at 16°C. The dsDNA was purified and then the volume of dsDNA solution was adjusted using drying the solution or adding the nuclease free water to make a final volume of 14 μl. 4 μl of 10X reaction buffer, 12 μl of ATP, CTP, GTP mixture (25 mM), 3 μl of UTP (50 mM), 3 μl of amino allyl UTP and 4 μl of T7 enzyme were added into 14 μl of dsDNA solution for the IVT (in vitro transcription) reaction. The reaction mixture was incubated for 14 h at 37°C and then cRNA was purified. cRNA yield

was quantified by measuring the UV absorbance at 260 nm, and 5 μg of cRNA for each sample was coupled with Cy5-dye (GE Healthcare, UK). 2 μg of Cy5-dye labeled cRNA (target) was fragmented for hybridization.

Fragmented target was added into 2X Hi-RPM hybridization buffer (Agilent Technologies, USA). Hybridization solution was applied onto Human GE 4x44K v2 Microarray (Agilent Technologies, USA) and then microarray was hybridized for 16 h at 60°C. Microarray was washed with wash solution I (6X SSC, 0.00005% Triton-X 102) for 1 min at 37°C and then microarray was washed with wash solution II (0.1X SSC, 0.00005% Triton-X 102) for 1 min at room temperature.

Microarray was scanned using Agilent High-Resolution Microarray Scanner (Agilent Technologies, USA), and the scanned image were analyzed using Feature Extraction Software (Agilent Technologies, USA) to obtain the signal intensity of spots. The signal intensity was normalized by median normalization method. Each experiment was repeated twice and unpaired t-test was performed between control group and test group.

4.3 Results and Discussion

4.3.1 Mechanism

The combined stimulation of internalized BMPs and external SMF exposure to cells induced morphological changes, improved cell growth and inhibited apoptosis of HeLa cells (described in Chapter 3). The primary mechanism of the responses is elucidated in accordance with the shrunk bodies of cells under the exposure of 480 mT SMF (shown in Fig. 3-5 and 3-6).

The diamagnetic anisotropy of cell membrane which is composed of phospholipid bilayer elicited the conformational changes. The negative anisotropy of lipids leads to the rearrangement of cell membrane, a lipid molecule tends to align perpendicular direction of applied magnetic field. The cells attached and spread on the surface without exposure to the magnetic field, which means that most of lipid molecules in cell membrane arranged vertically (Fig. 4-6 (a)). The SMF was applied with vertical direction of cells in experiments, thus most of the lipid molecules rearranged horizontally; perpendicular direction of the field (Fig. 4-6(b)). This realignment of the cell membrane could cause conformational and functional alterations of transmembrane proteins including ion channels and GPCRs [17, 28-32].

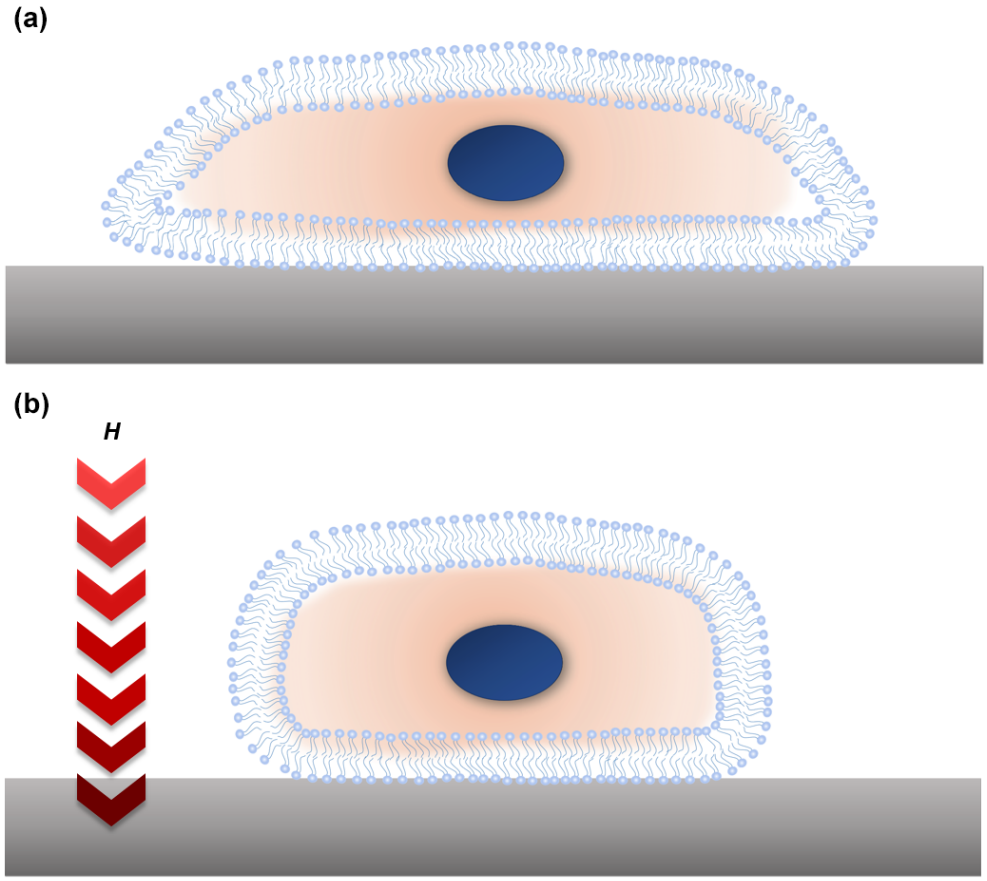

Figure 4-6. Schematic diagram of lipid bilayer arrangement in cell membrane (a) without the SMF exposure and (b) with the SMF exposure

In addition to the external SMF exposure, the BMPs internalized in cells were contributed to local enhancement of the magnetic field intensity inside cells. The increasing intensity of magnetic field was evaluated to verify the effectiveness by simulation using COMSOL multiphysics 3.5 (Appendix). These results suggested

the synergistic effect of BMPs and SMF on the magnetic flux density.

The diamagnetic anisotropic property of cell membrane and magnetic field intensification around BMPs are considered to give rise to the responses of cells described in Chapter 3. However the specific effects of internalized BMPs is remained to be discovered by further research.

4.3.2 Proposed Signaling Pathway

In order to explore the modulation of genes induced by the synergistic effect of the BMPs and an SMF, microarray analysis was performed using the Human GE 4x44K v2 Microarray (Agilent Technologies, USA). The intensity of genes was normalized for the three samples (non-exposed BMP-HeLa cells, exposed HeLa cells, and exposed BMP-HeLa cells to the SMF) to control background HeLa gene expression.

The genes were selected, which showed a p-value of less than 0.1 at least for one of the three samples. Then up and down regulated genes over 1.5-fold in the BMP-HeLa cells under the SMF compared with the other cells were reselected. The selected genes were categorized according to their function using the Database for Annotation, Visualization and Integrated Discovery (DAVID) v6.7 to find biological meaning and classify the selected genes into significant functional groups. Heat maps were generated for all up or down regulated genes over 1.5 fold in BMP-HeLa cells under SMF exposure compared with other cells (Fig. 4-7). The value of classified genes was compared using hierarchical clustering by complete linkage (cluster 3.0).

Figure 4-8 represents the predicted model of signal transduction in the context of up-regulated genes caused by the synergetic effect of the internalized BMPs and the external SMF. A number of up-regulated genes were found to be related to the

transmembrane receptor and ion transport protein. GPCRs-mediated signaling was particularly noticeable among the up-regulated genes (Table 4-3). GPCRs are key regulators for cellular communication, mediating the efficient coordination of a cell's responses to extracellular stimuli. As shown in Figure 3-5 and 3-6, external SMF was primarily responsible for the alteration of cellular structure. Therefore, it is supposed that external SMF alters the cell membrane because of the diamagnetic anisotropy of membrane phospholipids [33], which in turn initiate the modulation of GPCR with chemokine-chemokine receptor binding. SMF-initiated GPCRs related signal transductions, and then, should be stimulated by multiplied local MF around internalized BMPs.

Activated GPCRs promote a wide spectrum of intracellular biochemical remodeling, resulting in the modulation of many aspects of physiology, growth, development, and disease control [34]. This activation is mediated by coupling to intracellular heterotrimeric G-protein associated with the inner surface of the plasma membrane [35]. Thus, the G-proteins in the cell system regulate downstream signaling, resulting in the eventual modulation of transcription, gene expression, and proliferation via ERK/PI3K/p38 [34, 36]. The increased ATP level in the BMP-HeLa cells under the SMF (Fig. 3-8) may be involved in ERK and PI3K signaling pathways [37]. ERK has been reported to mediate anti-apoptotic effects in DNA-damaged cells, and p53 transactivation activity has been linked with the sustained activation of ERK [38].

These observations are in agreement with the results regarding the response of cisplatin-treated BMP-HeLa cells under the SMF. Ion transport is also affected by up-regulation of G-protein combined stimuli with somatostatin receptors, which modulate Ca^{2+} and K^{+} ion channels [39]. Ca^{2+} represents the most important intracellular signaling pathway, governing almost all physiological functions in differentiated cells; particularly, cytoplasmic Ca^{2+} determines the rate of cell proliferation [40].

Down-regulated genes were found to be involved in hydrolase, endoplasmic reticulum, and Golgi apparatus regulation. However, a significant signal transduction stream was not identified within the examined genes.

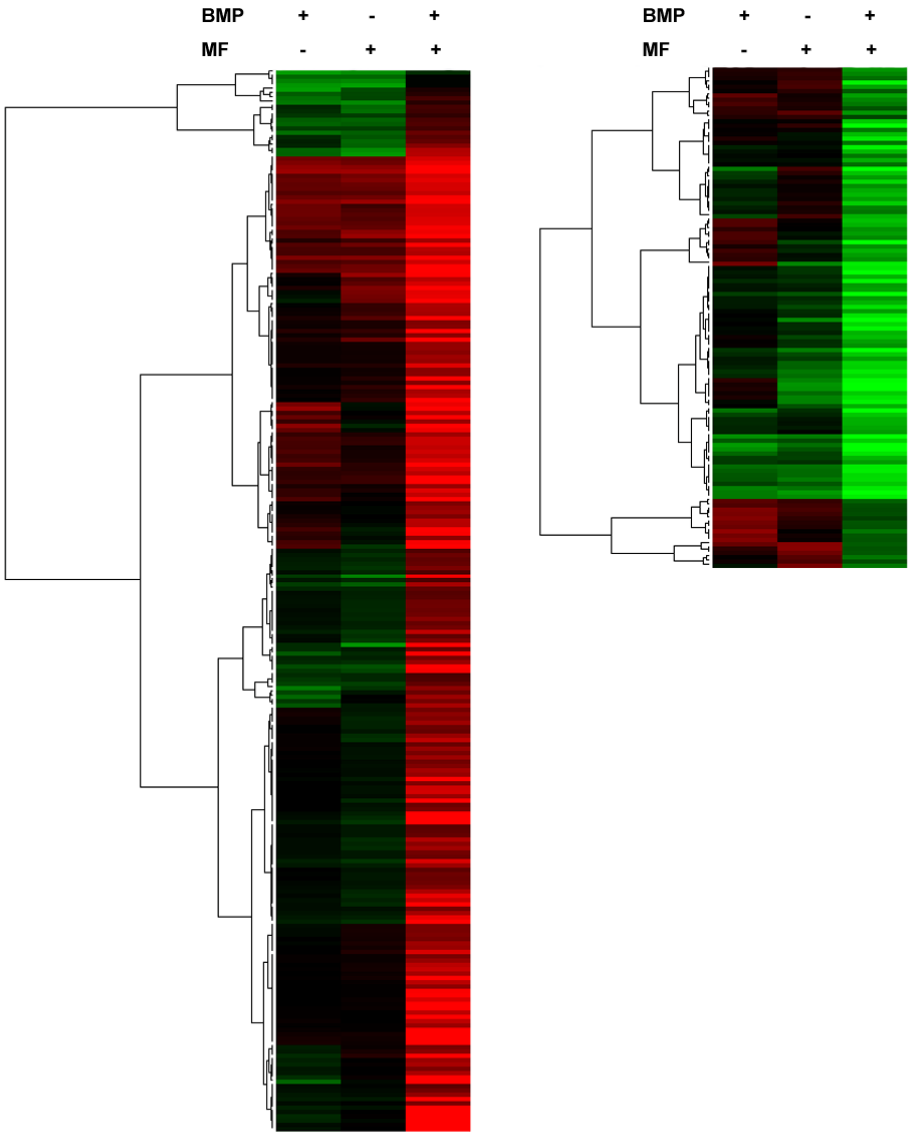

Figure 4-7. Heat maps of up (left) and down (right) regulated genes; the red represents up-regulation and the green represent down regulation

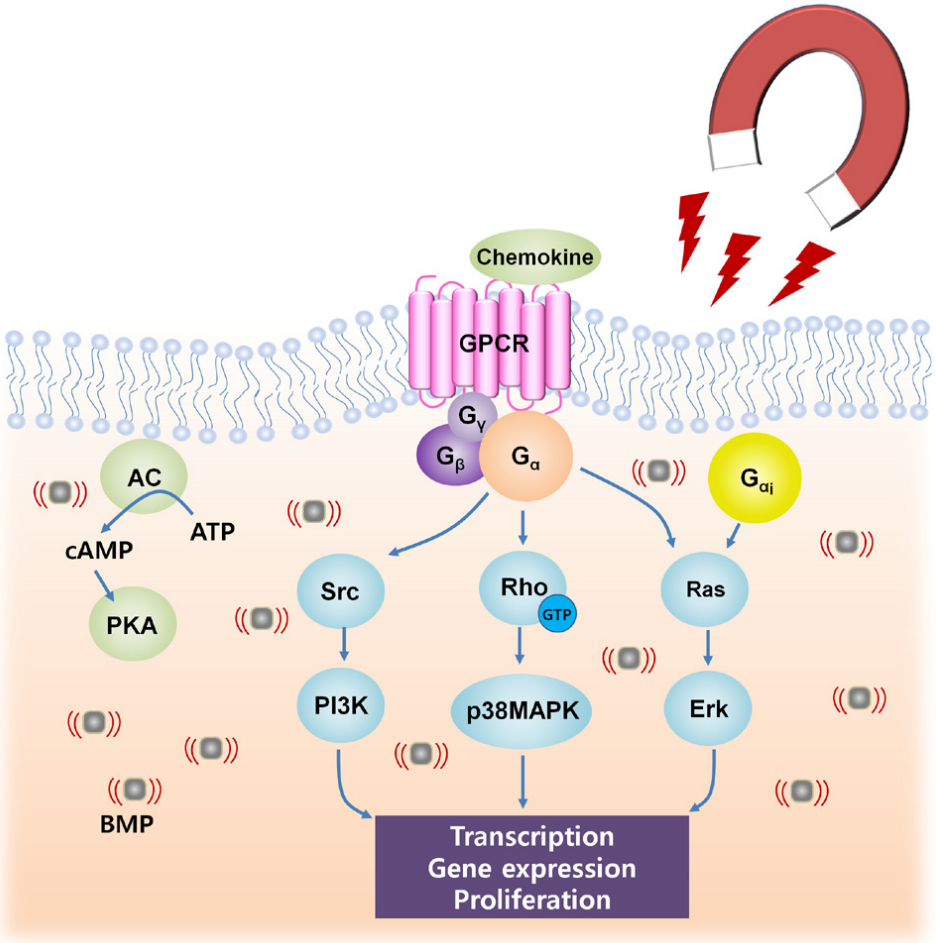

Figure 4-8. A model of the GPCR mediated intracellular signal transduction pathway induced by internalization of BMPs and external exposure of SMF

Table 4-3. Expression level of genes involved in the model of GPCR mediated signaling pathway

	Gene Name	Log_2 ratio		
		BMP-HeLa/HeLa	HeLa w SMF/HeLa	BMP-HeLa w SMF/HeLa
GPCR	G protein-coupled receptor, family C, group 5, member B	0.192	0.017	0.632
	G-protein coupled receptor family C, group 5, member C Precursor	-0.269	-0.160	0.653
	G protein-coupled receptor 146	-0.103	0.066	0.615
	G protein-coupled receptor 160	0.684	0.443	1.063
	leucine-rich repeat-containing G protein-coupled receptor 4	-0.071	0.146	0.780
G-Protein	guanine nucleotide binding protein (G protein) alpha 12	0.444	0.496	0.774
PI3K	phosphoinositide-3-kinase, catalytic, beta polypeptide	0.846	0.872	1.217
	phosphoinositide-3-kinase, catalytic, alpha polypeptide	0.093	0.571	0.766

Table 4-3.–Continued

Chemokine	chemokine (C-X-C motif) ligand 12 (stromal cell-derived factor 1)	0.098	0.118	0.981
AC	adenylate cyclase 1	-0.198	-0.321	0.751
PKA	protein kinase, X-linked	0.542	0.707	0.908
Src	hemopoietic cell kinase	-0.011	0.040	1.547
p38MAPK	mitogen-activated protein kinase 13	0.081	0.358	1.012
Rho	Rho family GTPase 1	-0.003	0.214	1.330
Ras	v-Ki-ras2 Kirsten rat sarcoma viral oncogene homolog	0.317	0.035	1.203
	neuroblastoma RAS viral (v-ras) oncogene homolog	0.119	0.381	0.608
	Ras-like without CAAX 1	-0.053	0.252	0.524
ERK	extracellular signal-regulated kinase 2	0.119	0.074	0.213
SSTR	somatostatin receptor 2	-0.031	-0.151	0.676

4.4 References

(1) Chalazonitis, N.; Chagneux, R.; Arvanitaki, A., Rotation of external segments of photoreceptors in constant magnetic field *C. R. Acad. Sci. Hebd. Seances Acad. Sci. D.* **1970,** *271*, 130.

(2) Hong, F. T.; Mauzerall, D.; Mauro, A., Magnetic anisotropy and the orientation of retinal rods in a homogeneous magnetic field *Proc. Natl. Acad. Sci. U. S. A.* **1971,** *68*, 1283.

(3) Geacintov, N. E.; Van Norstrand, F.; Becker, J. F.; Tinkel, J. B., Magnetic field induced orientation of photosynthetic systems *Biochim. Biophys. Acta* **1972,** *267*, 65.

(4) Breton, J., The state of chlorophyll and carotenoid in vivo. II. A linear dichroism study of pigment orientation in photosynthetic bacteria *Biochem. Biophys. Res. Commun.* **1974,** *59*, 1011.

(5) Neugebauer, D. C.; Blaurock, A. E.; Worcester, D. L., Magnetic orientation of purple membranes demonstrated by optical measurements and neutron scattering *FEBS Lett.* **1977,** *78*, 31.

(6) Maret, G.; Schickfus, M. v.; Mayer, A.; Dransfeld, K., Orientation of Nucleic Acids in High Magnetic Fields *Phys. Rev. Lett.* **1975,** *35*, 397.

(7) Nilakantan, P., Magnetic anisotropy of naturally occurring substances *Proc. Indian Acad. Sci. Sect. A* **1938,** *7*, 38.

(8) Arnold, W.; Steele, R.; Mueller, H., ON THE MAGNETIC ASYMMETRY OF MUSCLE FIBERS *Proceedings of the National Academy of Sciences* **1958,** *44*, 1.

(9) Worcester, D. L., Structural origins of diamagnetic anisotropy in proteins *Proc. Natl. Acad. Sci. U. S. A.* **1978,** *75*, 5475.

(10) AZANZA, M. J.; MORAL1, A. D., Cell membrane biochemistry and neurobiological approach to biomagnetism *Prog. Neurobiol.* **1994,** *44*, 517.

(11) BOROSKE, E.; HELFRICH, W., Magnetic anisotropy of egg lecithin membranes *Biophys. J.* **1978,** *24*, 863.

(12) Scholz, F.; Boroske, E.; Helfrich, W., Magnetic anisotropy of lecithin membranes. A new anisotropy susceptometer *Biophys. J.* **1984,** *45*, 589.

(13) Rosenblatt, C.; Yager, P.; Schoen, P. E., Orientation of lipid tubules by a magnetic field *Biophys. J.* **1987,** *52*, 295.

(14) Azanza, M. J.; Blott, B. H.; del Moral, A.; Peg, M. T., Measurement of the red blood cell membrane magnetic susceptibility *Bioelectrochem. Bioenerget.* **1993,** *30*, 43.

(15) Maret, G.; Dransfeld, K., Macromolecules and membranes in high magnetic fields *Physica B+C* **1977,** *86–88, Part 3*, 1077.

(16) Hong, F. T., Photoelectric and magneto-orientation effects in pigmented biological membranes *J. Colloid Interface Sci.* **1977,** *58*, 471.

(17) Rosen, A. D., Studies on the effect of SMF on biological systems *PIERS online* **2010,** *6*, 133.

(18) Speyer, J. B.; Sripada, P. K.; Das Gupta, S. K.; Shipley, G. G.; Griffin, R. G., Magnetic orientation of sphingomyelin-lecithin bilayers *Biophys. J.* **1987,** *51*, 687.

(19) GM, C., Structure of the Plasma Membrane. In *The Cell: A Molecular Approach*, 2nd ed.; Sinauer Associates: Sunderland (MA), 2000.

(20) Tillman, T. S.; Cascio, M., Effects of membrane lipids on ion channel structure and function *Cell Biochem. Biophys.* **2003,** *38*, 161.

(21) Nelson, D. L.; Cox, M. M., *Lehninger Principles of Biochemistry*. 5th ed.; W. H. Freeman and Company: 2008.

(22) New, D. C.; Wong, Y. H., Molecular mechanisms mediating the G protein-coupled receptor regulation of cell cycle progression *J Mol Signal* **2007,** *2*, 2.

(23) Pierce, K. L.; Premont, R. T.; Lefkowitz, R. J., Seven-transmembrane receptors *Nature reviews. Molecular cell biology* **2002,** *3*, 639.

(24) Ji, T. H.; Grossmann, M.; Ji, I., G protein-coupled receptors. I. Diversity of receptor-ligand interactions *J. Biol. Chem.* **1998,** *273*, 17299.

(25) Herr, D. R., Potential use of G protein-coupled receptor-blocking monoclonal antibodies as therapeutic agents for cancers *International review of cell and molecular biology* **2012,** *297*, 45.

(26) Tuteja, N., Signaling through G protein coupled receptors *Plant signaling & behavior* **2009,** *4*, 942.

(27) Filmore, D., It's a GPCR world *Mod. Drug Discovery* **2004,** *7*, 24.

(28) Rosen, A. D., Membrane response to static magnetic fields: effect of exposure duration *Biochim. Biophys. Acta* **1993,** *1148*, 317.

(29) Rosen, A. D., Inhibition of calcium channel activation in GH3 cells by static magnetic fields *Biochim. Biophys. Acta* **1996,** *1282*, 149.

(30) Rosen, A. D., Effect of a 125 mT static magnetic field on the kinetics of voltage activated Na+ channels in GH3 cells *Bioelectromagnetics* **2003,** *24*, 517.

(31) Shen, J. F.; Chao, Y. L.; Du, L., Effects of static magnetic fields on the voltage-gated potassium channel currents in trigeminal root ganglion neurons *Neurosci. Lett.* **2007,** *415*, 164.

(32) Iwasaka, M.; Suzuki, K.; Sugawara, T., Observations of cellular responses to diamagnetic forces acting on cell components *Science and Technology of Advanced Materials* **2008,** *9*, 024216.

(33) Rosen, A. D., Mechanism of Action of Moderate-Intensity Static Magnetic Fields on Bological Systems *Cell Biochem. Biophys.* **2003,** *39*, 163.

(34) New, D. C.; Wong, Y. H., Molecular mechanisms mediating the G protein-coupled receptor regulation of cell cycle progression *Journal of Molecular Signaling* **2007,** *2*, 2.

(35) Teicher, B. A.; Fricker, S. P., CXCL12 (SDF-1)/CXCR4 pathway in cancer *Clin. Cancer. Res.* **2010,** *16*, 2927.

(36) Goldsmith, Z. G.; Dhanasekaran, D. N., G protein regulation of MAPK networks *Oncogene* **2007,** *26*, 3122.

(37) Wilden, P. A.; Agazie, Y. M.; Kaufman, R.; Halenda, S. P., ATP-stimulated smooth muscle cell proliferation requires independent ERK and PI3K signaling pathways *Am J Physiol heart Circ Physiol* **1998,** *275*, H1209.

(38) Heo, J.-I.; Oh, S.-J.; Kho, Y.-J.; Kim, J.-H.; Kang, H.-J.; Park, S.-H.; Kim, H.-S.; Shin, J.-Y.; Kim, M.-J.; Kim, S. C.; Park, J.-B.; Kim, J.; Lee, J.-Y., ERK mediates anti-apoptotic effect through phosphorylation and cytoplasmic localization of p21Waf1/Cip1/Sdi in response to DNA damage in normal human embryonic fibroblast (HEF) cells *Mol. Biol. Rep.* **2010,** *38*, 2785.

(39) Akopian, A.; Johnson, J.; Gabriel, R.; Brecha, N.; Witkovsky, P., Somatostatin modulates voltage-gated K^+ and Ca^{2+} currents in rod and cone photoreceptors of the salamander retina *J. Neurosci.* **2000,** *20*, 929.

(40) Gartzke, J.; Lange, K., Cellular target of weak magnetic fields: ionic conduction along actin filaments of microvilli *American journal of physiology. Cell physiology* **2002,** *283*, C1333.

Chapter 5. Application: Magnetic Manipulation of Neurosphere

5.1 Introduction

5.1.1 Cell Therapy

Cell therapy is defined as the therapy in which cellular materials such as stem cell and progenitor cell are injected into a patient. This therapy is targeted to multiple organs by delivery several modes of cell which facilitate therapeutic action. The delivered cells via local or systemic administration, stem cell or progenitor cell, differentiate into a specific cell type after reaching the site of injury. Then damaged tissue is replaced by integrating with injected cells and facilitated improved function of the organ.

The clinical application of stem cells has shown promise for cell transplantation therapies [1-6]. However, identifying the optimum delivery strategy of the cells to the injury site remains a major challenge. Specific targeting of cells to sites of tissue damage and delivery of high numbers of transplanted cells to lesion tissue in vivo are critical parameters for the success of cell-based therapies. Targeting and differentiation of stem cells at sites of injury and repair of damaged tissue are exciting areas of research in regenerative medicine.

Delivery of stem cells to specific targets in vivo has been achieved via direct needle injection to the site of delivery [3, 6-9], local infusion [3, 10-11], or preferential homing or distribution following systemic administration. Despite of the

achievement, these delivery methods generally suffer from a lack of precise localization, low repeatability, and local damage to the injection site.

The versatile intrinsic properties of magnetic particles render them useful for targeted cell therapy, where magnetic carriers loaded with cells can be directed or guided by means of a magnetic field gradient toward biological targets [12-13]. Recent studies have shown that magnetic labeling of cells is relatively easy and safe [14-16]. However, only a few studies have used magnetic fields to guide magnetic particle-loaded cells to specific targets because of low uptake at the site of injury [17-18].

5.1.2 Neurosphere

The neurosphere culture system was the first in vitro system to unequivocally demonstrate the presence of cells in the adult brain with characteristics of true neural stem cells [19-20] and remains an extremely useful tool to analyze proliferation, self-renewal capacity, and multipotency of neural stem and progenitor cells. The culture system comprised of free-floating clusters of neural stem cells. Generally, neurospheres are derived from a single-cell suspension of neural stem and progenitor cells isolated from the adult or fetal central nervous system (CNS), but neurosphere cultures can also be established from ES cells (Figure 5-1) [21]. The composition and properties of cells are affected by variation in detail culture method, thus it is required to culture under the right circumstances [22].

The neurosphere culture system has also the potential to offer an unlimited number of neural stem and progenitor cells initially derived from either the fetal or adult CNS, thereby enabling the production of an on-demand source of cells that can be standardized, quality tested, and relatively easily genetically modified if needed. Some successful researches have been reported that a considerable number of neurons were obtained after transplantation of neurosphere expanded cells into neurogenic areas of the brain [23-25].

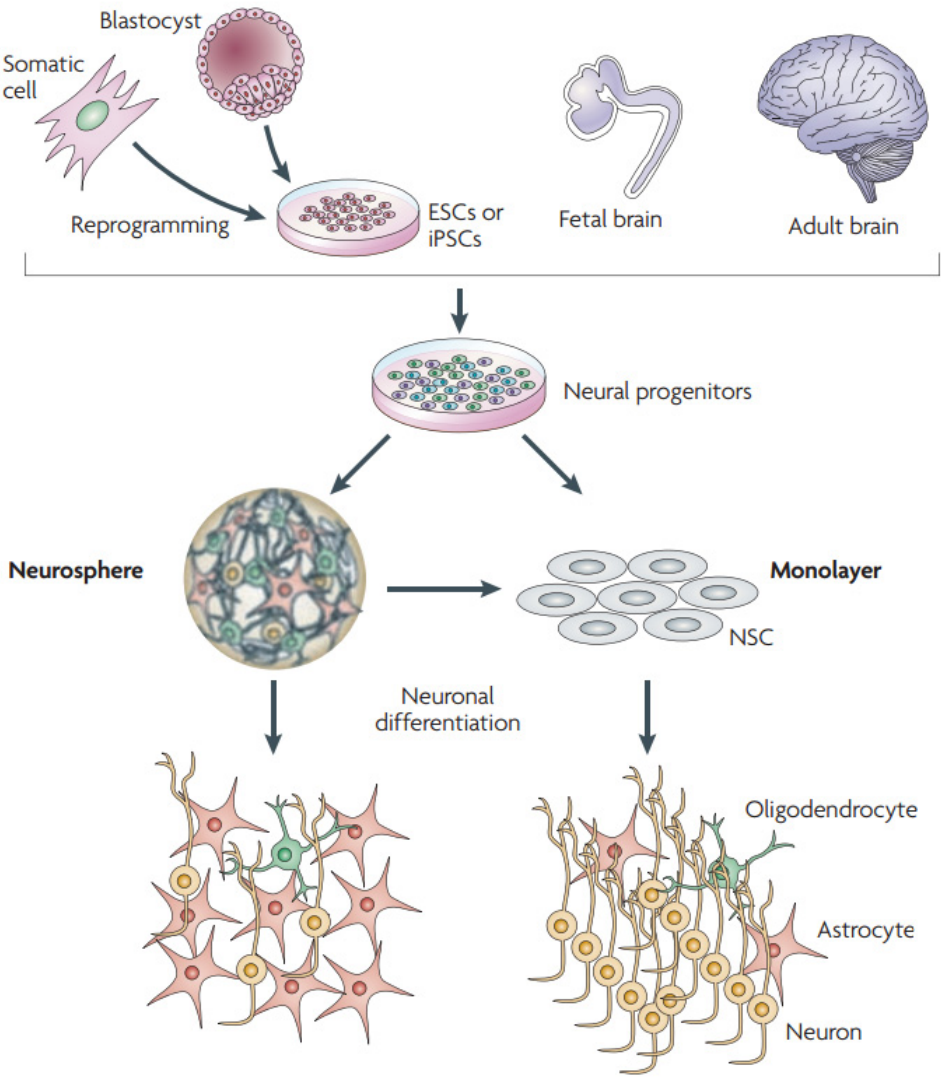

Figure 5-1. Sources of neurospheres and monolayer Nscs and results of differentiation [26]

5.2 Materials and Methods

5.2.1 Neurosphere Culture

5.2.1.1 Neurosphere formation

The cells were cultured to 80% confluency in BMP-free culture medium and then treated with BMPs (10 μg/ml applied to more than 10^6 cells) in serum-reduced medium (1% FBS) and incubated overnight to allow internalization of BMPs. The BMP-loaded cells (BMP-SH) were separated from non-BMP-loaded cells using a magnet. For neurosphere formation, the cells were cultured in floating culture for 5 days.

5.2.1.2 Cell Membrane Staining

The cell membrane of SH-SY5Y cells was labeled with red fluorescent dye (PKH26, Sigma-Aldrich, USA) for tracking of single cells and neurospheres in the target site. The labeling of cell membrane using PKH26 followed protocol provided by manufacturer, as briefly described here. Cultured cells (10^7 cells) were trypsinized and collected by centrifuge at 1000 rpm for 5 min. The cells were washed with serum (FBS) free medium by immersing and centrifuge. Then the cells were dispersed in 500 μl of Diluent C (Sigma-Aldrich, USA) and mixed with solution, the 1 μl of PKH26 dye dissolved in 500 μl of Diluent C. After 5 min incubation at room temperature, the cell samples were incubated with 1 ml of serum containing culture

medium for 1 min. The cells were separated the dye containing solution by centrifuge and discarding the remaining solution, then washed with fresh medium tree times to remove remaining dyes. Finally the cells were dispersed in adequate medium for subsequent studies.

Individual cells were cultured under the appropriate conditions for the subsequent experiments and neurospheres were formed. Stained cells were examined using a fluorescence microscope (Nikon, Japan) and a confocal microscope (LSM710, Carl Zeiss, Germany).

5.2.2 BMP-loaded Neurosphere Manipulation

5.2.2.1 Non-Flow

In the non-flow condition, the magnetic field was produced by placing an NdFeB magnet one side. The motion of the membrane labeled BMP-NSs was observed within 2 mm from the magnet, where the field gradient was approximately 40 T/m, using an inverted microscope (Nikon, Japan).

5.2.2.2 Neurosphere Capture in Capillary Tube

To study the delivery of BMP-SHs and BMP-NSs into a simulated spinal cord under flow conditions, a glass capillary tube with a diameter of 1 mm was employed. The inner surface of the tube was coated with fibronectin to permit attachment of the cells on the surface after delivery. The sterilized capillary tube was filled with a solution of 100 μg/ml fibronectin in 1× PBS, incubated overnight at room temperature, and then dried. A syringe pump (KD Scientific, USA) was used to introduce the cells dispersed in culture medium (10^4 cells or spheres) into the capillary tube with a stable flow rate of 22.6 ml/h. As the cells flowed in the tube, a focused magnetic field was applied to a target point to capture the cells using an edge of the magnet that generated approximately 100 T/m of field gradient. The capillary tube filled with the culture medium, and captured cells were incubated at 37°C for 20 h in a humidified

5% CO_2 atmosphere after delivery of the cells. The movement of the BMP-SHs and BMP-NSs under flow conditions and attachment of the cells on the inner surface of the tube were examined using a fluorescence microscope (Nikon, Japan).

5.3 Results and Discussion

5.3.1 Neurosphere

5.3.1.1 Neurosphere Formation

A neurosphere is a free-floating spherical cluster of neural stem cells obtained from floating cultures in vitro [27]. Neurosphere-derived cells have been successfully used in models of neurological injury such as experimental autoimmune encephalomyelitis and spinal cord injury [28-30]. Therefore, neurospheres may be useful for the delivery of therapeutic cells to lesion sites.

SH-SY5Y human neuroblastoma cells can grow in neurospheres under floating culture conditions without requiring special treatment such as serum and growth factors. It was confirmed that the BMP-SH cells formed neurospheres with morphological features similar to those of spheres formed by the control SH-SY5Y cells without BMP (Figure 5-2). The size of the neurospheres was heterogeneous and varied from 50 to 300 μm after from 5 to 10 days of free-floating culture. Also, as shown in Figure 5-3, the green spots indicating FITC-labeled BMPs were maintained in the cells as they grew into neurospheres. The neurospheres formed from single BMP-SH cell theoretically have the same amount of BMPs found in individual BMP-SH cells.

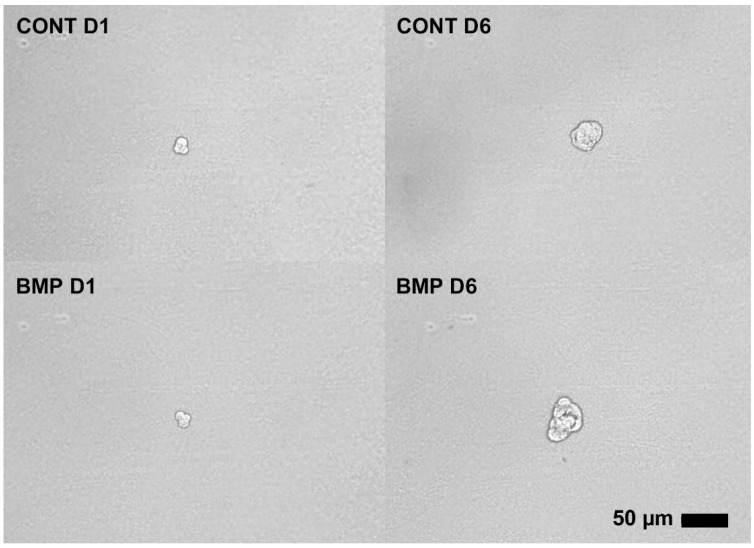

Figure 5-2. Neurosphere culture of control SH-SY5Y cells and BMP-loaded cells after incubation for 1 day; D1 and 6 days; D6

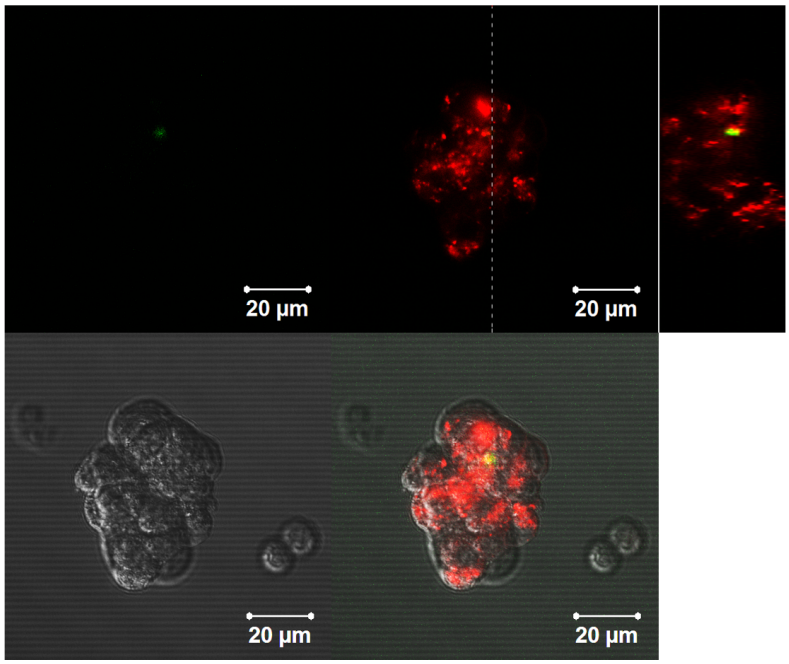

Figure 5-3. Confocal image of BMP-NS with cross section view, green: BMPs; red: cell membrane

5.3.1.2 Attachment of Neurosphere on Surface

Moderately grown neurospheres (diameter, ~100–200 μm) were isolated and cultured on an extracellular matrix (ECM) coated surface to investigate transplantation of neurospheres after delivery to target the site. The neurospheres attached to the surface, and individual cells from the neurospheres migrated to the surrounding area (Fig. 5-4) by way of similar pattern with control cells (Fig. 5-5). The results shows that the BMP-NSs could be applied for delivery of therapeutic cells with similar functionality of neurospheres from control cells.

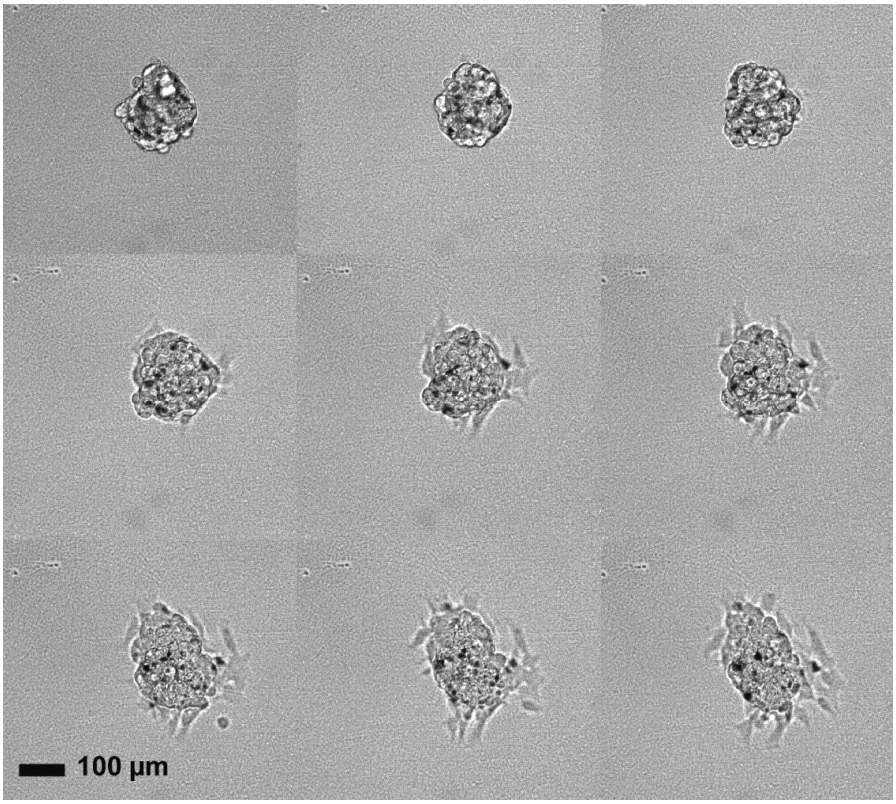

Figure 5-4. Attachment and spreading of BMP-NS observed hourly for 8 h

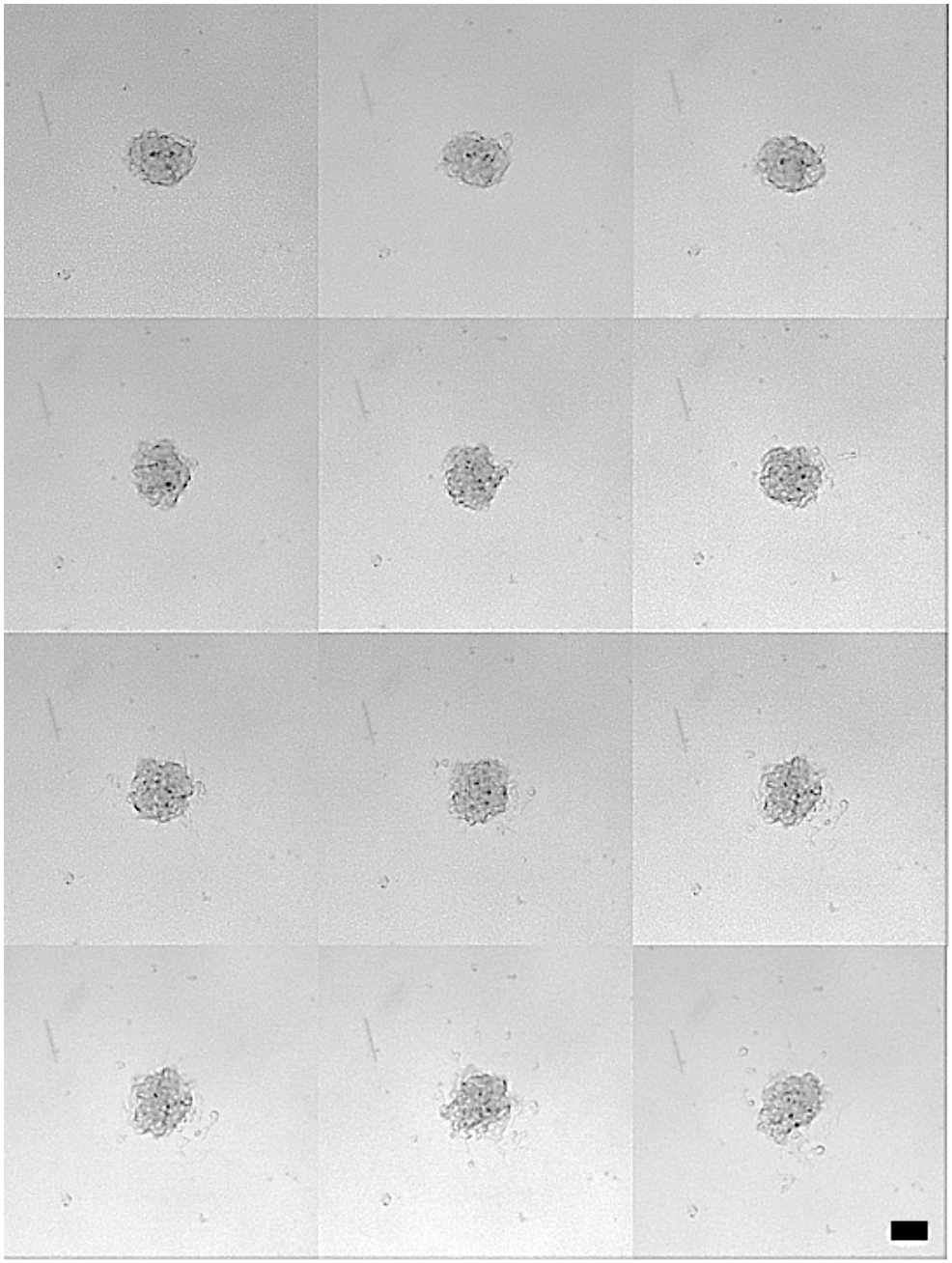

Figure 5-5. Attachment and spreading of a BMP-free neurosphere observed hourly for 11 h, scale bar: 100 μm

5.3.2 Manipulation

5.3.2.1 Non-Flow

The BMP-NS has the potential to be spatially manipulated by virtue of its free-floating form and the magnetic reactivity of the BMPs it contains. Therefore, we investigated the potential of magnetic manipulation to translocate the BMP-NSs to target sites. Initially, a one-dimensional (1-D) model of BMP-NS dynamics was generated under non-flow conditions. The transport of BMP-NSs in fluid is influenced by both hydrodynamic and magnetic forces. The Newtonian relationship for a neurosphere motion with absolute velocity $\vec{v}_{NS}$ is described as

$$\left(\frac{\pi {d_{NS}}^3}{6}\rho_{NS}\right)\frac{d\vec{v}_{NS}}{dt} = \vec{F}_m + \vec{F}_d + \vec{F}_g$$

, with the magnetic, drag, and gravitational forces on the right side [31]. In the 1-D model, the gravitational force is not relevant and the inertia force can be neglected with extremely low acceleration. Thus, the magnetic force balances the drag force of the BMP-NS as

$$\mathrm{F}_m = F_d$$

$$\mu_{\mathrm{f}} V_{BMP} \mathrm{M}_{\mathrm{s,BMP}} \frac{\mathrm{dH_a}}{\mathrm{dx}} = 6\pi \boldsymbol{\eta} R_{NS}\left(v_{NS} - v_f\right),$$

where μ_f is the permeability of the transport fluid, which is similar to the permeability of free space μ_0; $4\pi \times 10^{-7}$, V_{BMP} is the volume of a cluster of BMPs in BMP-NS; 1.68×10^{-18} m^3, $M_{s,BMP}$ is the saturation magnetization of BMPs; 437.90 kA/m, H_a is

the externally applied magnetic field intensity at the center of the BMP-NS, $\boldsymbol{\eta}$ is the fluid viscosity; 0.72×10^{-3} kg/s, R_{NS} is the radius of BMP-NS, υ_{NS} is the velocity of BMP-NS, and υ_f is the fluid velocity.

The uptake of BMPs in an SH-SY5Y cell was determined to be 8.69 pg/cell (described in section 2.3.2.2), and it is assumed that the cluster of internalized BMPs is located in the centre of a BMP-NS. The magnetic force exerted on a BMP-NS from the media was estimated identically to the previous section 3.3.1. The 1-D distribution of H_a is thus described as

$$H_a = \frac{M_s}{\pi}\left[\left[\tan^{-1}\frac{\mathrm{WL}}{2x(4x^2+\mathrm{W}^2+\mathrm{L}^2)^{\frac{1}{2}}}\right] - \tan^{-1}\left[\frac{\mathrm{WL}}{2(x+\mathrm{T})[4(x+\mathrm{T})^2+\mathrm{W}^2+\mathrm{L}^2]^{\frac{1}{2}}}\right]\right] H_a$$

$$= \frac{M_s}{\pi}\left[\left[\tan^{-1}\frac{\mathrm{WL}}{2x(4x^2+\mathrm{W}^2+\mathrm{L}^2)^{1/2}}\right] - \tan^{-1}\left[\frac{\mathrm{WL}}{2(x+\mathrm{T})[4(x+\mathrm{T})^2+\mathrm{W}^2+\mathrm{L}^2]^{1/2}}\right]\right],$$

where M_s is the saturation magnetization of the NdFeB magnet; 909.46 kA/m, W is the width; 25 mm, and L is length of the magnet; 50 mm. In this non-flow model, R_{NS} was 50 μm and υ_f is 0. According to the equations, the speed of BMP-NS transport toward the magnet is 29.42 μm/s when x is 2 mm from the magnet.

Figure 5-6 shows that a BMP-NS with a radius of 50 μm moved approximately 1.93

mm in 60 s. The theoretical prediction, 1.77 mm of movement in 60 s, matched well with the experimental data under non-flow conditions.

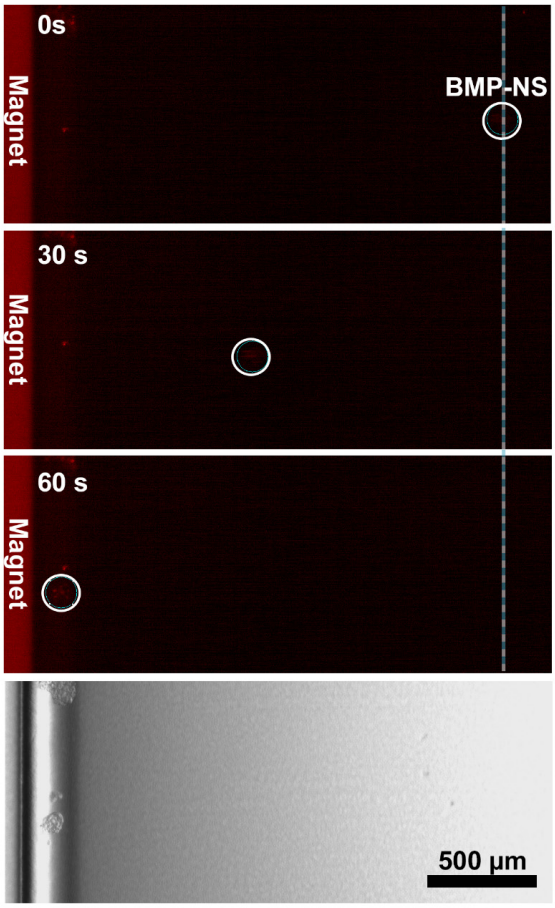

Figure 5-6. One-dimensional motion of a BMP-NS in non-flow condition under the magnetic field gradient

5.3.2.2 Flow in Capillary Tube

The capture of BMP-NSs at a target site was performed under steady flow conditions. The flow rate was 2 mm/s in a capillary tube with an internal diameter of 1 mm, which mimics the physiological condition of rat spinal fluid (Fig. 5-7(a)) [32].

An external magnetic field was applied around the capillary tube using an NdFeB magnet. The intensity of the two-dimensional magnetic field around the capillary tube was evaluated using the COMSOL Multiphysics 3.5 (Fig. 5-7(b)). The magnetic flux density decreased rapidly as the distance from the surface of the magnet increased. The magnetic field gradient generated by the NdFeB magnet was approximately ~100 T/m in the capillary region, with the goal of capturing neurospheres with a diameter of ~50 μm. The BMP-SH cells and BMP-NSs dispersed in culture medium (10^4 cells or spheres) were introduced to the capillary using syringe pump.

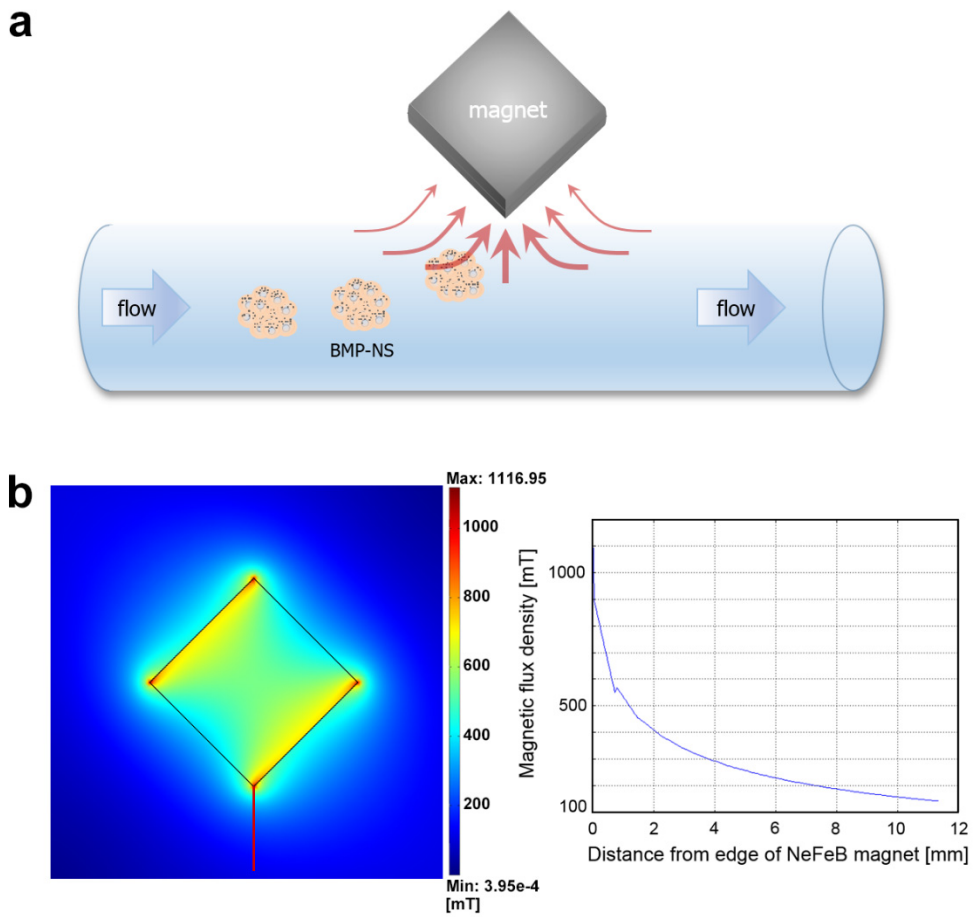

Figure 5-7. (a) Schematic of in vitro model system to capture BMP-NSs (b) magnetic flux density on surface (2D surface plot; left) and perimeter of the magnet (graph; right, magnetic flux density at the red line in 2D surface plot)

Effective targeting of the magnetic nanoparticle-incorporated cells depended on the magnetic susceptibility of the cells and their linear velocity within the tube. The magnetic susceptibility of the cells was related to the degree of cellular uptake of the magnetic nanoparticles. Interestingly, as shown in Figure 5-8(a) and (b), more cells were captured in the target site (magnetic field-focusing region) in the BMP-NSs than in the BMP-SHs, although the amount of BMPs internalized in a BMP-NS and a BMP-SH cell was theoretically identical.

A BMP-NS composed of many individual BMP-SH cells, which facilitate to capture more cells at once. Furthermore, BMP-NSs captured earlier on the surface acted as a stopper with a large volume and reduced the speed of the following neurospheres in flow, which were then more easily affected by magnetic force (Fig. 5-9). These advantages of the neurosphere rendered the capture efficiency of the BMP-NSs to be increased at the target site.

The captured cells were incubated overnight in the presence of the magnetic field under normal cell culture conditions, i.e., 37°C in humidified atmosphere containing 5% CO_2. The individual BMP-SH cells and BMP-NSs were well attached to the inner surface of the capillary tube coated with fibronectin after overnight incubation (Fig. 5-8 (c, d)). This study confirmed that the BMP-NSs were more effective for transplantation of a large amount of neuronal cells at once in an in vitro model system.

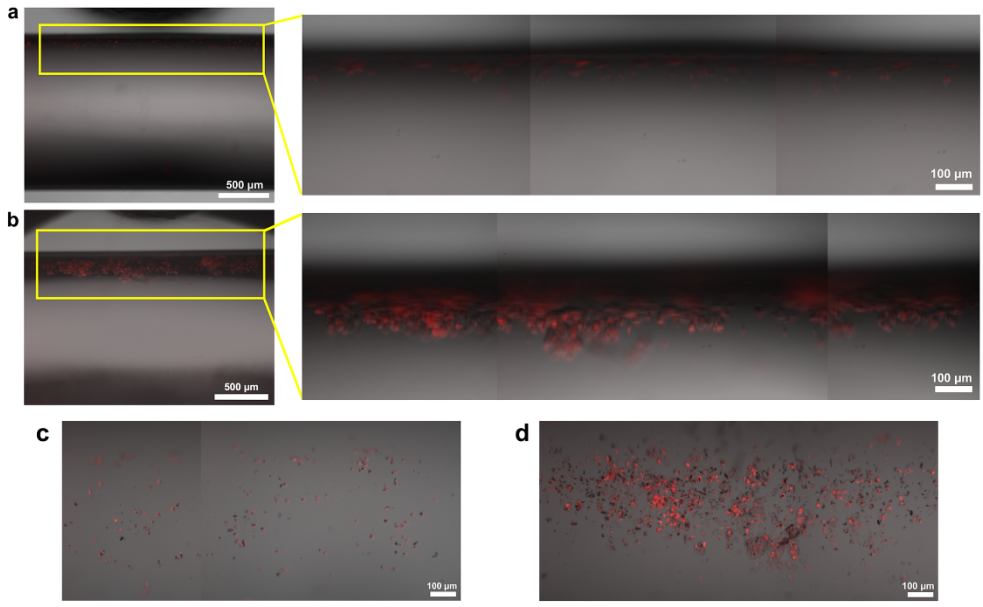

Figure 5-8. Images of captured BMP-SH cells (a) BMP-NSs (b) in capillary with 2 mm/s of flow rate, and images after overnight culture of BMP-SH cells (c) and BMP-NSs (d), the red represents PKH26-stained cell membrane; scale bars: 100 µm

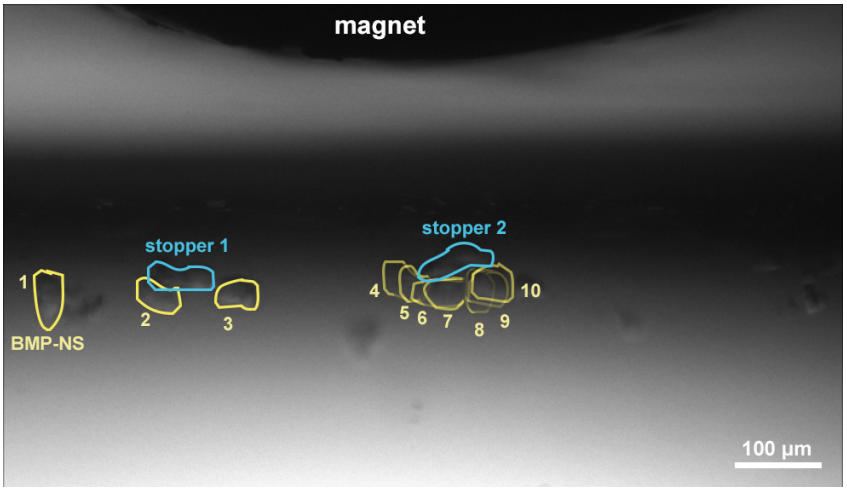

Figure 5-9. Tracking a BMP-NS every 2 s; yellow circles, stoppers; pre-captured BMP-NSs

5.4 References

(1) Al Mheid, I.; Quyyumi, A. A., Cell therapy in peripheral arterial disease *Angiology* **2009,** *59*, 705.

(2) Wollert, K. C.; Drexler, H., Clinical applications of stem cells for the heart *Circ. Res.* **2005,** *96*, 151.

(3) Yeo, C.; Mathur, A., Autologous bone marrow-derived stem cells for ischemic heart failure: REGENERATE-IHD trial *Regen. Med.* **2009,** *4*, 119.

(4) Snowden, J. A.; Martin-Rendon, E.; Watt, S. M., Clinical stem cell therapies for severe autoimmune diseases *Transfus. Med.* **2009,** *19*, 223.

(5) Borlongan, C. V., Cell therapy for stroke: remaining issues to address before embarking on clinical trials *Stroke* **2009,** *40*, S146.

(6) Tateishi-Yuyama, E.; Matsubara, H.; Murohara, T.; Ikeda, U.; Shintani, S.; Masaki, H.; Amano, K.; Kishimoto, Y.; Yoshimoto, K.; Akashi, H.; Shimada, K.; Iwasaka, T.; Imaizumi, T., Therapeutic angiogenesis for patients with limb ischaemia by autologous transplantation of bone-marrow cells: a pilot study and a randomised controlled trial *The Lancet* **2002,** *360*, 427.

(7) M., G.; M., L.; J., D.; D., C.; J., P.; P.R., B., Autotransplantation of Unmanipulated Bone Marrow Into Scarred Myocardium Is Safe and Enhances Cardiac Function in Humans *Cell Transplant.* **2004,** *13*, 7.

(8) Brinkman, D. M.; de Kleer, I. M.; ten Cate, R.; van Rossum, M. A.; Bekkering, W. P.; Fasth, A.; van Tol, M. J.; Kuis, W.; Wulffraat, N. M.; Vossen, J. M., Autologous stem cell transplantation in children with severe progressive systemic or polyarticular juvenile idiopathic arthritis: long-term follow-up of a prospective

clinical trial *Arthritis Rheum.* **2007,** *56*, 2410.

(9) van Ramshorst, J.; Atsma, D. E.; Beeres, S. L.; Mollema, S. A.; Ajmone Marsan, N.; Holman, E. R.; van der Wall, E. E.; Schalij, M. J.; Bax, J. J., Effect of intramyocardial bone marrow cell injection on left ventricular dyssynchrony and global strain *Heart* **2009,** *95*, 119.

(10) Wollert, K. C.; Meyer, G. P.; Lotz, J.; Ringes Lichtenberg, S.; Lippolt, P.; Breidenbach, C.; Fichtner, S.; Korte, T.; Hornig, B.; Messinger, D.; Arseniev, L.; Hertenstein, B.; Ganser, A.; Drexler, H., Intracoronary autologous bone-marrow cell transfer after myocardial infarction: the BOOST randomised controlled clinical trial *The Lancet* **2004,** *364*, 141.

(11) Janssens, S., et al., Autologous bone marrow-derived stem-cell transfer in patients with ST-segment elevation myocardial infarction: double-blind, randomised controlled trial *The Lancet* **2006,** *367*, 113.

(12) Ruan, J.; Ji, J.; Song, H.; Qian, Q.; Wang, K.; Wang, C.; Cui, D., Fluorescent magnetic nanoparticle-labeled mesenchymal stem cells for targeted imaging and hyperthermia therapy of in vivo gastric cancer *Nanoscale research letters* **2012,** *7*, 309.

(13) Park, S.; Shin, J.; Lee, J.; Cha, M., Manipulation of NIH3T3 cells with functionalized single-walled carbon nanotubes under a magnetic field *Mater. Lett.* **2012,** *68*, 378.

(14) Loebinger, M. R.; Kyrtatos, P. G.; Turmaine, M.; Price, A. N.; Pankhurst, Q.; Lythgoe, M. F.; Janes, S. M., Magnetic resonance imaging of mesenchymal stem cells homing to pulmonary metastases using biocompatible magnetic nanoparticles

Cancer Res. **2009,** *69*, 8862.

(15) Tang, C.; Russell, P. J.; Martiniello-Wilks, R.; Rasko, J. E.; Khatri, A., Concise review: Nanoparticles and cellular carriers-allies in cancer imaging and cellular gene therapy? *Stem Cells* **2010,** *28*, 1686.

(16) Tiefenauer, L. X., Magnetic nanoparticles as Contrast Agents for Medical Diagnosis. In *Nanotechnology in Biology and Medicine: Methods, Devices, and Applications*, Vo-Dinh, T., Ed. CRC Press: Boca Raton, 2007; pp 1-20.

(17) Wilhelm, C.; Bal, L.; Smirnov, P.; Galy-Fauroux, I.; Clement, O.; Gazeau, F.; Emmerich, J., Magnetic control of vascular network formation with magnetically labeled endothelial progenitor cells *Biomaterials* **2007,** *28*, 3797.

(18) ARBAB, A. S.; JORDAN, E. K.; WILSON, L. B.; YOCUM, G. T.; LEWIS, B. K.; FRANK, J. A., In Vivo Trafficking and Targeted Delivery of Magnetically Labeled Stem Cells *Hum. Gene Ther.* **2004,** *15*, 351.

(19) Reynolds, B. A.; Tetzlaff, W.; Weiss, S., A multipotent EGF-responsive striatal embryonic progenitor cell produces neurons and astrocytes *J. Neurosci.* **1992,** *12*, 4565.

(20) Reynolds, B. A.; Weiss, S., Clonal and population analyses demonstrate that an EGF-responsive mammalian embryonic CNS precursor is a stem cell *Dev. Biol.* **1996,** *175*, 1.

(21) Tropepe, V.; Hitoshi, S.; Sirard, C.; Mak, T. W.; Rossant, J.; van der Kooy, D., Direct neural fate specification from embryonic stem cells: a primitive mammalian neural stem cell stage acquired through a default mechanism *Neuron* **2001,** *30*, 65.

(22) Jensen, J. B.; Parmar, M., Strengths and limitations of the neurosphere culture

system *Mol. Neurobiol.* **2006,** *34*, 153.

(23) Flax, J. D.; Aurora, S.; Yang, C.; Simonin, C.; Wills, A. M.; Billinghurst, L. L.; Jendoubi, M.; Sidman, R. L.; Wolfe, J. H.; Kim, S. U.; Snyder, E. Y., Engraftable human neural stem cells respond to developmental cues, replace neurons, and express foreign genes *Nat. Biotechnol.* **1998,** *16*, 1033.

(24) Fricker, R. A.; Carpenter, M. K.; Winkler, C.; Greco, C.; Gates, M. A.; Björklund, A., Site-specific Migration and Neuronal Differentiation of Human Neural Progenitor Cells after Transplantation in the Adult Rat Brain *J. Neurosci.* **1999,** *19*, 599.

(25) Englund, U.; Fricker-Gates, R. A.; Lundberg, C.; Bjorklund, A.; Wictorin, K., Transplantation of human neural progenitor cells into the neonatal rat brain: extensive migration and differentiation with long-distance axonal projections *Exp. Neurol.* **2002,** *173*, 1.

(26) Conti, L.; Cattaneo, E., Neural stem cell systems: physiological players or in vitro entities? *Nature reviews. Neuroscience* **2010,** *11*, 176.

(27) Bez, A.; Corsini, E.; Curti, D.; Biggiogera, M.; Colombo, A.; Nicosia, R. F.; Pagano, S. F.; Parati, E. A., Neurosphere and neurosphere-forming cells: morphological and ultrastructural characterization *Brain Res.* **2003,** *993*, 18.

(28) Cao, Q.; Benton, R. L.; Whittemore, S. R., Stem cell repair of central nervous system injury *J. Neurosci. Res.* **2002,** *68*, 501.

(29) Pallini, R.; Vitiani, L. R.; Bez, A.; Casalbore, P.; Facchiano, F.; Di Giorgi Gerevini, V.; Falchetti, M. L.; Fernandez, E.; Maira, G.; Peschle, C.; Parati, E., Homologous Transplantation of Neural Stem Cells to the Injured Spinal Cord of

Mice *Neurosurgery* **2005,** *57*, 1014.

(30) Pluchino, S.; Zanotti, L.; Rossi, B.; Brambilla, E.; Ottoboni, L.; Salani, G.; Martinello, M.; Cattalini, A.; Bergami, A.; Furlan, R.; Comi, G.; Constantin, G.; Martino, G., Neurosphere-derived multipotent precursors promote neuroprotection by an immunomodulatory mechanism *Nature* **2005,** *436*, 266.

(31) Sinha, A.; Ganguly, R.; De, A. K.; Puri, I. K., Single magnetic particle dynamics in a microchannel *Phys. Fluids* **2007,** *19*, 117102.

(32) Hazel, R. D.; McCormack, E. J.; Miller, J.; Li, J.; Yu, M.; Benveniste, H.; II, J. P. M.; Egnor, M.; Wagshul, M. E., Measurement of Cerebrospinal Fluid Flow in the Aqueduct of a Rat model of Hydrocephalus *Proceeding of Internal Society for Magnetic Resonance in Medicine* **2006,** *14*, 30.

Conclusions

The combined effect of MNPs and magnetic field on cell was examined with BMPs and SMF, which is required by increasing use of MNPs and magnetic field for biomedical applications.

The BMPs produced from the *Magnetospirillum* sp. AMB-1 were successfully extracted and delivered into the cells, HeLa, C2C12 and SH-SY5Y. The uptake of BMPs by cells was confirmed using confocal microscopy and TEM. Insignificant cytotoxicity of BMPs was tested up to 3 days culture of cells and the uptake efficiency was about 40% of added BMPs to 10^4 of HeLa cells and 10^6 of SH-SY5Y cells. The BMP-loaded cells could be selectively separated using magnetic field with strong magnetic reactivity of BMPs, and is used for investigating the synergistic effect of the BMPs and SMF exposure on cells.

The biological effect of internalized BMPs and SMF exposure was investigated in the context of cell structure, growth, apoptosis and neuronal differentiation. Cell bodies were tend to shrink in the condition of SMF exposure independent of the internalization of BMPs. Cell growth was modulated by the combined magnetic stimulation of internalized BMPs and an exposure to external SMF. The growth of the BMP-internalized cells was significantly increased under the external SMF, which was investigated using MTS and ATP assay. An anti-apoptotic effect was also

induced by the synergistic interaction of the BMPs and SMF exposure. The apoptotic progress induced by an anticancer drug was inhibited in terms of cell death rate, DNA fragmentation and p53 gene expression in the BMP-loaded HeLa cells exposed to the SMF. In addition, improved neuronal differentiation of SH-SY5Y cells were evaluated by measuring the neurite outgrowth length.

These responses of cells to the synergistic stimulation were initially caused by the structural change of the cell membrane, which was observed with fluorescence microscope. The lipid molecules comprising cell membrane were rearranged in favorable direction originated from their diamagnetic anisotropy under the moderate strength of SMF. The internalized BMPs in cells assisted the effect in increasing magnetic flux density around them. The alteration of cell membrane resulted in structural and functional modulation of the embedded transmembrane proteins. The microarray analysis suggested that these phenomena were involved in the alterations of GPCRs-mediated signal transduction originated from the interaction of the internalized BMPs and the external SMF.

A promising in vitro model system was suggested with the advantages of the improved cell growth and magnetic controllable BMP-loaded cells by virtue of the synergistic effect of the BMPs and SMF on cells. It is confirmed that the BMP-NS could be applied for delivery of therapeutic cells with similar functionality of neurospheres from control cells. The BMP-NS has the potential to be spatially

manipulated by virtue of its free-floating form and the magnetic reactivity of the BMPs it contains, and the BMPs enabled it to attach to the target site. The BMPs also rendered cells to facilitate growth and neuronal differentiation; therefore, BMP-NSs might be suitable for cell therapy for neurological damage. In this approach, focusing of cells at the target site was achieved by BMP loading, and efficiency was improved by delivering the neurosphere form of the cells in vitro. This study may be useful for stem cell therapy, and future research would apply this technology to in vivo studies.

Appendix

A. Analysis of Magnetic Field around BMPs

The BMP have own magnetic dipole due to their ferromagnetic property, which means that a BMP can be considered a nano-sized magnet. The magnetic flux density between two magnets is estimated by the formula below.

$$\mathbf{B} = \mathbf{B_1} + \mathbf{B_2}$$

Where, $\mathbf{B_1}$ is the flux density for a magnet at distance $\mathbf{x_1} = \left(\frac{\boldsymbol{d}}{\mathbf{2}} + \boldsymbol{x}\right)$, $\mathbf{B_2}$ is the flux density for the other magnet at distance $\mathbf{x_2} = \left(\frac{\boldsymbol{d}}{\mathbf{2}} - \boldsymbol{x}\right)$, **d** being the distance between the magnets. When the magnets are rectangular, the flux density is derived from the single rectangular magnet formula using the principle of superposition [1].

$$\begin{aligned} \mathrm{B} = \frac{B_{r1}}{\pi}\Bigg[& \tan^{-1}\left[\frac{W_1 L_1}{2x_1\left(4{x_1}^2 + {W_1}^2 + {L_1}^2\right)^{1/2}}\right] \\ & - \tan^{-1}\left[\frac{W_1 L_1}{2(x_1 + T_1)\left[\left(4(x_1 + T_1)^2 + {W_1}^2 + {L_1}^2\right)^{1/2}\right]}\right] \\ & + \frac{B_{r2}}{\pi}\Bigg[\tan^{-1}\left[\frac{W_2 L_2}{2x_2\left(4{x_2}^2 + {W_2}^2 + {L_2}^2\right)^{1/2}}\right] \\ & - \tan^{-1}\left[\frac{W_2 L_2}{2(x_2 + T_2)\left[\left(4(x_2 + T_2)^2 + {W_2}^2 + {L_2}^2\right)^{1/2}\right]}\right]\Bigg]\Bigg] \end{aligned}$$

Where, B_r is residual flux density, W is width, L is length and T is thickness of the magnet. This formula implies that the magnetic flux density in the surrounding area

of a BMP would be enhanced under the SMF environments.

Magnetic flux density changes around the BMPs, under an SMF, were analyzed using magnetostatics model in COMSOL multiphysics 3.5. Two different values of magnetic field intensity at the surface of NdFeB magnets, 120 and 480 mT were used to simulate conditions similar to experimental set-up. Two type of particle were considered, BMP and BMP agglomerate which described BMPs gathered in a cell. A BMP was modeled as a 50 nm square and a BMP agglomerate was a 500 nm square. The distance between center of a BMP or a BMP agglomerate and the magnet was 1 mm, which is the position of cells exposed to SMF. The magnetic flux density was visualized with 2D surface plot and cross-section line plot around the particle.

The increasing intensity of magnetic field was evaluated to verify the effectiveness by simulation using COMSOL multiphysics 3.5 (Fig. A-1).

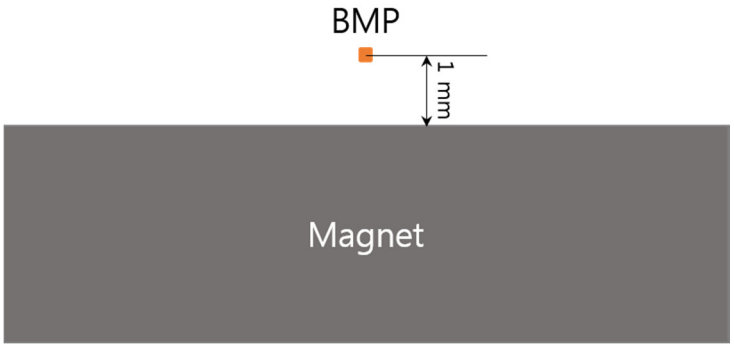

Figure A-1. A simplified model for the simulation of magnetic field intensity around a BMP

As shown in Figure A-2, the magnetic field intensity around a BMP is increased up to 625 mT within 0.6 μm from the particle. The internalized BMPs were observed using TEM that some of BMPs were gathered nearly (Fig. 2-6, 2-7), thus the magnetic field intensity around an agglomerate of BMPs having 500 nm diameter were also confirmed. The agglomerate is more effective to enhance intensity than a particle, up to 730 mT within 3 μm from it. In case of 120 mT exposure, the intensity is increased up to 275 mT around a BMP and 380 mT around an agglomerate (Fig. A-3). The effective area is similar to that under the 480 mT of SMF.

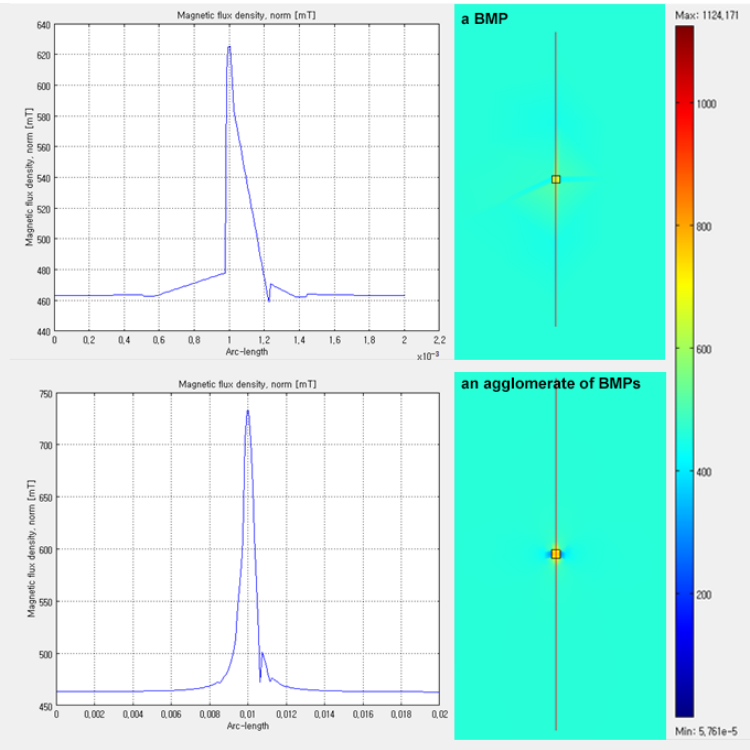

Figure A-2. Magnetic field intensity around a BMP and an agglomerate of BMPs under the 480 mT of SMF

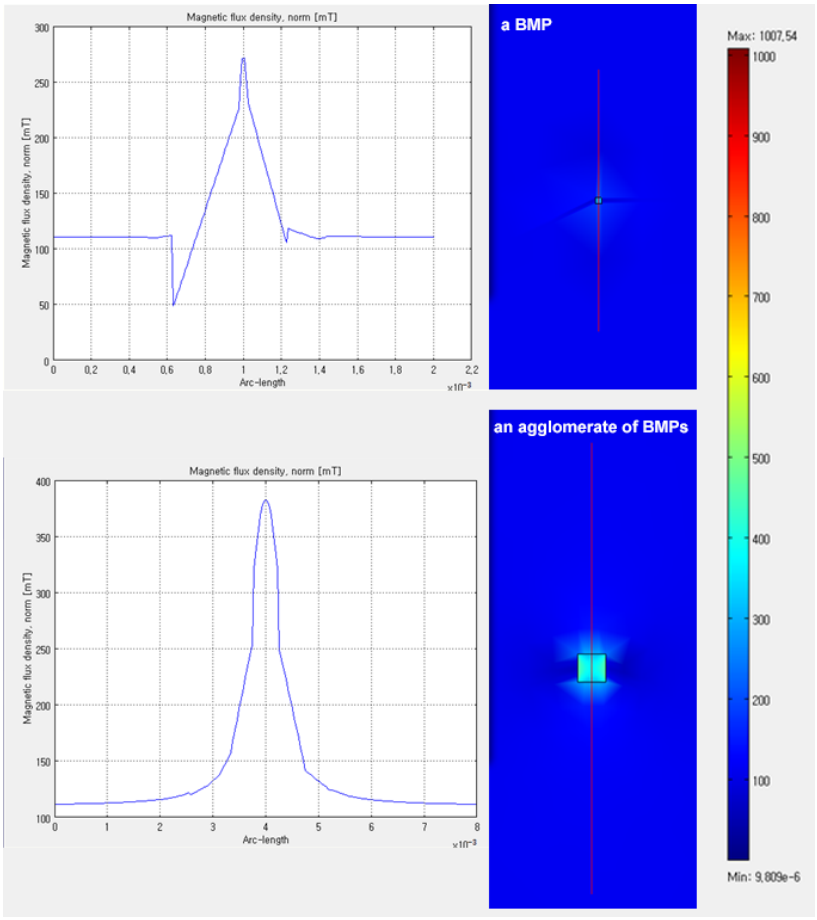

Figure A-3. Magnetic field intensity around a BMP and an agglomerate of BMPs under the 120 mT of SMF

B. Appendix References

(1) http://www.imstrading.com/magnet-formula.html#drs.

국문초록

자성나노입자와 자기장이 세포에 미치는 상승효과에 대한 연구

전기장과 자기장의 생체의학적 응용을 위한 연구는 수 십 년간 계속되어 왔다. 전기장은 물리치료, 재활, 암 치료 등에 이용되어왔고, 전기자극치료기가 시중에서도 판매되고 있다. 자기장을 이용하여 만성통증, 상처치유, 관절염 등의 치료를 하기 위한 연구도 계속되고 있으며, 자기장은 현재 영상의학에서 많이 사용되는 자기 공명 영상법에 이용되고 있다.

자성나노입자의 합성과 그 응용에 대한 연구 또한 전세계적으로 관심이 높고 활발히 진행되고 있는 추세이다. 이는 자성나노입자가 가지는 자기적 성질로 인해 외부자기장을 이용하여 제어가 가능하다는 장점으로부터 비롯된다. 전자기장과 자성나노입자를 여러 치료법에 응용하기 위한 연구들이 많이 진행되고 있고, 정자기장 또한 세포 분리와 표적화에 이용되고 있다. 따라서 자기장과 자성나노입자의 안전한 이용을 위하여 그것이 미칠 수 있는 생물학적 영향에 대한 주의 깊은 검토가 요구된다. 그러나 자기장과 자성나노입자의 복합적인 생물학적 효과에 대한 연구는 미미한 편이다.

이에 본 연구에서는, 박테리아 자성나노입자와 정자기장을 이용하여 자성나노입자와 자기장이 세포에 미치는 상승효과에 대해 알아보았다. 박테리아 자성나노입자는 주자성 박테리아에 의해 자연적으로 합성되는 자성나노입자를 일컫는다. 이 입자는 생체적합성을 가진 지질막에 쌓여진 상태로 합성이 되고 이러한 성질은 세포 내부로 입자가 전달되는 데에 도움이 된다.

세포막을 구성하고 있는 지질 분자들의 반자기적 이방성은 중간 강도의 정자기장이 인가된 환경에서 세포의 형상을 변화시키는 주된 요인이다. 더불어 페리 자성체인 박테리아 자성나노입자는 입자 주변부의 자기장을 강화시키는 역할을 한다. 자성나노입자가 내재된 세포가 자기장에 노출되었을 때, 이러한 두 특성이 복합적으로 세포에 작용함으로써 세포성장 촉진과 세포자멸사 감소의 현상이 나타난다. 세포 형상 변화를 초래한 세포막의 형상적 변화는 세포막에 박혀있는 막관통단백질의 형상적, 기능적 변화로 이어지고 세포의 유전자 조절을 일으켜 궁극적으로는 세포성장, 세포자멸사, 세포분화에 영향을 미치게 된다. 이러한 유전자 조절이 G단백질공역수용체를 매개로 한 신호전달의 조정으로 인해 발생됨을 마이크로어레이 분석 기법을 통하여 밝혔다.

체내에서 결손조직으로의 정확한 세포 이동과 가능한 많은 수의 세포를 이식하는 것은 세포를 기반으로 하는 치료요법의 성공을 결정하는 매우 중요한 요소이다. 자성나노입자와 자기장의 상승효과로 인한 세포성장

촉진은 자성나노입자를 내재한 세포의 자기장에 의한 제어성과 함께 세포치료요법에 효율적으로 이용될 수 있고, 결손조직의 신속한 재생을 유도할 수 있다.

본 연구에서는 자성나노입자와 자기장의 상승효과를 이용한 하나의 응용분야로써, 척수 손상으로 인해 손상된 신경세포 치료에 이용될 수 있는 체외 모델 시스템을 제시하였다. 이 모델 시스템에서는 박테리아 자성나노입자를 내재한 신경구세포가 유체흐름 속에서도 자기장에 의해 특정목표 지점으로의 위치 제어가 가능함을 보여주었다. 이러한 결과는 박테리아 자성나노입자가 유체내에서의 줄기세포 위치 제어에 적합함을 보여주며, 이는 체내 순환을 통한 줄기세포의 이동 및 이식을 이용한 조직 재생 치료에 적용될 수 있음을 시사한다.

본 연구에서 밝혀진 박테리아 자성나노입자와 자기장의 상승효과로 인한 세포성장 조절은 표적세포치료요법에 새로운 접근법으로 제시될 수 있다.

주요어: **자성나노입자, 자기장, 세포성장, 세포자멸사, 세포분화, 신경구세포, 세포치료**

학번: 2006-23090

감사의 글

무사히 학위를 마칠 수 있도록 끝까지 믿고 지켜봐 주며 도와준 나의 가족, 아버지, 어머니, 동생 직수 너무나 고맙고 사랑합니다.

그리고 여기까지 인도하여 주신 주님께 감사 드립니다.